May 2020

The Fabrication and Analysis of an Angle-Ply, Multi-Laminate Annulus Fibrosus Plug for Intervertebral Disc Repair

Alex Garon
Clemson University, alexrgaron@gmail.com

THE FABRICATION AND ANALYSIS OF AN ANGLE-PLY, MULTI-LAMINATE ANNULUS FIBROSUS PLUG FOR INTERVERTEBRAL DISC REPAIR

A Thesis
Presented to
the Graduate School of
Clemson University

In Partial Fulfillment
of the Requirements for the Degree
Master of Science
Bioengineering

---

by
Alexander Robert Garon
May 2020

Accepted by:
Dr. Jeremy Mercuri, PhD, Committee Chair
Dr. Dan Simionescu, PhD
Dr. Sanjitpal Gill, MD

ABSTRACT

The intervertebral disc (IVD) is a fibrocartilaginous tissue connecting adjacent vertebrae in the spinal column. Within the IVD is gelatinous core called the nucleus pulposus (NP) which is radially confined by the annulus fibrosus (AF). The AF is composed of concentric layers of fibrous lamellae rich in collagen type I and functions to support radial forces redistributed from the NP core.[15,1] Pathologic conditions of the IVD are often associated with low back pain (LBP) which has a lifetime prevalence of up to 80% and creates an annual economic burden of over $100 billion.[2,3] Discogenic pathologies associated with LBP include IVD degeneration (IVDD – a multifactorial breakdown of the IVD) and/or herniation (IVDH – when IVD tissue is forced beyond or out of the normal confines of the IVD).[4,35] This results in approximately 2.7 million back surgeries in the United States annually.[4,5] These surgeries are generally palliative, leaving patients susceptible to continued chronic LBP or chance of re-herniation.

Current methods aimed at repairing the IVD fail to address the focal defect created in the AF following discectomy. Furthermore, developing technologies that do effectively close AF defects (Intrinsic Barricaid™ and Annulex X-Close™) are made of synthetic materials that do not support IVD tissue regeneration.[71,74] Therefore, there has been an increased focus on using tissue engineering and regenerative therapies to develop an effective AF repair system to both restore IVD integrity and mechanics to slow or halt underlying degenerative processes.

Our group has previously developed an outer AF repair patch (AFRP) using sheets of decellularized pericardium.[122-124] Pericardium contains collagen type I and a fiber

orientation similar to native AF tissue. Stacking layers of fiber aligned pericardium effectively mimics the angle-ply lamellae of the AF. Despite many promising outcomes of the AFRP, it was identified that a biomimetic scaffold was needed that could fill a full-thickness AF defect, as opposed to only covering the defect in the outer AF. Thus, the goals of this research were to i) fabricate a full thickness, multi laminate annulus fibrosus repair plug (FT-AFRP) scaffold, ii) determine the scaffold's ability to mimic the mechanical properties of native, full-thickness AF tissue and restore spinal kinematics in a repair model, iii) determine the scaffold's influence on AF cell viability, alignment, and morphology.

The research herein resulted in the development of a repeatable method to fabricate FT-AFRPs which effectively mimicked the angle-ply, fiber aligned architecture of native AF using decellularized pericardium and an alginate hydrogel casing. FT-AFRPs moderately matched compressive mechanical properties of native AF tissue and partially restored spinal kinematic parameters in an IVD explant repair model. FT-AFRPs also demonstrated cytocompatibility and the ability to support AF cell alignment and morphology. Collectively, these results support the potential of the FT-AFRP to be used in conjunction with outer AF closure techniques to more effectively repair the AF following IVD surgery.

DEDICATION

This work is foremost dedicated to my parents, Susan and Bob, as well as my best friend, Jacqueline. Your constant love and support have pushed me to be the best version of myself as I continue to chase my dreams.

ACKNOWLEDGMENTS

First, I would like to thank my advisor, Dr. Jeremy Mercuri, for his trust in my ability to conduct research in the Ortho-X lab. His support, encouragement, and mentorship have helped to shape me into the researcher and person I am today. I would also like to thank my committee members, Dr. Dan Simionescu and Dr. Sanjitpal Gill, for their assistance on the progression of this project. I would like to recognize Dr. Yongren Wu and Martin Groke of the Medical University of South Carolina for their willingness to collaborate on portions of this project. I would like to thank past members of the Ortho-X lab, Specifically Ryan Borem and Joshua Walters, for setting the incredible foundation for this project as well as the continuous support. Lastly, I would like to thank the current Ortho-X lab members. Their intelligence and constant willingness to help made nearly any challenge seem feasible and made this experience one I will not soon forget.

TABLE OF CONTENTS

Page

Table of Contents (Continued)

LIST OF TABLES

LIST OF FIGURES

List of Figures (Continued)

Figure Page

List of Figures (Continued)

Figure Page

List of Figures (Continued)

Figure Page

List of Figures (Continued)

Figure Page

List of Figures (Continued)

Figure Page

CHAPTER ONE

LITERATURE REVIEW

1.1 Introduction to Lower Back Pain

Low back pain (LBP) affects a large majority of the population with a lifetime prevalence of up to 80%.[6] It is the second highest cause of disability in the United States with a 54% increase in years lived with disability from 1990 to 2015.[2,7] LBP is the leading cause of orthopedic and neurosurgeon visits, and the second most common reason for general physician visits.[8,9] Patients suffering from LBP experience symptoms ranging from persistent dull aches to debilitating sharp pain.[10] In addition to an overall reduction in quality of life, LBP brings with a significant individual and societal economic burden. Each year in the United States, approximately 149 million days of work are lost due to LBP.[2] The associated reduction in productivity and lost wages makes up approximately two-thirds of a total annual cost of over $100 billion.[2,3]

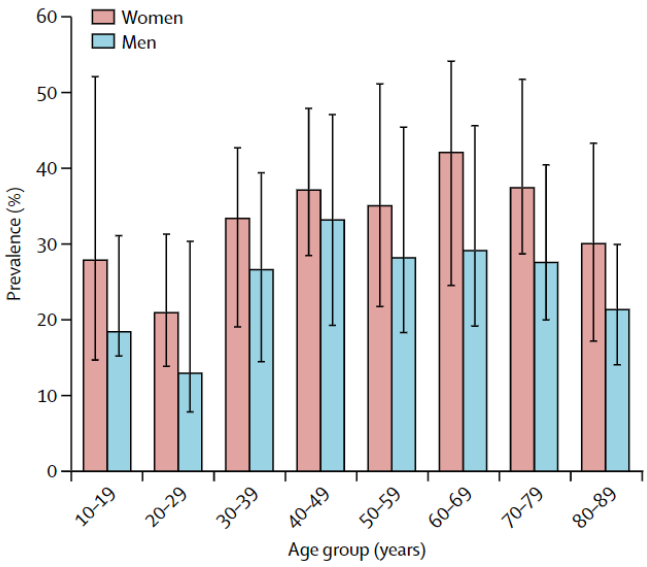

Figure 1: Median prevalence of lower back pain across sex and age groups.[7]

While the causes of LBP are often multifaceted and difficult to determine, a common progression can stem from intervertebral disc (IVD) pathologies. The breakdown of IVDs, called intervertebral disc degeneration (IVDD), has been suggested to imply the occurrence of both chronic and non-chronic LBP.[11] The pathogenic process of IVD degeneration also predisposes intervertebral disc herniation (IVDH) in which IVD tissue is forced out of the confines of the disc.[4] While IVDD and IVDH are two distinctly different challenges, they both often result in overall reduction of IVD height, loss of spinal motion, and increased pain and debilitation. Overall, these pathologies affect an additional 5% of the population in developed countries each year and result in 2.7 million annual back surgeries in the United States.[4,5] These surgeries, while performed often, are generally palliative, leaving patients susceptible to continued chronic LBP or chance of re-herniation. With an aging population and recent increasing trends in lumbar degeneration, continued development of widespread and effective IVD targeted treatment options are needed to address the significant pain and economic burden of LBP.[12]

1.2 Intervertebral Disc Physiology

The vertebral column is made up of individual functional elements called motion segments. Each of these segments contains an IVD linking two adjacent vertebrae as seen in **Figure 2**.

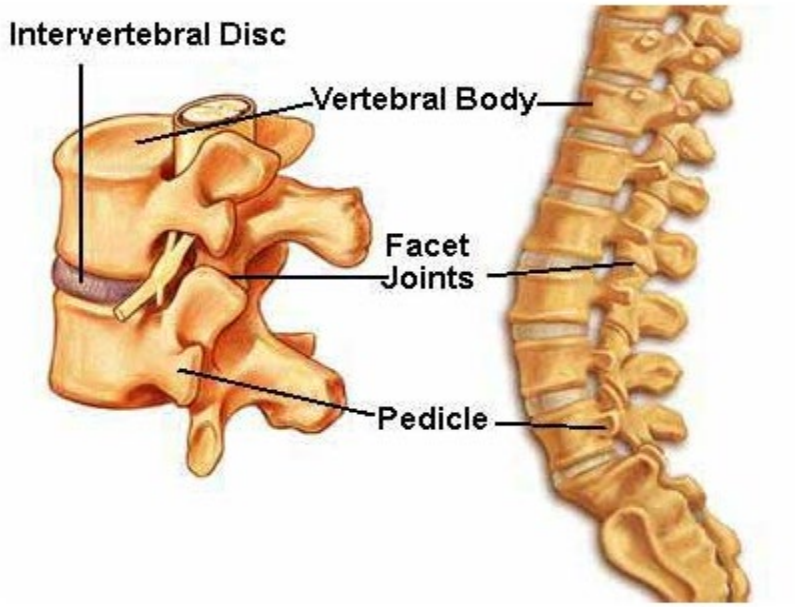

Figure 2: Overview of IVD location within the spinal column.[13]

There are 23 IVDs in the human spine which are classified in three different categories: 6 cervical, 12 thoracic, and 5 lumbar. While there are regional differences, the main structure of the IVD is common throughout the spine.[14] The overall shape of the IVD is approximately cylindrical with a slight posterior taper which becomes most prominent in the lumbar discs due to the natural curvature of the lower spinal region.[14] The IVD acts as a shock absorber in the spine, transferring loads throughout the vertebral column while maintaining proper mobility and support. To achieve this, the IVD is uniquely designed with multiple distinct regions, each interreacting and dynamically contributing to the overall functionality of the disc.[15]

1.2.1 IVD Anatomy and Function

The IVD is a fibrocartilaginous tissue with three regions: the nucleus pulposus (NP), the annulus fibrosus (AF), and the cartilaginous end plates (CEP).[16]

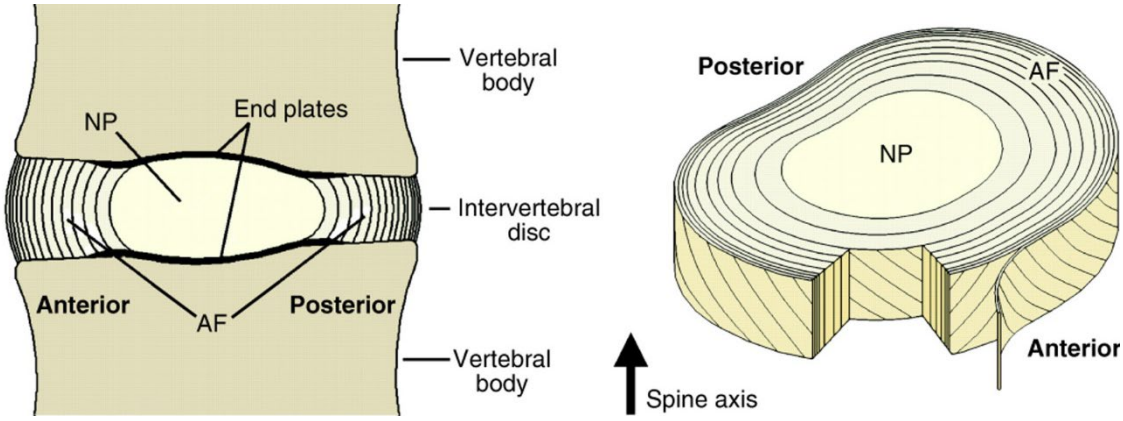

Figure 3: Overview of the Intervertebral Disc[16]

The NP is the central, gel-like core of the IVD largely responsible for distributing compressive spinal loads to the AF and CEPs.[1] The AF is a multi-layered ring structure, wrapping around the NP and confining it concentrically in the disc's core. The CEPs confine the disc vertically and act as the interface between the IVD and associated vertebral bodies.[17] Altogether, the IVD is the largest avascular tissue in the human body with oxygen concentrations dropping as low as 1% in the center of the NP.[14] Differences in these tissue regions can generally be attributed to the organization and proportion of the three main components of the IVD: water, collagen, and proteoglycans. The main collagen types throughout the IVD are types I and II.[1] The main proteoglycan is aggrecan, a cartilage specific proteoglycan.[16] The different distributions of these components contribute to the swelling pressure, permeability, and compressive properties of the IVD.

The NP plays an essential role in the flexibility and stability of the spine. High levels of collagen type II and proteoglycans help the NP to remain elastic and resist compression under spinal stresses.[1] The water content of the NP can be as high as 80%, compared to the AF which is approximately 70%.[18,19] Other components of the NP

structure include elastin as well as rounded chondrocyte like cells.[14] The proteoglycans of the NP contain a core protein with numerous covalently attached glycosaminoglycans (GAGs).[20] These carbohydrate chains extend throughout an irregular network of type II collagen fibrils.[16] The GAGs are sulfated with keratin and chondroitin, giving the NP a high charge density. The fixed negative charge causes the influx of counter ions which then results in water in-flow. This generates an osmotic swelling pressure, ultimately leading to a mix of fluid and solid mechanical behavior. This gelatinous, biphasic mechanical response of the NP gives it the ability to support spinal forces and re-direct them to the other portions of the IVD.[1]

The AF is composed of 15-25 concentric layers of fibrous lamellae rich in collagen type I. Between the layers is a proteoglycan and GAG rich gel interspersed with elastin.[14] The collagen fibers run parallel to each other within each individual layer. The fibers of each successive layer run perpendicular to the fibers of the previous layer at angles approximately $\pm 30^{o}$ from the horizontal axis of the IVD as seen in **Figure 4**.[14] Additional cross fibers provide further connection between different layers.

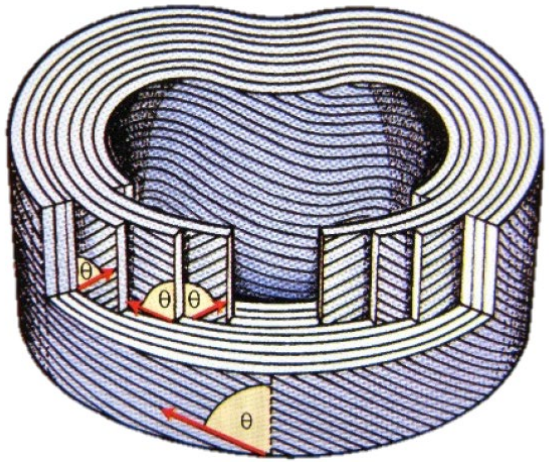

Figure 4: Angle-ply architecture of the AF lamellae.[21]

The ability of the AF to bear the forces redistributed by the NP can primarily be attributed to this angle-ply structure. While the AF appears as a ring structure, the lamellae tend to be discontinuous around the NP core and rather serve as connecting bands between adjacent CEPs.[22] The architecture and composition are heterogeneous throughout the AF. The organization of the lamellae and associated collagen fibers are highly ordered in the outer regions of the AF located closest to the edges of the IVD. Towards the center of the IVD, within the inner AF, there is a shift to collagen type II as well as an increased level of proteoglycans giving rise to a gradual transition from outer AF to the NP.[16] Cell type in the AF also follows a gradient with similarities to the NP found in the innermost AF regions. Elongated fibroblast-like cells are the predominant cell morphology in the outer AF. Like the collagen fibers of the matrix, the AF cells are highly organized. The cell processes align along the fiber structures of each lamellae, functioning to produce the aligned collagenous matrix and further contribute to the mechanical stability of the AF.[23] It has been suggested that cell alignment in this region is initiated by the constant tensile forces placed on the AF when the IVD is functioning in physiological conditions.[23] Cell phenotype shifts to a rounded, chondrocyte-like cell in the inner AF, although both cell types are still present. The innermost portion of the AF is often referred to as the transition region due to its increased similarity in cell and matrix composition compared to the NP.

The CEP is a thin layer of cartilage that acts as an interface between the vertebral body and the rest of the IVD. The CEP varies in thickness from 0.1 – 1.6 mm with the thinnest regions being above and below the NP.[14] While the CEP is primarily referred to as being hyaline cartilage, fibrocartilage can also be found in the region surrounding the

NP.[14,16,24] The primary functions of the CEPs are to act as a mechanical barrier between the NP and vertebral bodies as well as for nutrient transport from nearby vasculature.[24] With the avascularity of the IVD as a whole, there is a heavy reliance on nutrient and waste exchange to occur through the pores located in the CEPs.[25]

1.3 IVD Pathologies and Clinical Significance

Due to the mechanical interplay between the AF, NP, and CEPs, structural integrity of each part is essential to the functionality of the IVD as a whole. Clinically, the two most common pathologies are IVD degeneration (IVDD) and IVD herniation (IVDH). The progression of IVDD leaves patients susceptible to IVDH. Likewise, damages from IVDH can further induce IVDD, leaving a distinct difference but important relationship between the two pathologies.

1.3.1 Degenerative Disc Disease

IVDD is the accelerated breakdown of the IVD extracellular matrix (ECM), reducing its structural integrity and overall height in the spinal column while showing advanced signs of aging. While IVDD can occur anywhere in the spine, it is most common in the lumbar discs (L-1 through L-5), particularly L-4 and L-5.[4] Factors contributing to IVDD include; physical, environmental, and genetic, leaving underlying processes that cause the breakdown difficult to define. The prevalence of IVDD is widespread and can occur early in life as IVDs degenerate earlier than other musculoskeletal muscles.[26] First consistent signs of IVDD have been seen in the age group of 11-16.[27] Overall, around 20% of teens show mild signs of IVDD.[28] In addition to this, most mild cases of IVDD are asymptomatic, leaving early detection difficult. The progression of IVDD through older

populations is significant with 10% of 50 year old's and 60% of 70 year old's showing severe signs of degeneration in their discs.[26] IVDD has a grading scale with stages 0-4 (4 being the most severe) as seen in **Figure 5**.

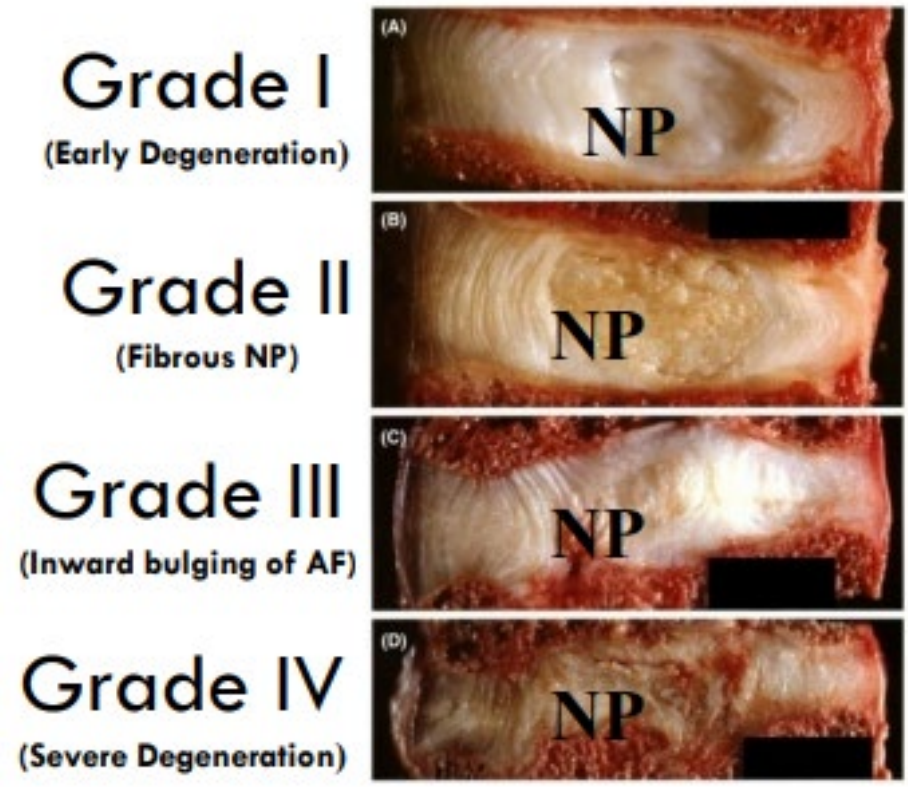

Figure 5: Progressive stages of intervertebral disc degeneration.[29]

IVDD is most distinguishable by a loss of tissue and reduction in the IVD's organizational structure.[30] This initial degeneration occurs through mild changes in the matrix of the NP and inner AF regions.[31] As IVDD progresses, the lamellae of the AF become irregular with collagen fibers becoming less organized.[26] Additional blood vessels are also seen in degenerated discs.[32] The overall process begins with biomolecular damage including a loss in proteoglycan and water content.[33] The drop in GAG content associated with the lowered proteoglycan content reduces the osmotic pressure of the IVD, leading to

the loss of hydration.[26] These biomolecular changes induce a cellular response including cell senescence and apoptosis as well as an irregularity in protein signaling.[33] The accumulated biomolecular changes of IVDD also lead to phenotype changes of AF and NP cells. While little change is seen in overall collagen content in degenerated discs, the types and distributions of collagen is altered through IVDD.[31] The compromised cellular and matrix components of the IVD lead to a negative change in biomechanics through an overall loss in hydraulic and viscoelastic properties of the tissue.

IVDD results in significant changes in the function of the IVD. With a lowered osmotic pressure and water content, a degenerated IVD loses height quickly under load.[34] This loss in height under load paired with a fluid flow out of the disc causes the IVD to bulge radially. The altered state of the IVD can place irregular stress concentration both internally on the AF and CEPs as well as throughout other portions of the spine.[26,27,30,31] When stress concentrations continue to accumulate on progressively degenerated tissue, an IVDH can occur.

1.3.2 Herniation

Herniation occurs when IVD material extends beyond the normal boundaries of the disc. This extended material can be from the NP, AF, or a combination of both. While herniations can occur without pain, as seen by MRI images of herniated discs in asymptomatic patients, the pathology can become problematic if nerve compression occurs.[35] Pinching of the spinal sciatic nerve (sciatica), results in numbness and pain in the lower back which can extend into the legs.[26,30] Overall, there are four primary classifications of IVDH as seen in **Figure 6:** 1) bulging discs: the AF remains intact but

the disc is extended over its normal boundary, 2) Protrusion: NP material pushes into the AF region without tearing AF layers, 3) extrusion: NP material is forced through AF layers and beyond the outer confines of the disc, 4) sequestration: the NP material extruded through the AF is no longer attached to the NP base material.[36]

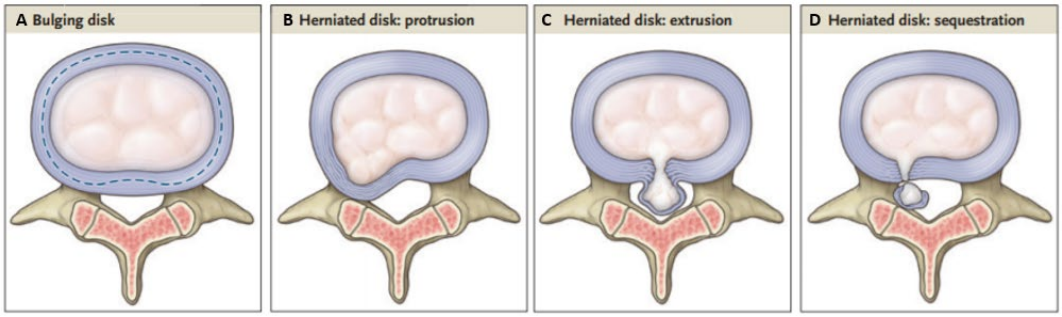

Figure 6: Stages of Intervertebral Disc Herniations.[36]

IVDH's occur most commonly posterolaterally where the AF is thinner and where there is no accompanying support from adjacent spinal ligaments.[37] While it has been thought that IVDH occurs purely through mechanical overload of the spine, studies done on healthy IVDs have shown that vertebral bodies usually fail before the IVD does under intense loading.[26] This points towards the predisposition of IVDD for IVDH.

1.4 Current Treatments of Intervertebral Disc Pathologies

There are a variety of treatment options for IVD pathologies ranging in aggressiveness and effectiveness. As emphasized by the grading severity scales of IVDD and IVDH, each pathologic IVD case is unique requiring a different form of treatment. Clinically, there are consistent recommendations for evaluating individuals with general lower back pain, but a lack of clarity on treatments.[30] Many of the available treatment options target the symptoms of discogenic lower back pain rather than the underlying

pathology of the IVD. The overlying objectives of any treatment option, at the most basic level, should be to alleviate painful symptoms while restoring mechanical function.[16]

1.4.1 Non-surgical solutions

Non-surgical management is often the most conservative treatment option for those suffering from LBP, making it a primary option for patients. Options include oral analgesics, physical- and psycho- therapy, acupuncture, and steroidal injections.[30,36,38] These treatment options are often appropriate for individuals with milder cases of IVDH or IVDD. It has been suggested that non-operative management consist of a multimodal approach including anti-inflammatory medication, physical therapy, and education.[39] It is important to manage the painful symptoms while simultaneously rehabilitating when possible. This rehabilitation can be done through specific exercise and manual spinal manipulations.[40,41] Another recent approach to discogenic back pain consists of electrothermal stimulation which has shown to increase function and decrease overall pain.[42] Long term conclusions are yet to be published on this form of therapy. Continued pain, especially caused from sciatica, can lead to the incorporation of corticosteroid injections in hopes to reduce nerve irritation and induce healing.

While these multimodal, non-surgical treatments offer a variety of options, they often show limited success. Ongoing and potentially ineffective treatment can become very expensive with the average patient spending $3,445 on conservative treatment measures before opting for a surgical approach.[43] All in all, when a patient's back pain points towards an IVD pathology and becomes a chronic issue after conservative treatment, surgical approaches are considered.

1.4.2 Surgical Interventions

Surgical procedures are often a last resort or an option for individuals with confirmed IVD pathologies that cannot be sufficiently treated with conservative measures. The main benefit of surgical approaches is that relief of pain can occur faster than non-surgical options. While pain may subside quicker, the overall advantage for total magnitude of pain relief is often smaller for surgical approaches.[44,45] Differences in surgical rates around the world have raised questions as to the potential over-use of surgical interventions in some areas. For example, The US has a rate of back surgery that is five times higher than that of the UK.[26] Additionally, cases can vary as different surgical approaches are used to treat IVDD and IVDH.

When IVDD reaches its later stages in a patient, one of two surgical strategies are often explored: spinal fusion or total disc replacement (TDR). These currently practiced procedures aim to reduce patient's symptoms rather than to restore the structure and function of the IVD. The current gold standard is spinal fusion.[46,47] Spinal fusion gained popularity in the early 2000's with a 137% increase in total number of fusion procedures between 1998 and 2008.[48] This trend has continued in more recent years with a 63% increase in lumbar specific fusion procedures between 2004 and 2015, totaling to 199,140 lumbar surgeries in 2015.[49] Spinal fusion consists of removing the damaged IVD and creating a bony fusion between the two adjacent vertebrae. Bone graft material is implanted where the IVD once was, inducing the bone segments above and below the space to fuse together. Metal fixation devices are often implanted to further increase the stability of the spine segment while bone is forming. The mobility of the spinal motion segment is

removed, but spinal height is maintained in an effort to reduce pain. The overlying problem associated with spinal fusion is the accelerated degeneration of adjacent IVDs. Removing the shock absorbing capacity of an IVD redirects the forces to adjacent IVDs. It has been reported that IVDD in adjacent spinal levels appear as soon as 3 years after fusion surgery.[50] In addition to the physiological issues, fusion procedures are expensive with an average cost of $102,000, further contributing to it being a last-resort option.[51] A variety of fusion techniques have been developed but little to no difference in success rates has been seen in recent studies.[52]

With continuing concerns associated with completely removing the spinal motion segment through fusion, many have focused on developing a device to completely replace the damaged IVD. Like fusion, TDR involves the removal of the damaged IVD. Unlike fusion, the implantation of a prosthetic replacement maintains portions of the mobility of the native spinal segment. The implant aims to restore harmonic load sharing between spinal levels to reduce the occurrence of adjacent segment disease. Implants are typically combinations of biocompatible polymers such as ultra-high molecular weight polyethylene and metals such as cobalt-chrome molybdenum. There are currently eight TDR devices on the market from companies such as Medtronic, Globus, and Zimmer Biomet.[53] While TDR has been commercially available since the 1980's, continued investigation is needed to confirm the overall success of the procedure. Recent studies have shown improved success for TDR compared to spinal fusion with improved patient reported outcomes at both 2 and 5 year follow ups.[54,55] Additionally, a decrease in adjacent level IVDD has also been reported.[56] While some have reported a reduction in re-operation rates compared to fusion,

others have reported no significant difference.[55,57] These short-term studies are beginning to present significant data to support the use of TDR over spinal fusion, but significant challenges for TDR remain. Implant collapse, subsidence, and dislocation can lead to severe complications. TDR is also incompatible for a variety of patients such as those with high spinal instability or vertebral osteoporosis.[53] The largest complication associated with TDR is implant wear.[58] Wear causes debris deposition which can induce an inflammatory response. The response mimics that of a foreign body reaction resulting in bone resorption, stimulation of sensory fibers, and the imminent return of pain.[59] Recent long-term studies confirm that TDR patients suffer a similar deterioration to fusion patients, but at a later time. Re-operation rates were as high as 31% for the Charité III lumbar TDR implant after a 12 year follow up.[60] These studies question the legitimacy of TDR as a successful alternative to spinal fusion. Both fusion and TDR are also often overly aggressive procedures for those with IVDH.

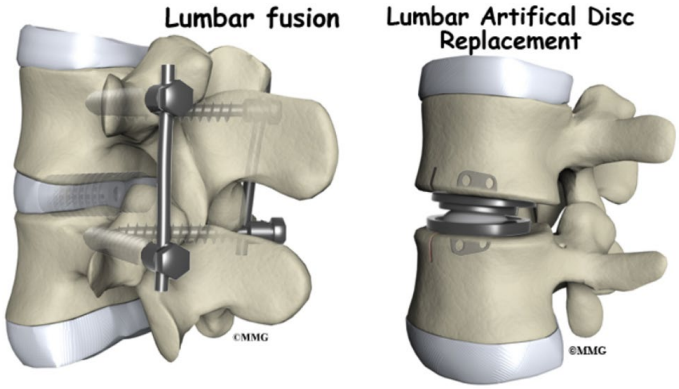

Figure 7: Spinal Fusion and Total Disc Replacement.[61]

One of the most common types of surgery, specifically associated with IVDH, is discectomy. This procedure includes making a small incision in the back, exposing the IVD, and cutting and removing material protruding from the IVD in order to reduce nerve

compression. A laminectomy, where a small portion of the vertebrae is removed, is often required in order to reach the site of the herniation.

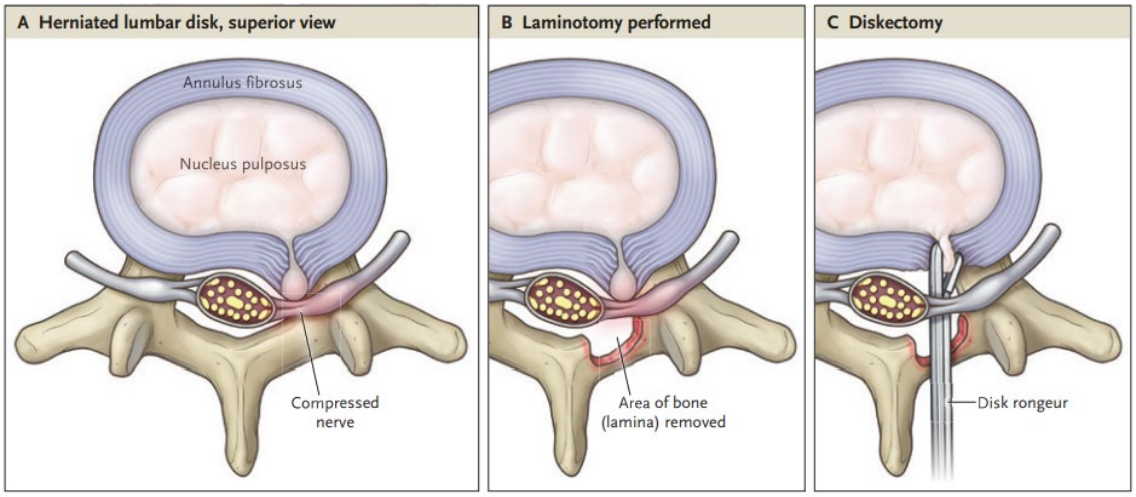

Figure 8: Discectomy procedure with laminectomy.[36]

Up to 300,000 of these procedures occur annually in the United States.[62] While many patients show positive outcomes following discectomy procedures, recurring issues occur for many. In a recent study examining discectomy success, 7% of cases required reoperation by year 1, 9% of cases by year 2, and up to 19% by year 4 with more than half due to re-herniations at the same disc level.[36,63] Reoccurring herniations are especially present in patients who have large protrusions with minimal IVDD elsewhere as well as with adolescents with IVDH.[62] These conditions are particularly troublesome as removing the herniated tissue from the disc requires rupturing the AF, leading to a depressurization of the NP. Additionally, disc height is reduced by 25% on average following discectomy procedures.[64,65] Advances have been made in the procedure, most of which involve trending towards a more minimally invasive technique and reducing recovery times. The challenge remains as to restoring the structure and function of the AF after discectomy

procedures. Long term studies done on discectomy patients showed similar outcomes to those opting for conservative treatments.[66] Techniques removing different portions of the herniated disc also resulted in no significant improvement.[67] Overall, the AF fissures associate with discectomy as well as the loss of biomechanical stability must be addressed in order to further prevent re-herniation and achieve superior clinical outcomes.

1.5 Repairing the IVD

Previously discussed clinical methods to combat IVD pathologies have focused on treating symptoms through conservative therapies or palliative surgical techniques. Conservative treatments show limited success for patients with higher severity level IVD pathologies while surgical options show high levels of implant failure and re-operation. For IVDD, Spinal fusion and TDR are generally end-stage procedures that could benefit from an earlier stage intervention. Current research is being done to develop an NP material to replace degenerated native tissue. Implanting this material would require a pathway to the center of the disc, leaving the AF compromised. Likewise, discectomies performed on patients with an IVDH result in a mechanically altered AF in order to remove excised native tissue.

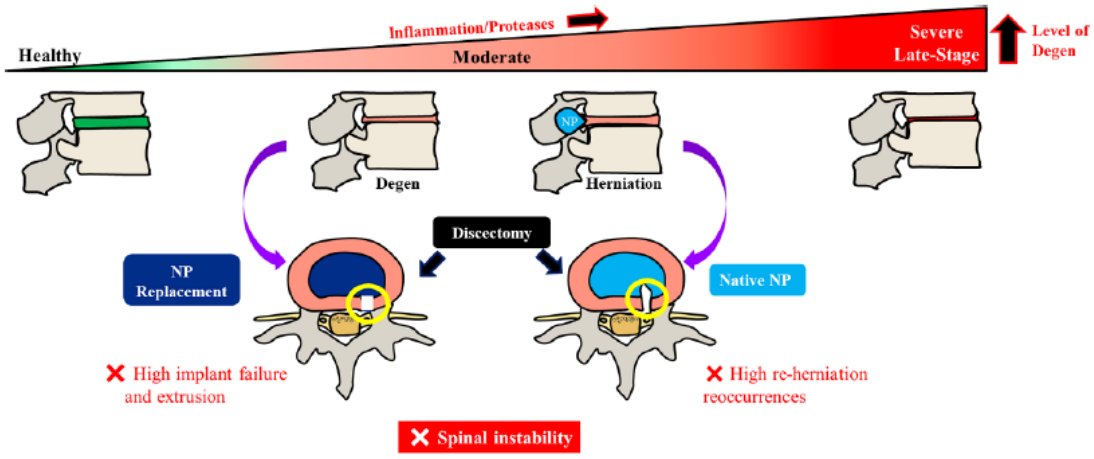

Figure 9: Depiction of the IVDD cascade and subsequent need for AF repair following NP replacement or discectomy procedures.[68]

In both cases, a method to replace damaged AF tissue, effectively closing off the IVD to re-herniation, would be beneficial. Techniques to address the damaged AF are increasingly recognized as an essential development for improved patient outcomes following repair procedures. With an additional challenge of slowing down the degenerative process when repairing the IVD, a primary focus on tissue engineered scaffolds has emerged.[62,69]

1.5.1 AF Closure Techniques

There have been a variety of attempts at closing the annular defects of the IVD with few options currently available. Initial attempts involved simply suturing the AF closed with traditional knots. Other techniques involve glues which are primarily composed of fibrin or cyanoacrylate. In vitro studies suggested that AF closure with solely suture or glue is insufficient but that a combination of both had potential promise.[70-72] Cyanoacrylate glues, which typically perform better mechanically than fibrin glues, have raised concerns of long term cytotoxicity.[73,74] Additionally, larger defects pose concerns that are difficult to overcome with suture and glue techniques alone.

Recent technologies have built on these findings. The Xclose system (Anulex Technologies, Minnetonka, MN) uses tension bands to close the AF.[72] One to three tension bands are stretched in parallel or cruciate patterns across the AF defect on the outside of the IVD. Each band is comprised of a suture loop with tissue anchors at either end. These anchors are placed approximately 12mm directly into the adjacent AF tissue. A pre-tied knot is used to tighten the bands and secure the anchors, theoretically repairing the AF. Despite closing off the outer AF, this technique fails to plug the void throughout the AF, leaving NP material to migrate out from the inter region of the IVD. This migration results in reduction of disc height and a loss of intradiscal pressure. Additionally, the anchoring relies on the structural integrity of AF tissue surrounding the defect. Many other suture-based products have suffered from similar pitfalls.

Barricaid™ (Intrinsic Therapeutics, Woburn, MA) is another system that uses a slightly different approach. A woven polyester mesh acts as a plug within the annular defect. The mesh is attached to a titanium anchor with is implanted into the adjacent endplate.[75] The incorporation of the mesh blocks material from re-herniating and also aids in maintaining disc height. Despite this, the system fails to seal the outer annulus and leaves little potential for tissue regeneration or remodeling. Recent follow-up studies have investigated the effectiveness of both the Barricaid and Xclose systems in repairing the AF compared to discectomies where AFs were left damaged. Studies showed that while these systems do reduce the occurrence of re-herniation, no improvements were made in disability and pain indexes for patients compared to discectomies performed without AF repair.[76]

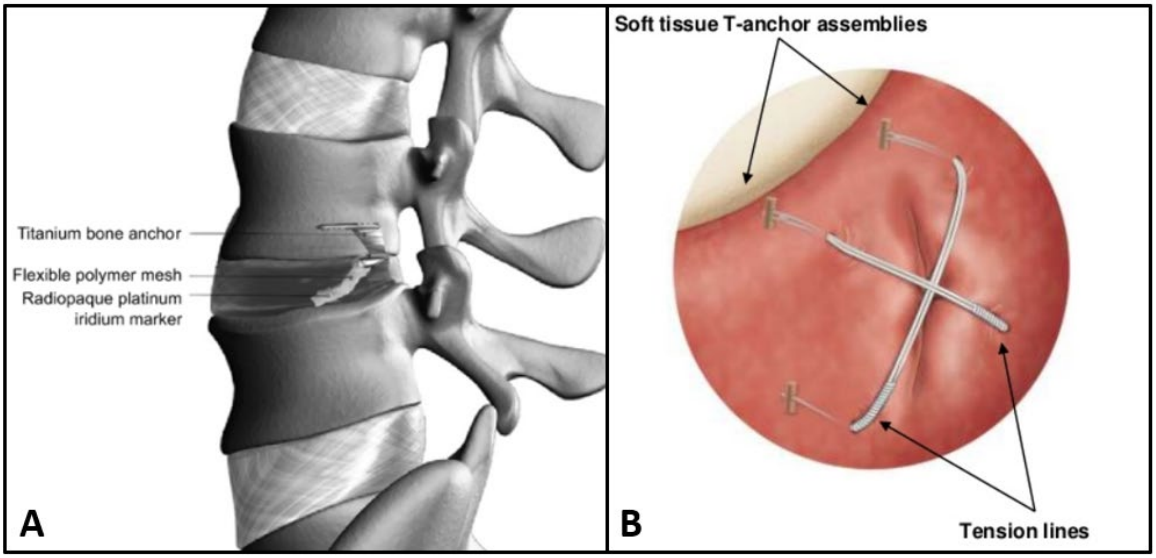

Figure 10: Current commercially available AF repair strategies A) Barricaid and B) Xclose system.[77]

Current systems focus solely on closing the AF; which they are marginally successful at. Pain and disability remain in patients even with reduced rates of re-herniation. This issue is most likely linked to both the migration of material in an IVD as well as the continued degenerative process after repair. Overall, a system is needed that 1) closes the outer AF defect, 2) keeps NP material in the center of the disc by filling AF defect space, 3) has potential to regenerate and remodel the damaged IVD tissue to slow the degenerative process. Mechanically, this system would need the best aspects of both the previously mentioned products: replacement material throughout the thickness of the AF as well as an outer seal. Combining these aspects would pair lowered rates of re-herniation with improved patient outcomes through maintained disc height and restored mechanical stability. The achievement of restored function paired with slowing the degenerative process further points towards the development of a biomimetic, tissue engineered system.

Currently, research is being done to develop a biomimetic scaffold for outer AF closure that is implanted onto the outside of the disc after discectomy or nuclear arthroplasty as seen in **Figure 11**.

Figure 11: An annulus fibrosus repair patch (AFRP) intended for outer AF closure.

While such a system may prevent NP material from leaving the confines of the disc, it does not keep the NP in the center of the IVD where it possesses the most mechanical functionality. This problem constitutes the need for a scaffold that occupies the entire full thickness of the AF defect, aiding in the retention of the NP as well as the overall restoration of mechanical stability in the IVD.

1.6 Tissue Engineering the Annulus Fibrosus

With the challenge of both preventing re-herniation as well as promoting healing and/or slowing the degenerative process, tissue engineering and regenerative medicine have moved to the forefront of research. The breakdown of the IVD is attributed to cellular and biomolecular changes. These changes lead to a change in tissue morphology, and ultimately, lost biomechanical performance. Considering this, the overlying aspect of

IVDD is matrix structure. This structure is dependent on the balance of cell metabolism within the IVD in order for proper maintenance of the matrix.[78] Overall, while a mechanically competent replacement is needed to aid in closing the AF, the cellular aspect is equally as important in achieving total clinical success through a slowed degenerative process. This is the aspect that many commercially available AF closure techniques fail to address.

Gene and protein therapies have opened a potential option to stimulate matrix and aid in repairing the IVD. These strategies have been administered through techniques such as direct injection into degenerated discs. Despite this, the progressive nature of IVDD has garnered suggestions for continued therapeutic administration for sustained stimulation.[79,80] One leading option constitutes the incorporation of cell therapies with a mechanically competent scaffold. Achieving this requires a biomimetic scaffold that follows the structure of native AF tissue in order to provide correct cellular stimulus for the repaired IVD. In addition to cellular signaling, similar matrix structure between an engineered and native AF could also provide similar mechanical properties, ultimately leading to corrected mechanical function of a repaired IVD. In order to best create this scaffold, it is important to understand the native AF structure and healing capacity as well as previous attempts at engineering AF scaffolds.

1.6.1 Native AF Healing Capacity

The intrinsic healing potential of the IVD is generally considered poor.[62] Low mean cell counts in the IVD of 6000 cells/mm^3 paired with an avascular and biomechanically demanding environment make natural regeneration a significant challenge.[81] This is

supported clinically by the progressive and high prevalence of degeneration. Despite this, minor repair processes have been observed in the AF.[81] The healing capacity that is present is potentially connected to the chemotactic mechanisms of chemokines. Chemokine receptors have been identified on human AF cells.[62] The ability of chemokines to recruit AF cells has also been confirmed.[82] Whether the process is chemotactic or not, low but continuous proliferation rates have been shown in different parts of the IVD including the AF.[83] Furthermore, stem cell niches around the border of the IVD have been reported and there is evidence that these cells migrate into the AF to work with local progenitor cells towards tissue regeneration.[83] Increasing evidence of mesenchymal stem cell (MSC)-like progenitor cells have been reported in AF, NP, and CEPs of both healthy and degenerated human IVDs.[84-86] The overall function of these repair mechanisms may be disturbed by the inflammatory and catabolic processes associated with degeneration and IVD damage.[87] Overall, this leads to an insufficient natural healing process, especially when damage has been initiated through events such as IVDH and discectomy.

Smith et al. suggested that the healing process of the AF occurs in three different phases.[88] First, a proliferative reaction in the fibrous tissue induces healing of the outer AF. This process begins at the outermost portions and works towards the median portions of the wound. Secondly, the healing process continues to the inner AF in a similar manner to the healing of the outer region in the first phase. This process begins within a few weeks and lasts up to a year post-operation. Lastly, collagenous fiber density begins to increase in the NP material that protruded into and remained in the AF wound after injury. This ultimately leads to a fibrous and stiffer structure than healthy tissue.

The healing process of the AF has been investigated further in many different animal studies.[88-95] Key and Ford used a dog model with different induced posterior annulus lesions.[89] The lesion groups included a transverse incision, puncture with a 20-gauge needle, and an open square annulus window. The lesions were initially found to fill with blood, fibrin, bone, and cartilage debris. This was slowly replaced by a thin layer of fibrous tissue over the course of 22 weeks. Some lesions developed disc protrusion, which was most common in the transverse incision group but also seen in the annulus window group. The needle puncture group showed no abnormalities and the lesions could not be identified after 22 weeks. This finding was challenged by a more recent study through an organ culture model with rabbit IVDs.[96] This study concluded a progressive mechanical and biologic consequence from needle puncture in longer term follow-ups.

From these various studies it is evident that a healing process occurs in the AF following injury, but that it is very limited in regenerating the IVD to a healthy and functional state. Various theories have been proposed for this limited healing potential, but much remains unknown. One potential reason for clinical insufficiencies is that the exterior AF repairs associated with intrinsic healing do not adequately recruit fibers to the tensile forces demanded by the IVD. Mechanical shifting of axial load in the NP to circumferential tension in the AF requires keeping NP tissue volume elastic and contained. Scarred tissue changes the AF's ability to contain the NP, ultimately leading to accelerated herniation and propagation of annular fissures.

1.6.3 Regenerative Medicine and Cell Therapies

The value of cells to the metabolic health of the IVD prompts the strategy of replacing, regenerating, or augmenting the native cell population under pathologic conditions. This would work towards the goal of correcting matrix deficiencies to aid in the restoration of proper biomechanics in the IVD.[62] A variety of techniques have been tried to achieve this goal. One approach is to stimulate disc cells to produce more matrix through the introduction of growth factors.[97] In contrast, cytokine inhibitors have also been tried in order to prevent the breakdown of matrix.[98] The direct injection of these factors has shown little success due to their inability to maintain effectiveness over extended periods of time. Cell implantation is another approach to directly address the scarcity of healthy cells in damaged AF tissue. The incorporation of analogous or autologous cells has shown success for other applications such as articular cartilage and has therefore been applied to IVD repair. The implantation of autologous cells in small populations of patients has shown success but long term outcomes need further investigation.[78] The ability for these cells to live in the damaged AF long term remains a challenge. Similar to the injection of growth factors, cell implantation has limited long term success when proper nutrient supply and scaffold conditions are not present as with many IVDH and IVDD cases. Other than low chance of survival, challenges for cell implantation include cell leakage out of the intended injury site, unwanted osteophyte formation, and general difficulty of implantation into the IVD.[99,100] Cell sources are also a potential issue which will be addressed in subsequent sections.

When cells are successfully implanted and viable, it has been shown that they respond to matrix and mechanical stimulation, ultimately contributing to a modulation of inflammation and promotion of repair.[101] These implanted cells repopulate regions of the AF where native cells and extracellular matrix (ECM) have been lost through a deposition of matrix proteins. This is supported by studies showing that cultured AF cells retain proliferative capacity, demonstrate an ability to generate correct matrix, and undertake expression consistent with the phenotypic demands of IVD anatomy.[78] Obtaining AF cells requires direct implantation of the correct cell type or the implantation of stem cells that have the potential to differentiate into the correct cell type. Therefore, it is essential to provide a scaffold that AF or stem cells can live on in order to achieve their benefits surrounding regeneration.

1.6.4 AF Cell Sources

One of the major issues limiting the use of biological AF repair is a suitable cell source.[102] Often, the first consideration in identifying a cell source is if cells should be autologous, allogenic, or xenogeneic. Another consideration is the way in which the cells are cultured once isolated as certain conditions can aid in proper integration with tissue once implanted. Cells can also be harvested from a tissue type that is different than the one intended to be repaired. Lastly, stem cells can be considered with their potential to differentiate into desired cell types. Overall, there are many options for cell sources, each with their own advantages and limitations. These items to be considered for cell therapy must therefore also be considered when choosing a cell source to supplement a tissue engineered scaffold.

Using the Intervertebral disc as a source of autologous cells is an obvious first approach, but one which possesses significant limitations. Low cell counts and regional phenotypic changes make isolating a significant number of the correct cells difficult. Additionally, taking a biopsy punch of tissue to extract cells inevitably means puncturing the AF. With the heathiest cells coming from the least degenerated discs, this would mean potentially inducing IVDD and eventual IVDH to repair an IVD at a different spinal level. Another issue associated with human adult AF cells is that the majority of them are reported to be dead or dying through necrosis or apoptosis.[27] Senescence is another common occurrence associated with adult AF cells which unfavorably alters cell metabolism and growth.[103] The same concerns apply to allogenic or xenogeneic AF cells with additional challenges of disease transmission and immune responses. Despite these challenges, autologous AF cell therapy has been incorporated clinically with discectomy procedures. A European study of 112 patients compared outcomes for patients undergoing discectomy procedures with and without subsequent autologous AF cell treatment.[78] The study reported moderate success of AF cell treatment to preserve disc structure. Reported limitations of the study included potential inclusion of inflammatory cells as well as the requirement of a second procedure for cell implantation. Overall, the use of AF cells shows promise, but there is a significant challenge in obtaining them autologously in a healthy state without inducing damage to the transplant site.

With the challenges associated with obtaining heathy AF cells, focus has shifted towards the use of stem cells for regenerative therapy.[62] As with AF cells, autologous cells pose the least clinical hurdles in terms of patient compatibility. A popular choice is

mesenchymal stem cells (MSCs) which can be obtained autologously from various locations including bone marrow, adipose tissue, muscle and dermis, umbilical blood, and others.[104] MSCs are known to be able to differentiate into many different cell types associated with bone, cartilage, adipose tissue, and muscle.[102] The ability of MSCs to differentiate into disc like phenotypes is still under investigation. Studies have reported that MSCs can adopt a gene expression profile similar to native disc cells.[103] Co-culturing MSCs with disc cells has also shown a sped up process of discogenic phenotype expression but these studies have focused on the chondrocyte like phenotype of NP cells.[105] MSCs aid in the repair process of the IVD in a few different ways, including: 1) by differentiation into disc-specific cells to replace lost or damaged cells and to form new ECM, 2) indirectly, through the release of growth factors to enhance regeneration, 3) by modulating the inflammatory response.[104]

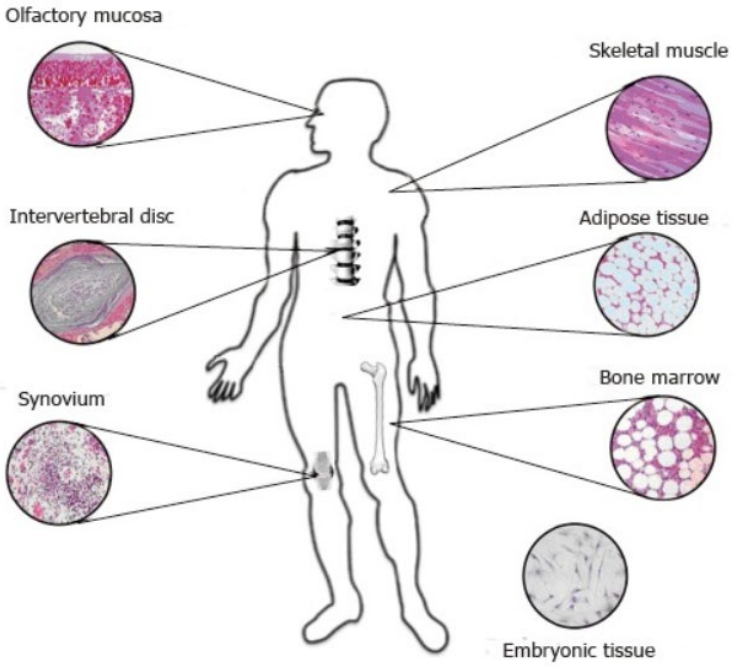

Figure 12: Major sources of stem cells used for IVD engineering.[100]

One of the main limitations of MSCs is that many patients with back pain are middle-aged, giving their stem-cells little expansion potential. To limit this challenge, a potential allogenic source could be younger donors. Another option for allogenic or potentially autologous stem cells is from umbilical tissue. This is a continuously more achievable source as tissue banks are established. An additional challenge is for MSCs to repair the IVD in a useful amount of time. Studies done on MSC's production of GAG and aggrecan, two important molecules lost through IVDD, have suggested that stem cell injection by itself is not enough to restore the disc.[106] From a clinical standpoint, trials done with stem cells have shown varying success. The injection of undifferentiated hematopoietic stem cells into patient's IVDs showed no clinical success.[105] A more recent study using bone marrow concentrate cells did show pain reduction.[107] Companies have continued entering the market for clinical trials on cell-based therapies in recent years. Studies done have supported that a variety of cell sources, homologous and non-homologous, autologous and allogenic, can retard the degenerative process of the IVD following IVDH.[108] The challenge remains of having a viable cell source and scaffolding for cellular support.

1.6.5 Scaffolds Under Development

An ideal biomaterial for AF repair would provide instant and prolonged mechanical stability and allow new healthy tissue to form.[62] It has been suggested that a biocompatible scaffold that mimics the angle-ply architecture of the native AF would be the holy-grail for AF repair.[109] Many scaffolds are currently being developed with several overlying focuses as described in **Table 1**. Many different strategies have been used to engineer such a

scaffold with materials ranging from injectable hydrogels, to decellularized extracellular matrix, to synthetic polymers.

Table 1: Overlying goals for AF repair scaffolds from Bowles et al. and Cruz et al.[101,109]

General Goals and Qualities of AF Repair Scaffolds
Restoration of mechanical function of the damaged or diseased AF.
Prepared scaffold architecture that supports AF or other relevant cell types.
Ability to delivers biologics to promote ECM production and tissue formation.
Allow easy translation to current surgical procedures.
Seal irregular shaped AF defects to prevent re-herniation and cell leakage.
Restore IVD height and mechanical behavior.
Withstand prolonged exposure to the mechanically demanding environment of the IVD.

Due to the high levels of collagen in native AF, cell scaffolds have been developed using injectable collagen-based gels.[110-112] Different combinations of collagen type I and II have been used to mimic the collagen content in the inner and outer regions of native AF. Advantages of collagen based scaffolds include a weak immunogenicity and the ability to support a variety of cell types.[62] These gels have been supplemented with fibrin as well as GAGs such as chondroitin sulfate or hyaluronan, which are natively seen within the AF.

In 2018, Moriguchi et al. published a paper on the use of high density collagen gels seeded with AF cells as a repair strategy in an in vivo rat model.[111] These gels consisted of collagen type I extracted from rat tail tendons which was digested and diluted to 20 mg/mL. The collagen solution was gelled with a 0.75 mM solution of riboflavin and mixed with ovine AF cells before implantation into rat tail defects. This study concluded that the high-

density collagen gel improved disc height, NP size, and disc hydration after 5 weeks when seeded with AF cells. Demonstration of durability and NP retention was shown, but little was done to legitimize the gels ability to restore mechanical function.

In 2014, Guterl et al. proposed an optimized fibrin gel for AF repair (FibGen).[113] The initial fibrin gel was enhanced through genipen crosslinking as well as the addition of cell adhesion molecules, fibronectin, and collagen. In vitro tests demonstrated durability and mechanical tunability through slowed degradation rates compared to fibrin only gels as well as shear stiffness values similar to native AF. Culturing AF cells in FibGen gel resulted in an elongated morphology. This could potentially be advantageous when seeking the fibroblast like cell type associated with native AF tissue. While the FibGen gel shows promise for very small annular defects, it is incapable of sealing larger defects without accompanying scaffolds. Additionally, further studies by this group demonstrated that the material is cytotoxic when cells are incorporated into the gel before gelation occurs.

Analogous gels have been developed using other natural hydrogels such as agarose, alginate, and chitosan.[114,115] Altogether, the gels discussed have widely shown advantageous cellular support as well as easy implantability. What these materials lack is a robust mechanical strength comparable to native AF tissue as well as a fiber aligned architecture. Thus, focus has shifted towards developing scaffolds that better mimic the mechanical properties and organization of the native AF.[62]

One natural material that has been identified to have both advantageous mechanical properties as well as a high affinity for cell attachment is silk.[62] Various processing techniques also give the potential to create a silk scaffold that mimics native architecture.

In 2007, Chang et al. studied the ability of AF cells to attach to and grow on porous silk scaffolds supplemented with RGD peptides.[116] It was concluded that AF cells attach to silk scaffolds, proliferate, and synthesize ECM. In addition, the inclusion of RDG peptides showed changes in cell morphology that could aid in replicating cell type differences between inner and outer AF regions. In 2018, Bhunia et al reported that these silk scaffolds were able to be processed into a mimetic angle-ply construct.[117] Lamellar sheets were fabricated using a directional freezing method. Aligning multiple layers together resulted in an angle-ply structure with compressive properties similar to native AF. While these scaffolds show promise, they are primarily used as part of a whole IVD replacement. The silk sheets are intended to wrap completely around an NP replacement core rather than to close an annular defect. Further research may be needed to develop a suitable closure technique using this material.

Various synthetic materials have also been used to create a full thickness scaffold with a focus on polymeric biomaterials. Polymeric biomaterials have been used in many other tissue engineering applications due to their lack of immunogenicity, predictable mechanical properties, reproducibility, and ease of processing into desirable structures.[62] Popular biodegradable polymers for AF tissue engineering are polycaprolactone (PCL), Polylactic acid (PLA), and polyglycolic acid (PGA). Various techniques of processing these polymers have included freeze-drying, salt-leaching, weaving, thermal phase separation, and electrospinning. The most often used method to produce porous structure for AF repair is electrospinning.[62] It has been shown that depositing electrospun nanofibers

onto a rotating mandrel can dictate both fiber alignment as well as mechanical anisotropy needed to mimic native AF.[118]

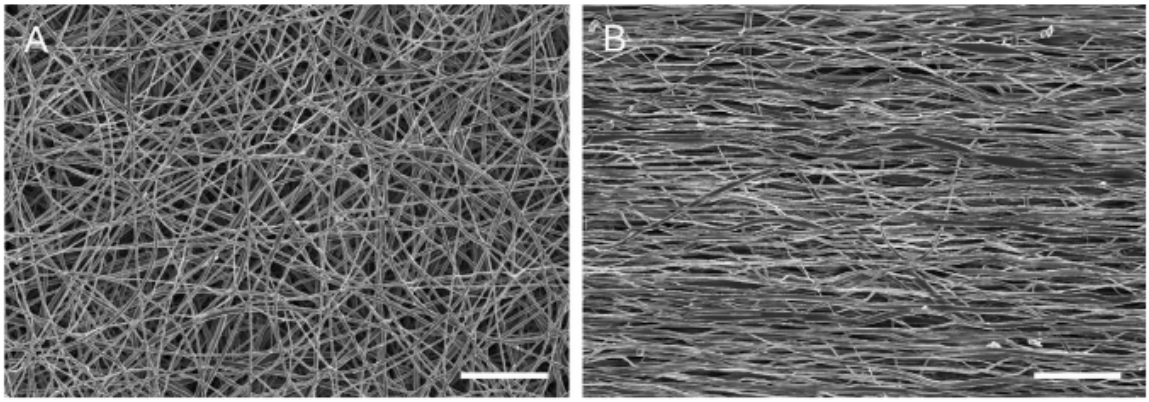

Figure 13: Scanning electron microscopy images of non-oriented (A) and oriented (B) electrospun PCL.[62]

In 2007 Nerurker et al. detailed the electrospinning of PCL to produce AF-like tissue.[118] Their processing technique resulted in singular sheets of aligned fibers. Although these sheets are not a full thickness annular repair, they are the base units needed to develop a full annular closure scaffold. Uniaxial tensile testing on the sheets resulted in the most similar results to native AF lamellae when fibers were oriented between 28º-44º, demonstrating the mechanical mimicry of the material. In addition, seeded AF cells aligned along the fiber structure and deposited matrix when scaffolds were placed under physiological loads. Further developments for this scaffold have focused on developing a whole disc replacement with agarose as a central NP replacement.[119] Other labs with electrospun PCL and PLA scaffolds have yielded similar results mechanically and cellularly.[120]

In 2017, Kang et al. used similar electrospinning techniques as previously described but fabricated cylindrically shaped scaffolds with multiple layers of fiber-oriented lamellae

of PCL.[121] These cylinders were formed by thermally fusing 13 individual lamellae and punching out both 4- and 6-mm diameters with a biopsy punch. Scaffolds were seeded with porcine bone marrow derived MSCs and used to repair induced annular defects in an in-vivo porcine model. The repair consisted of the PCL scaffold to plug the defect, a cyanoacrylate closure glue, and an outer suture closure method. Follow up studies at 6 and 12 weeks concluded that repairs successfully restored nucleus volume and slowed the degenerative process as observed trough MRI imaging. Aligned collagen was also observed integrating with the PCL plug at 12 weeks. Further studies are needed to determine the integration and mechanical outcomes as the PCL scaffolds degrade. Insufficient integration upon complete degradation of the scaffold would result in the return of pain and herniation potential.

Other synthetic, full thickness annular plugs have been developed using stereolithography (SLA) techniques. Blanquer et al. used poly(trimethylene carbonate) (PTMC) processed with SLA to achieve a gyroid-porous structure as seen in **Figure 14**.[122]

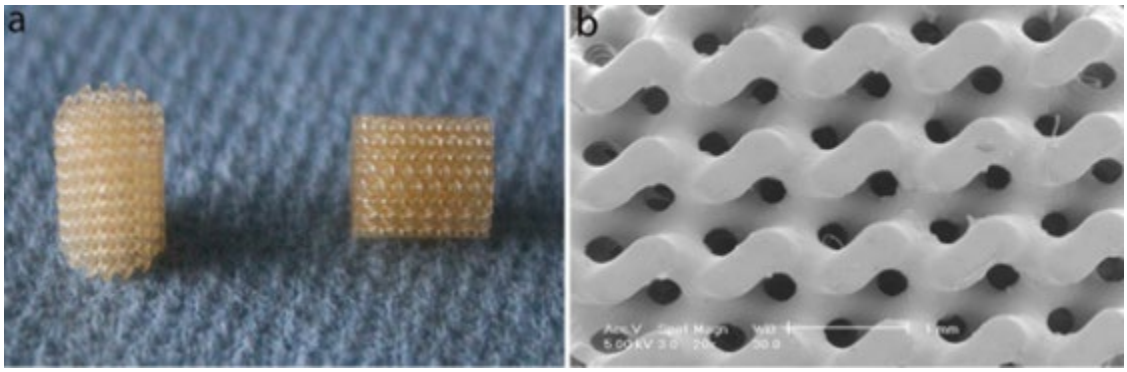

Figure 14: A) Cylindrical poly(trimethylene carbonate) AF repair scaffolds and B) scanning electron microscopy image of porous scaffold structure.[122]

Repair studies were done with PTMC scaffolds in a bovine injury model.[112] Bovine caudal spinal segments (vertebrae-IVD-vertebrae) were extracted and injuries were induced by a 5 mm biopsy punch. Repairs consisted of implantation of the cylindrical PTMC scaffold, injection of FibGen gel, and closure of the defect with a combination of a polyurethane membrane, fibrin adhesive, and suturing. The motion segments were put through a complex loading regimen and kinematic parameters of the repaired motion segments were compared to uninjured control groups. The repairs partially restored IVD biomechanics but posed a high risk for re-herniation.

Overall, there have been many different attempts at creating a scaffold to both replace the damaged AF as well as to act as a carrier for regenerative cells. Natural gels show abundant cell support and implantability but lack adequate closure and mechanical functionality. Silk and electrospun polymers can correctly mimic angle-ply architecture and support cell life but have widely been used as part of a whole intervertebral disc replacement. Plug shaped synthetic scaffolds show mechanical and cellular promise but have yet to be studied long term as they degrade. The overall important findings throughout studies outlined that AF scaffolds must 1) mimic the mechanically anisotropic quality of native AF, 2) support relevant cell types ultimately leading to scaffold integration with native tissue, and 3) be used in conjunction with supporting techniques to achieve complete AF closure.

1.7 Towards A Tissue Engineered, Full-Thickness AF Repair Scaffold

LBP is a widespread clinical problem that can often be traced to IVD pathologies such as IVDD and IVDH. In the case of IVDH, the AF is inevitably damaged through the

initial herniation process or subsequent discectomy repair procedures. There are currently few commercially available options to repair the damaged AF, resulting in high rates of re-herniation and continued LBP. Repair strategies that do exist are able to prevent re-herniation, but do not play any role in modulating the continued degenerative process. Regenerative medicine approaches and tissue engineered scaffolds have been developed in hopes to combine solutions to the mechanical and cellular aspects of discogenic LBP, but none have shown all-around success. While some scaffolds under development have shown either mechanical or cellular advantages, few have shown both. Those scaffolds that do satisfy both needs are made of synthetic materials that do not provide additional ECM for re-integration. Others are simply unsuitable for an AF point defect and instead are focused towards whole IVD engineering.

The research herein aims to build off the most successful aspects of previously developed commercial products and scaffolds currently under development to step closer to an all-encompassing AF repair strategy. The intended strategy will fill the void of annular defects to prevent herniation and restore overall IVD mechanics. The strategy will also allow for the delivery of gene- or cell-based therapies to manage the onset of IVDD. Lastly, the strategy will include a scaffold that is biomimetic to provide proper cellular cues as well as add additional ECM to re-incorporate with intact native AF tissue. Investigating such a strategy will include developing a scaffold fabrication method, studying the mechanical mimicry of the scaffold compared to native AF tissue, and identifying the ability of the scaffold to support relevant cell types.

CHAPTER TWO

AIM 1

2.1 Introduction and Purpose

Previous efforts have identified decellularized porcine pericardium as a potential material for AF repair scaffolds.[123-125] Pericardium is comprised of both dense regular and irregular connective tissue. Most of this connective tissue is type I collagen which is organized in directional fibers as seen in native AF tissue.[123] Multiple sheets of pericardium were overlaid such that the fiber preferred directions mimicked the fiber structure of AF tissue. Specifically, three layers of pericardium were adhered together via a sewing machine and ultimately used as a patch to close the outside of annular defects. This resulted in a mechanical response similar to AF tissue as well as a partially restored kinematic response when used to repair an injury model.[124] Additionally, the decellularization of the pericardium resulted in a cytocompatibility that supported cell viability, penetration, and proliferation.

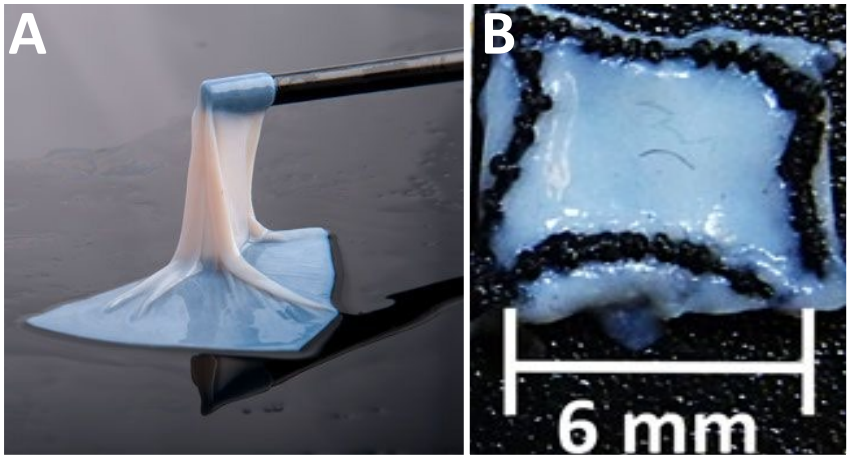

Figure 15: A) Decellularized pericardium and B) a 3-layer angle-ply AF repair patch (AFRP).

While major advances were made in developing the AF repair patch (AFRP), the scaffold is only intended to close the outside of an annular defect. The AFRP does not replace AF tissue throughout the disc resulting in a failure to keep NP material in the center of the IVD.

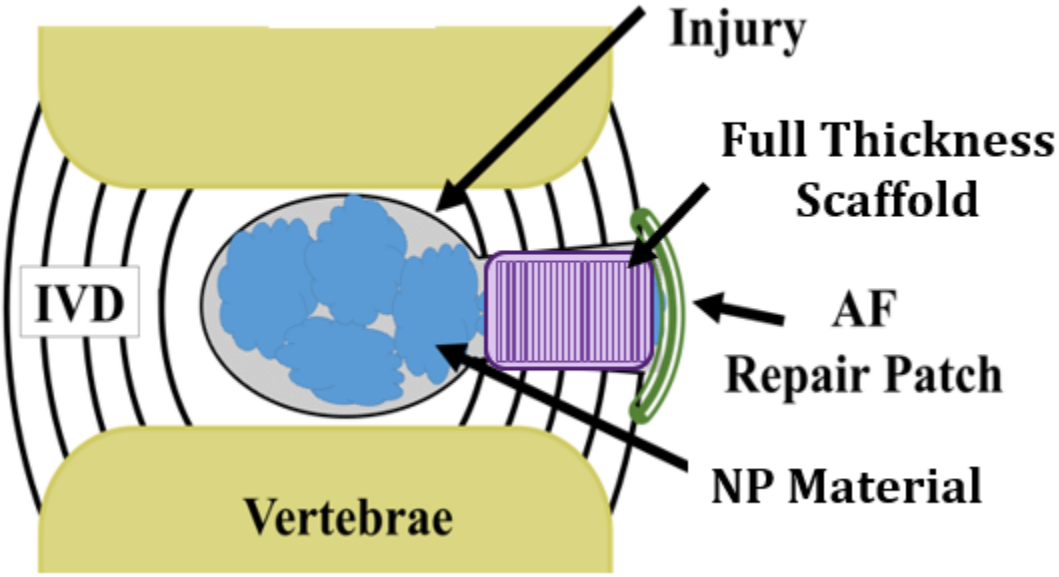

Figure 16: Schematic depicting outer AF closure of an IVD defect using the AFRP as well as the needed full-thickness AF scaffold.

Thus, the objective of this aim was to fabricate a full thickness, multi-laminate annulus fibrosus repair plug scaffold (FT-AFRP). The FT-AFRP was developed beginning with fabrication techniques of the AFRP, involving multiple layers of decellularized porcine pericardium. The FT-AFRP scaffold was intended to work in conjunction with the AFRP as a total AF replacement strategy. The studies performed herein include the trials in extending the AFRP into a full thickness plug, refining the scaffold to a proper size and fiber orientation, adhering layers of pericardium together, the potential inclusion of a GAG

gel between plug layers, developing a repeatable process to manufacture the plugs, and the potential to freeze dry the fabricated scaffolds. Outcome measurements were primarily qualitative involving repeatability and consistency in fabrication methods of the FT-AFRP. Quantitative measurements included size comparisons to potential AF defect sizes.

2.2 Materials and Methods

2.2.1 Specimen Procurement, Dissection, and Treatment

Porcine hearts were obtained within 4 hours of slaughter from a local abattoir. All tissue was put on ice upon procurement. The parietal layer of pericardium was separated from the rest of the heart. Excess fat and connective tissue was manually removed from the pericardium using tweezers and scalpel. The parietal layer of pericardium is fused and inseparable from the fibrous layer which is the outermost layer of the pericardium. The dense, regular connective tissue associated with the fibrous layer of pericardium is comprised of collagen fibers running in parallel directions to one-another. The subsequent decellularization of the pericardium was adapted from methods described by Tedder et al and modified by McGuire and Borem et al.[123,126] Before fabricating scaffolds, pericardium was crosslinked using 6 mM 1-ethyl-3-(3-dimethylaminopropyl)carbodiimide hydrochloride (EDC), 1.2 mM N-hydroxysuccinimide (NHS), 50 mM MES buffer solution. Sheets of pericardium were clamped together and submerged in the crosslinker solution overnight (12 hours).

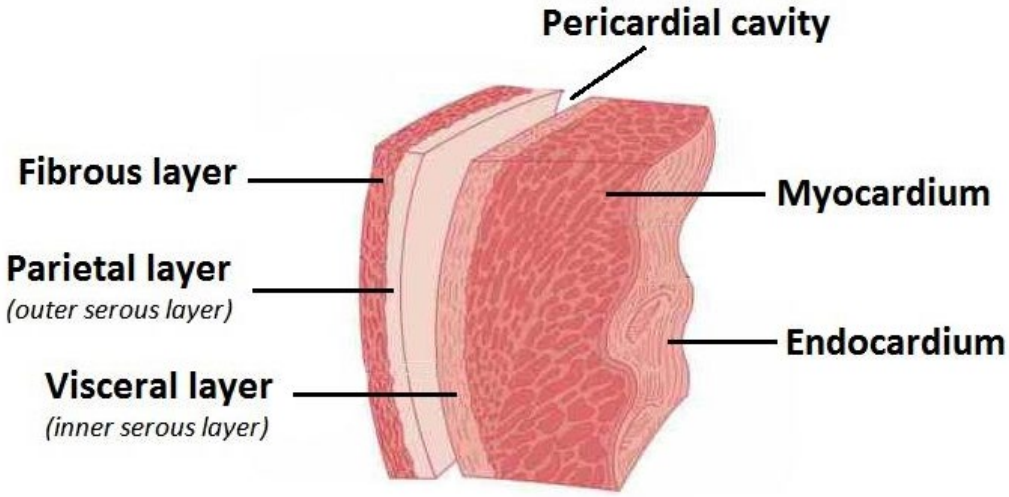

Figure 17: Layers of pericardium.[127]

2.2.2 Initial Strategies for FT-AFRP Fabrication

Initial attempts at fabricating the FT-AFRP were developed from previous methods of AFRP fabrication. The fabrication of AFRPs included placing single layers of pericardium on a light box to identify fiber orientation. Layers were stacked on top of each other at ± 30° to re-create the native angle-ply fiber configuration. Stacked layers were then placed on a water-soluble backing material (solvy-ultra) and sewn together with a sewing machine in squares with dimensions of 8 x 8 mm^2. Patches were then stored in ddH_2O for 4 hours to ensure complete dissolution of backing material. Three-layer patches had a thickness of 0.8 mm. Each subsequent approach described aims to move further towards a full thickness, angle-ply annulus fibrosus repair scaffold.

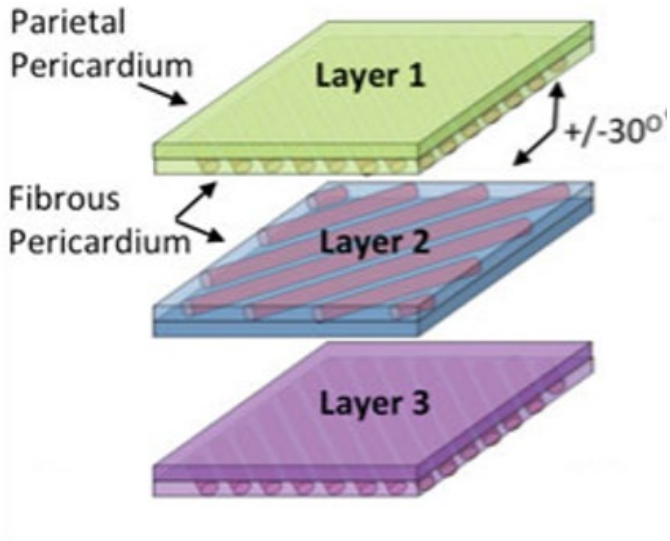

Figure 18: Angle-ply layer structure of three layer AFRP.[123]

Fabrication Approach 1

To begin to extend the multi-layer patch into a full thickness scaffold, trials of stacking 6 layers of pericardium together were done to determine if an increased layer count could be sewn together successfully. The patch dimensions were also increased for this trial to approximately 2 x 2 cm^2. Subsequent trials of sewing together 6 layers of pericardium involved partially drying the tissue by dabbing with a Kimtech wipe before stacking as well as replacing needle and foot components of the sewing machine. Another approach was to initially sew two separate 3-layer patches and then to sew together the two different 3-layer patches.

Fabrication Approach 2

Next, 8-layer patches were fabricated with an extended length, resulting in dimensions of 9 mm x 4.5 mm. These patches were fabricated using the same method as the 3-layer AFRPs. The patches were folded in half, perpendicular to the long axis, to increase total scaffold thickness to 16 layers while maintaining the fiber-oriented architecture. To secure

the patches in their folded orientation, a simple interrupted knot was tied into each the four corners using a 3-0 suture. It was ensured that knots tied into the two corners on the folded side of the patch did not wrap around the rounded edge. This was done to allow the folded edge to be cut with a scalpel once all four corners were secured. Doing this opened the folded-up end and exposed all 16 layers like the other three sides of the patch.

Fabrication Approach 3

In order to obtain a cylindrically shaped plug, the use of a biopsy punch in the fabrication method was trialed. Initially, a reusable metal 6mm biopsy punch was used. This punch was determined to have too large a wall thickness and an insufficient sharpness. Disposable 6mm biopsy punches were used. 6 mm was the chosen size for the punch due to the classification of AF defect sizes switching from the category of large to small at 6 mm in diameter.[128] Four 6-layer patches with dimensions 2 x 2 cm^2 were fabricated using the sewing method described previously. The tissue was marked to note the fiber alignment direction within each patch. The four patches were stacked. The 24 layers of pericardium were punched through with the 6 mm disposable biopsy punch. The stacked plug of pericardium was removed from the biopsy punch using tweezers. Punches of 12 layers of pericardium were also taken and compared for overall height. Height measurements were taken with a ruler.

Fabrication Approach 4

In order to better hold pericardium layers in place while punching, layers of pericardium were stacked onto a needle system. A U-100 insulin needle tip was taped to the lab bench in an upright position. A cutting surface was placed over the needle with a

hole cut out for proper needle clearance. 24 layers of pericardium were individually stacked onto the needle. With the needle inserted through the layers, a plug was punched out using a biopsy punch. Both 6- and 8-mm diameter plugs were fabricated.

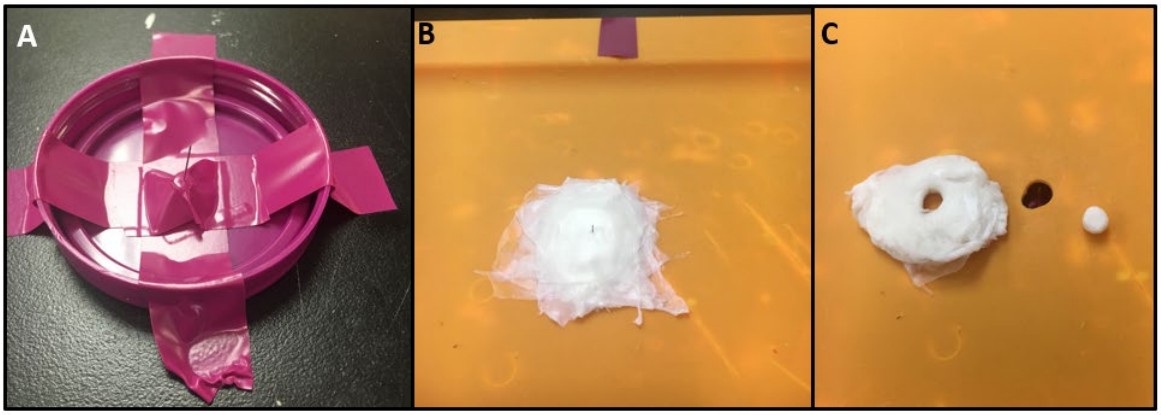

Figure 19: Needle guided AF plug fabrication showing A) needle set-up, B) stacked pericardium layers, and C) plug and excess pericardium after biopsy punching.

2.2.3 Adhering Pericardium Layers

Various techniques were tried to keep the individual layers of pericardium together once punched. These techniques included suturing, a hyaluronic acid (HA) hydrogel, a commercial grade wound sealant, and an alginate gel. The approaches described could be applied to any the scaffold formation approaches described in the previous section. The main goal in adhering layers was to maintain integrity of the layers during implantation.

Adhering Approach 1

Hyaluronic acid (HA)-gel was prepared by reconstituting 1% sodium hyaluronate in PBS. Preliminary attempts to asses the ability of the HA hydrogel to adhere pericardium layers was done by injecting the HA gel between layers of 2 x 2 cm^2 3-layer patches. Patches were clamped shut and submerged in 6mM EDC, 1.2 mM NHS, 50 mM MES crosslinker solution overnight. Qualitative assessments of layer adherence were conducted.

Additional studies were done to directly incorporate the HA hydrogel into the AF repair plug fabrication method. 24-layer stacks of 6 mm diameter punched pericardium were placed into the caps of centrifuge tubes. The diameter of the centrifuge tube cap was 8 mm. HA gel was pipetted into the centrifuge tube to surround the AF scaffold. The centrifuge tube was closed, turned upside down, and the bottom was cut off to create an opening to pipette in crosslinker solution. Scaffolds remained in crosslinker solution overnight. Once the HA gel was solidified, scaffolds were removed from the centrifuge tube caps with forceps and qualitatively assessed for adherence and durability. The plug was squeezed vertically and laterally, and layers were attempted to be pulled apart.

The procedure was repeated with the use of a commercial grade sealant instead of the HA hydrogel. Tisseel (Baxter Int. Deerfield, IL), a fibrin sealant often used for wound closure was used. The provided injection kit was used to surround AF plugs with sealant in centrifuge tube caps. The sealant was allowed to solidify for 30 minutes before removing scaffolds from centrifuge tube caps and assessing.

Adhering Approach 2

A dip coating method was developed to encase the stacked layers of pericardium in an alginate gel. A 2.4% alginic acid sodium salt solution was created. 24-layer plugs were punched using a 6 mm biopsy punch and excess pericardium was removed. The plugs were picked up with forceps, dipped in the alginate solution, and slowly removed to ensure an even coating around the plug. A 102 mM $CaCl_2$ co-factor solution was used to crosslink the alginate into a solidified state. The alginate coated plugs were dropped into the co-factor solution and left for 10 minutes. Plugs were removed and qualitatively analyzed for

alginate coverage, adherence, and durability. Additional trials were done in which plugs were dipped in co-factor solution first and then dropped into the alginate solution.

Adhering Approach 3

24 layers of pericardium were stacked without the use of a fixation needle. A 4-0 braided suture with a curved diamond point needle was used to pierce through all layers of the pericardium. Suture thread was pulled through the layer of pericardium and a simple stop knot was tied to anchor into the bottom layer of pericardium. The thread was subsequently fed through a disposable biopsy punch to ensure the suture was not cut when punching out the pericardium layers. The 6 mm biopsy punch was used to punch through the 24 layers of pericardium. The punched layers were removed from the excess tissue and the suture was unfed from the biopsy punch.

In alignment with the development of stacking pericardium on a needle, further suture-based trials were done with a 4-0 straight needle suture. The 60 mm straight needle was positioned like the insulin needle previously described. 24 layers of pericardium were stacked and punched with a 6 mm biopsy punch. The needle and connected suture were pulled through the pericardium plug. A stop knot was tied at the end of the suture. The suture line was cut so to leave approximately 5 cm of additional suture on the side opposite the stop knot.

Combinational Approach

With multiple approaches having certain desirable qualities of a repeatable and consistent fabrication method, a combinational approach was taken. 24 layers of pericardium were stacked onto a straight needle with suture attached. A plug was punched

out with a 6 mm biopsy punch and removed from the excess pericardium. A stop knot was tied on the bottom side of the plug and 5 cm of excess suture was left on the stop side of the plug. The excess suture was used to dip the plug in alginate solution without handing the scaffold with forceps. The alginate encased plugs were then crosslinking in the co-factor solution previously described for 10 minutes. Suture was removed from the plugs by pulling the stop knot out away from the scaffold with forceps.

2.2.4 Plug Fabrication Jig Design

To create a repeatable and consistent method of FT-AFRP fabrication, a 3-D printed base was created. The base was designed to hold multiple needles in an upright position as well as to aid in securing the pericardium in place while punching. SolidWorks (Dassault Systèmes, Vélizy-Villacoublay, France) computer aided design software was used for drawing models. The system included a base and a clamping plate as seen in **Figure 20**. The base designed had a 35 x 35 mm^2 platform to house the suture needles and mount the pericardium. The clamping plate was designed to fit around the mounted pericardium and platform to provide additional support while biopsy punching the pericardium scaffolds. The SolidWorks part files were used to 3-D print the system with nylon PA12 fiber.

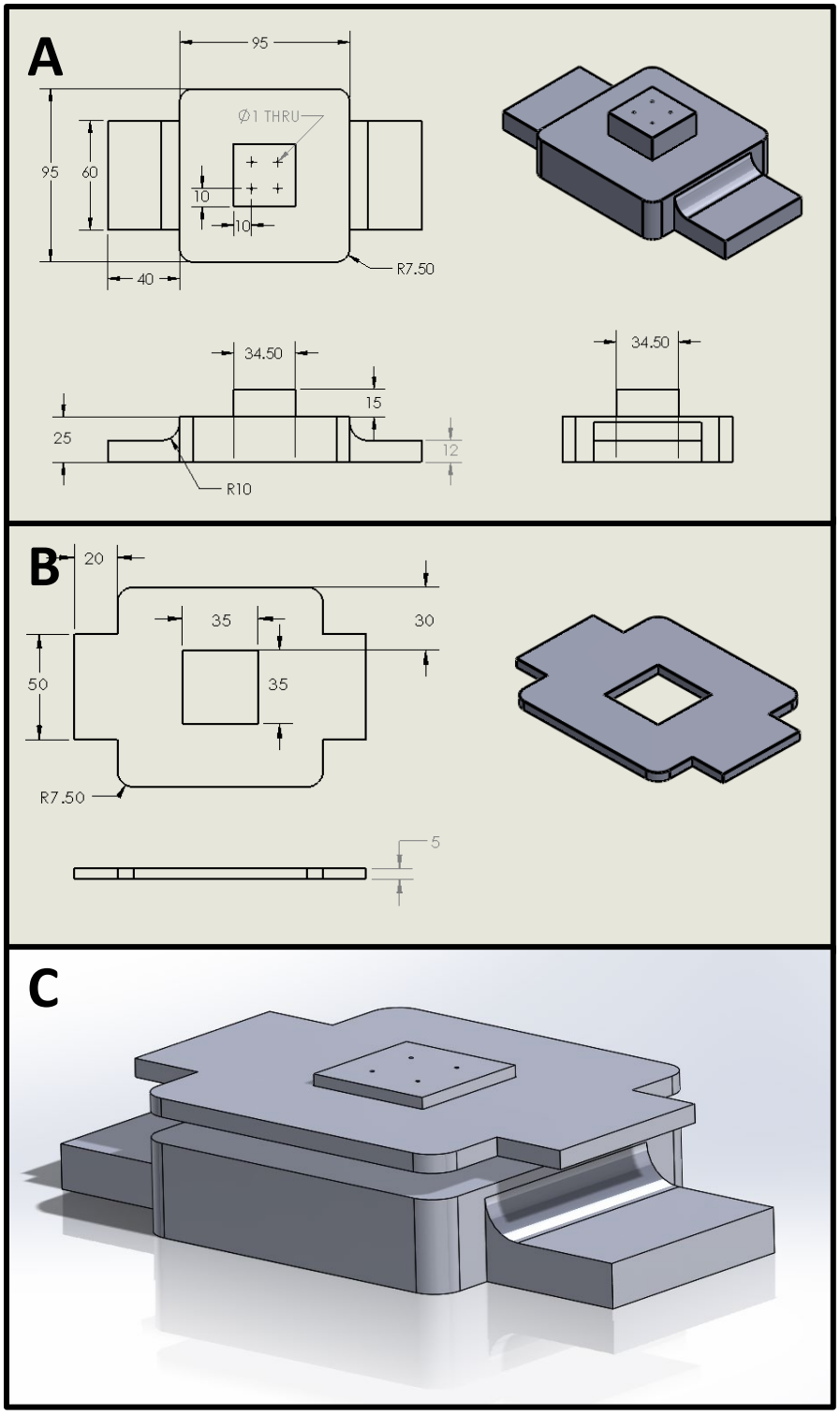

Figure 20: Engineering drawings with dimensions in mm of the A) base and B) clamp plate as well as C) a 3-D rendering of the multi-component system.

To fabricate plugs using the 3-D printed system, four straight needle sutures were first fed through the holes in the base platform. The base was secured to the benchtop using spring clamps. Pericardium layers were cut into squares 40 x 40 mm^2 as to be slightly larger than the mounting platform. A single layer of pericardium was separated. The fiber direction of the pericardium layer was identified by holding up the tissue to a light source. The layer was gently stretched, manually aligned to the center of the mounting platform, and pushed downward to puncture with all four needles. Once down to the base platform, curved forceps were used to flatten out any wrinkles in the individual layer of pericardium.

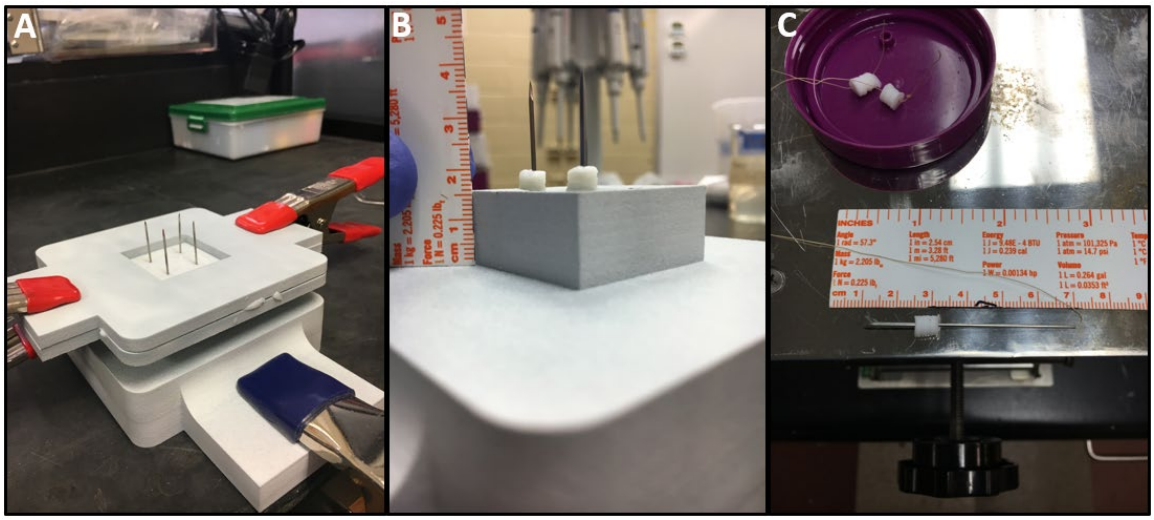

Figure 21: Steps of the final plug fabrication process using the 3-D printed base including A) stacking pericardium layers, B) punching plugs and removing excess tissue, and C) removing needles from base and sliding plugs down onto suture thread.

This process was repeated for each subsequent layer of pericardium until the desired height or layer number was achieved. The 3-D printed clamp plate was then placed over the pericardium and gently pressed down onto the base to wedge the layers of pericardium against the sides of the mounting platform of the base. A 6 mm biopsy punch

was used to punch through all layers of the pericardium. Once all four plugs were punched, the clamp plate and excess pericardium were removed from the system. The straight needles, with stacked pericardium plugs attached, were pulled through the top of the base plate. Plugs were pushed off the needles and onto the suture using forceps. The combinational technique previously described was then applied to secure the plug to the suture and to coat the plug in alginate gel.

2.2.5 Freeze Drying and Rehydration of AF Plugs

Additional studies were done to assess the ability of FT-AFRPs to be freeze dried. The ability of scaffolds to be dried and rehydrated could play an important factor in storage and transportation. While only assessed qualitatively, the ability of FT-AFRPs to return to their pre-dried state after rehydration was under investigation. After fabrication, FT-AFRPs were frozen at -80^{o} C and transferred to a freeze-drying system. A FreeZone 6 Plus (LABCONCO, Kansas City, MO) freeze dryer was used to expose the plugs to a 0.1 mBar and -88^{o} C atmosphere for 12 hours. Plugs were removed from the freeze dryer and qualitatively assessed for structure. A rehydration assessment was done to investigate the freeze-dried FT-AFRP's ability to reabsorb liquid and return to their previous state. Freeze-dried FT-AFRPs were placed in conical tubes and 1.5 mL of 1x Phosphate buffered saline (PBS) solution was added. The FT-AFRPs were left to rehydrate for 24 hours. After rehydration, FT-AFRPs were removed from PBS solution and the pericardium and alginate was compared to its state before freeze drying.

2.3 Results

2.3.1 Specimen Procurement, Dissection, and Treatment

Our group has previously confirmed the decellularization of porcine pericardium through agarose gel electrophoresis, immunohistochemistry, and Nanodrop DNA analysis.[123] These studies demonstrated the complete removal of alpha-Gal, a porcine antigenic epitope, and a DNA content of 96.2 ± 13.4 ng/mg of dry weight tissue; a 95.3% decrease as compared to fresh porcine pericardium.[123] Additionally, the crosslinking treatment of pericardium was found to significantly lower mass loss from collagenase digestion while not significantly altering tensile properties.[124]

2.3.2 Strategies for AF Repair Plug Fabrication

Initial attempts at sewing together 6 layers of pericardium in a similar method to AFRP production was initially unsuccessful. With an increased layer count, pericardium slid out from its flat orientation when attempting to sew. Replacing the needle of the sewing machine and partially drying the pericardium gave improved outcomes. Ultimately, 6- and 8-layer patches were able to be manufactured with practice. The technique of folding patches resulted in a 16-layer thick square with sutures at all four corners. The height of 16 layers was approximately 3.1 mm. The scaffold was essentially an extension of the AFRP with a square shape.

Biopsy punched plugs, without the use of a needle support, produced cylindrical but irregularly shaped plugs as seen in **Figure 22**. 12-and 24 layer plugs measured 3.2 ± 0.1 and 5.8 ± 0.2 tall respectively. The diameter measurements varied slightly due to the inconsistency in layer alignment throughout the plug.

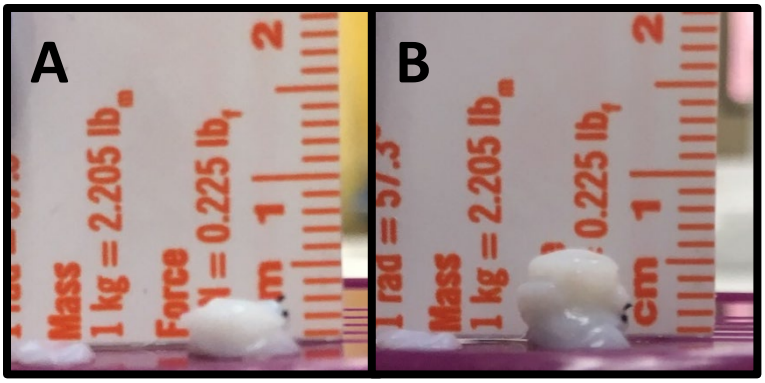

Figure 22: A) 12 and B) 24 stacked layers of pericardium punched with 6 mm biopsy punch.

The insulin needle system used to hold pericardium layers together while punching resulted in more uniformly aligned plugs as seen in **Figure 23**. Plugs punched with 6- and 8-mm biopsy punches measured consistent diameters equivalent to punch diameter. Height measurements average 4.6 ± 0.3 mm across all 6 and 8 mm diameter plugs.

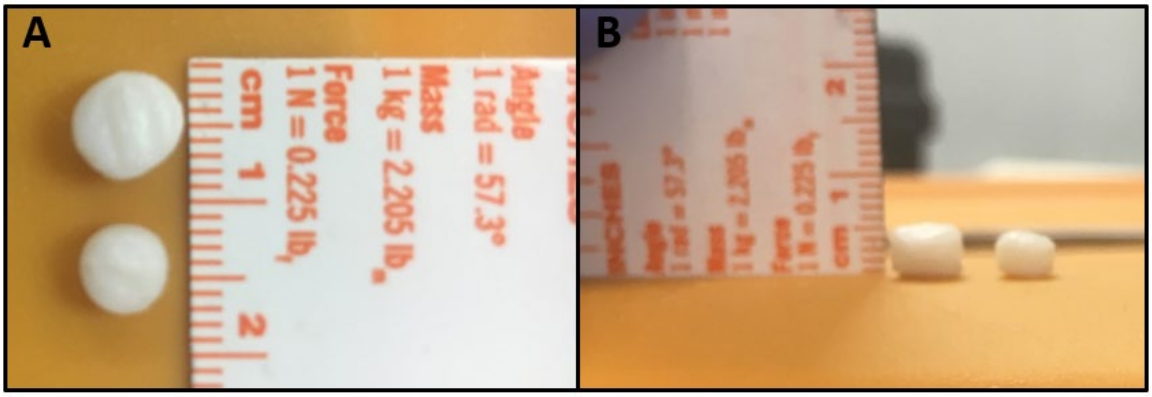

Figure 23: A) top and B) side views of 6- and 8-mm diameter plugs fabricated with insulin needle support.

2.3.3 Adhering Pericardium Layers

The injection of HA gel between enlarged 3-layer patches was unsuccessful through multiple trials. The patches were found to have little to no gel between layers upon removal from crosslinking solution. No adherence was felt between layers upon manual shearing of the layers. Direct incorporation of HA gel around punched AF repair plugs showed better

but still little overall promise. The gel was not able to be properly crosslinked into a rigid coating through the procedure described. Gel that did crosslink on the top of the scaffold was not able to aid in the overall adhering process of the scaffold. Using the commercial grade fibrin sealant, Tisseel, showed better adhering outcomes. The application of the sealant resulted in a non-uniform but rigid layer surrounding the plug as seen in **Figure 17**. The sealant was not able to properly coat the bottom of the plug that was on the bottom of the centrifuge tube. Portions of the sealant also migrated between the layers causing them to split. Sticking to the centrifuge tube also resulted in difficulty of removing the plugs from the cap. Diameter and height measurements averaged 7.0 ± 0.1 and 6.3 ± 0.3 mm respectively, indicating an approximate 0.5 mm thick layer of sealant around the outside of the plug.

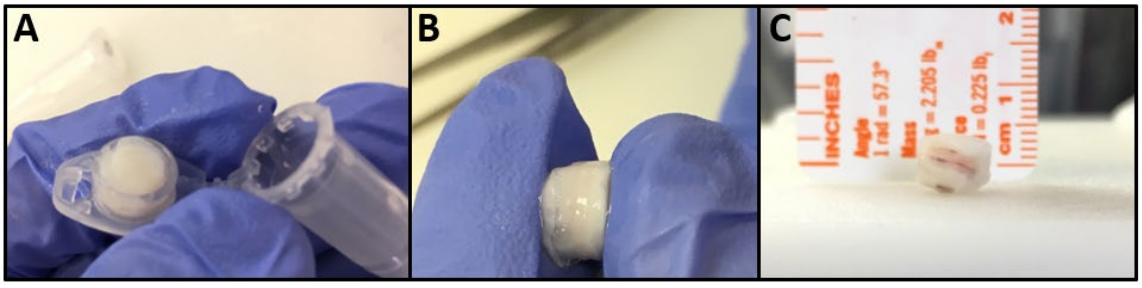

Figure 24: A 24-layer AF repair plug A) before removal from centrifuge tube, B) from a side profile, and C) with inconsistent sealant coverage.

The dip coating method used with the alginate gel resulted in consistent and complete coverage of AF repair plugs, successfully holding all layers together. Inconsistencies in the alginate coating resulted partial blockage of the areas being directly held by the forceps. A slightly rounded top was also consistent throughout plugs on both

the tops and bottoms. Average diameter and height for 24-layer plugs were 6.0 ± 0.2 mm and 5.5 ± 0.1 mm respectively.

The use of suture was able to hold together layers of pericardium. Overall, consistency was more achievable when a straight needle suture was used. Overall heights of 24 layer plugs were smaller than other fabrication methods at 4.2 ± 0.2 mm. A knot was not able to be tied tightly onto the top side of the plug.

The combinational approach of using needle, suture, and an alginate dip coating resulted in the most consistent and robust plugs. A complete alginate coating around all edges of the plug was seen. The alginate encased the plug in a slight oval-like shape with the edges of the plug being relatively flat but the tops and bottoms being rounded. The average height and diameter for these 24-layer plugs was 6.3 ± 0.4 and 7.0 ± 0.1 mm respectively. The largest inconsistencies were seen in the shape and overall height of the rounded edges of alginate on the plugs.

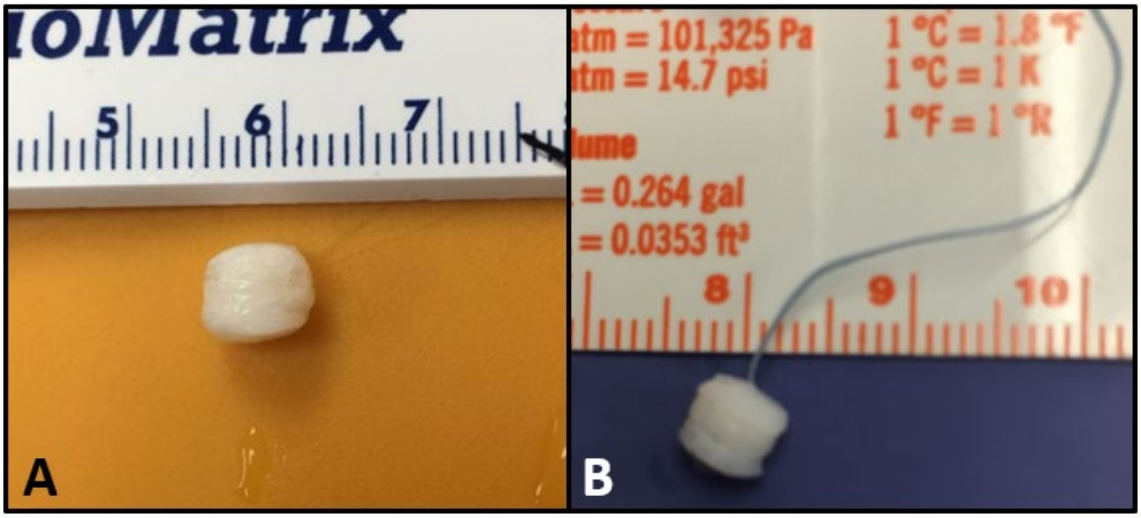

Figure 25: 24-layer plugs fabricated with straight needle, suture, and an alginate dip coat with A) suture removed and B) suture left in the scaffold.

2.3.4 Plug Fabrication Jig Design

The 3-D printed scaffold properly housed the straight needle sutures during fabrication. Additionally, the clamping plate successfully aided in the proper alignment and tension of the pericardium while biopsy punching. The needles and attached suture were easily fed through the base upon completion of plug punching. The resulting plugs were produced in consistent batches of four and were comparable to the plugs using the combinational approach previously described.

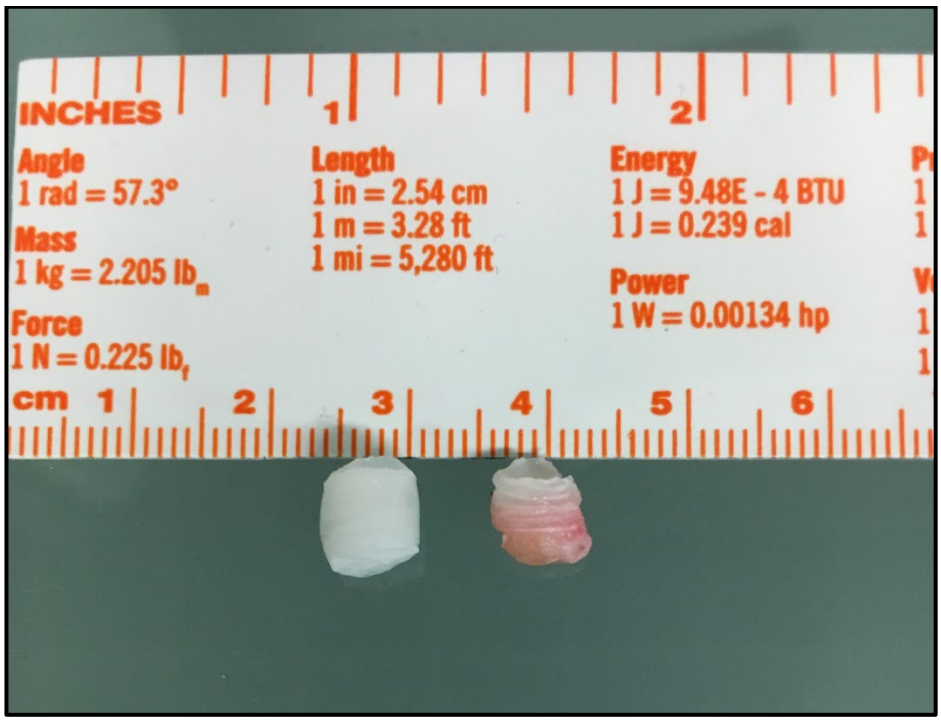

Figure 26: A 30-layer AF repair plug fabricated using the 3-D printed base (left) compared to a 6-mm punch of native bovine AF tissue (right).

2.3.5 Freeze Drying and Rehydration of AF Plugs

The alginate coating appeared to remain intact when plugs were freeze dried. Upon rehydration, plugs regained their original shape with a slight decrease in size. The alginate coating did return and was comparable to its original shape. For samples in which the

alginate coating did not completely surround the plug, individual layers of pericardium flaked off after freeze drying.

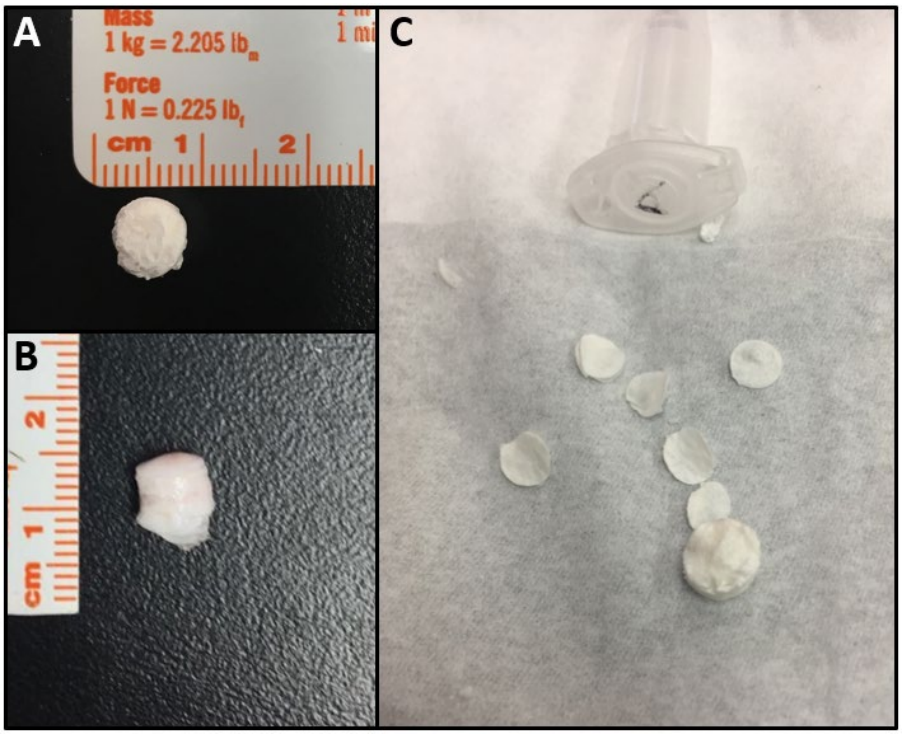

Figure 27: Freeze drying study showing A) top view of a dried plug, B) a 30-layer re-hydrated plug, and C) individual layers of pericardium falling off plug.

2.4 Discussion

2.4.1 AF Repair Plug Fabrication

The concept of the FT-AFRP was based off previous studies done on the AFRP for outer AF closure. Thus, extending the AFRP method of fabrication was an obvious starting point to increase the layer count of the scaffold to achieve a full annular thickness. Sewing of an increased number of layers generally did not work due to slipping of pericardium layers while sewing. That being said, a consistent method of creating 6-layer, large-sized

patches was useful in advancing the overall fabrication technique. Layers of pericardium were sewn into 6-layer squares for the crosslinking process as well as for more efficient stacking for subsequent fabrication techniques. The process of folding over patches and suturing corners was not sufficient as it resulted in square scaffolds and could not be applied for high layer counts of 24. While AF defects can often be irregularly shaped, a cylindrical shape is most applicable to a range of potential defects. Additionally, defects could potentially be shaped or punched to proper size also constituting a cylindrical scaffold. The biopsy punch easily cut through pericardium layers and gave the required cylindrical shape. Continued issues of layer slippage required a mechanical holder of pericardium layers which was implemented in the form of an insulin needle.

Once cylindrical plugs of up to 30 pericardium layers were able to be fabricated consistently, a method to adhere layers together was still needed. While native AF tissue is made up of individual lamellae, they have an innate adherence to each other through overlapping collagen matrix and an interlamellar GAG gel.[14] Previous investigation of the incorporation of a GAG gel between layers AFRPs resulted in improved mechanical properties, specifically, impact resistance.[125] While the incorporation of an HA gel was an attractive strategy due to its re-incorporation of GAGs and potential to adhere layers, the methods used to implement the gel were insufficient. While the use of a GAG gel is certainly a future need for the AF repair plug, the HA gel was not robust enough, even if applied successfully, to hold the plug together. Future research will be conducted to incorporate GAG between layers of the plug, but the gel was not be able to serve as the main adherence method.

The commercial grade sealant, Tisseel, provided a stronger outer layer for the plug. Tisseel is primarily used for wound closure and therefore posses the correct mechanical strength to properly hold the AF repair plug together. Additionally, it has been shown to be biocompatible and has been used for other tissue engineering applications.[129] While the application kit allowed for easy injection of the sealant around the plug, only small amounts were obtainable at a time. The method of injecting into a centrifuge tube cap was insufficient in producing a consistent outer layer around the plug, even when a high-quality sealant was used like Tisseel. With the identified need for a dip coating method paired with expense concerns over fibrin sealant, alginate was identified as an alternative.

Alginate was a readily available alternative that had increased durability compared to HA gel and which could also be obtained in much higher quantities than Tisseel. Alginate hydrogels are commonly used in tissue engineering applications due to their ability to support cell life and tunable mechanical properties.[130] 3-D alginate scaffolds have also produced more relevant gene expression profiles when AF cells are cultured in them as compared to monolayer culturing.[131] These characteristics made alginate an attractive and potentially dynamic outer adhering sealant. The proper amount of alginate gel to allow for dip coating was also easily produced. This technique resulted in the most consistent plugs, especially when the combinational technique which included the straight needle suture was used. The gel casing on the outside of the plug was only intended to hold layers together well enough for potential handling and implantation. This was achieved by the alginate gel. Mechanical and cellular contributions of the alginate to the overall scaffold characteristics was yet to be determined.

The sizing of the AF repair plug was generally targeted to be 6 mm in diameter and 24 layers thick. The diameter was based off AF defect size characterization categories. The height of plugs was not specified to an exact requirement as sizes could vary. General thickness of human lumbar AF is 5-6 mm.[68] All fabrication techniques needed to be tunable to different biopsy punch sizes as well as a variety of total layer numbers. This was achievable by the combination fabrication technique previously described.

2.4.2 Plug Fabrication Jig Design

Streamlining the fabrication process was important as nearly every initial attempt at making FT-AFRPs resulted in a different geometry and overall quality. The 3-D printed base achieved the consistency needed. The ability to make four plugs out of each batch of stacked pericardium greatly improved overall consistency. It also reduced the time needed to create plugs. While initial designs intended to use two clamping plates to hold together all layers of pericardium at once, it was found that stacking layers directly onto the needles one at a time was much easier. One potential issue with the technique was the danger associated with manually forcing biopsy punches directly towards suture needles that were sticking up out of the base. Despite this, future manufacturing implications for scalability could easily be achieved with machine automation of a similar but larger scale process.

2.4.3 Freeze Drying and Rehydration of AF plugs

The ability to freeze dry resulting scaffolds was inconclusive. Qualitatively, plugs that were initially fabricated with a complete alginate coating were able to maintain their structural integrity upon freeze drying and rehydration. This could be an important long-term factor for packaging and shipping implant materials. A common problem was that

plugs did not dry as complete scaffolds, but rather as individual pericardium layers resulting in the flaking reported previously. The continued improvement in consistency and overall alginate coverage could potentially improve freeze drying capability as well.

2.4.4 FT-AFRP Development: Key Takeaways

The research in this section produced a repeatable method to fabricate a full thickness AF scaffold using sheets of fiber-aligned decellularized pericardium, an alginate hydrogel, and a 3-D printed jig. While FT-AFRPs contained a similar ECM and fiber alignment compared to native AF, it was still undetermined whether that translated into appropriate mechanical and cellular behavior. Subsequent sections focus on the characterization of the biomimetic FT-AFRP scaffold to investigate its ability to act as an AF replacement.

CHAPTER THREE

AIM 2

3.1 Introduction and Purpose

Human lumbar IVDs undergo complex compressive loading during activities of daily living. Axial compressive spinal loads imparted on lumbar IVDs generate intradiscal pressures (IDPs) ranging from 0.1-2.3 MPa.[132] These IDPs can fluctuate based on body position and can abruptly increase through activities such as lifting heavy objects, jumping, and valsalva maneuvers. These IDPs are redirected by the NP into radial and circumferential tensile forces on the AF. When abrupt increases in IDPs occur in degenerate IVD, herniations can occur. The damage done to the AF directly through IVDH or subsequently through discectomy or NP replacement procedures requires a viable method of AF repair. This repair must aid in restoring the mechanical interplay between the NP and AF by properly responding to forces redirected from IDPs imparted by the NP. To achieve this, many have focused on creating void filling biomaterials to replace missing AF tissue throughout the full thickness (5-6 mm) of the AF. These scaffolds have widely shown the ability to support cell life but have produced varying results in terms of mechanical mimicry of native AF tissue. Additionally, focus has been placed on developing an outer AF closure device to prevent re-herniation that works in conjunction with full thickness AF scaffolds towards AF repair. Thus, our lab has developed both an outer closure (AFRP) and full thickness (FT-AFRP) scaffold using fiber aligned sheets of decellularized porcine pericardium. The FT-AFRP is the most recent addition to an IVD repair system involving the AFRP as well as a previously developed NP replacement

(ABNP) material. The research herein aims to determine the FT-AFRP's ability to mimic the mechanical properties of native AF tissue and restore spinal kinematics in an IVD repair model.

To compare the FT-AFRP to native AF tissue, confined compression was chosen due to useful outcome parameters such as hydraulic permeability and aggregate compressive modulus as well as well documented data of healthy and degenerated AF tissue. Studies have shown that radially punched samples of human AF tissue possess hydraulic permeability and aggregate compressive modulus values of $2.1 – 5.0 \times 10^{-16}$ m^4/N s and 0.40 – 2.5 MPa respectively.[133]

While mechanical mimicry of the AF repair plug is an important indicator in replicating native AF tissue, the ultimate requirement is the ability to restore overall disc mechanical function. Previous studies have been done using the AFRP and ABNP in a spinal repair model.[125] These studies concluded that the repair system only partially restored spinal kinematics. It was concluded that the repair did prevent re-herniation in the spinal model but that many kinematics parameters may have remain altered due to the migration of NP replacement material into the AF defect region. These studies not only justify the need for a full thickness AF repair scaffold but also warrant follow up studies to identify the FT-AFRP's ability to restore spinal kinematics.

3.2 Materials and Methods

3.2.1 Analysis of FT-AFRPs in Confined Compression

FT-AFRPs were fabricated using decellularized sheets of porcine pericardium. Pericardium was crosslinked as previously described. Test frame and confining chamber

setup required plug dimensions of 5 mm in diameter and 1 – 3 mm in height. FT-AFRPs were fabricated through 12 individual layers of fiber aligned pericardium, a 5 mm biopsy punch, and a dip coating of alginate. The slightly rounded edges on the tops and bottoms of the 12-layer plugs were sheared to be flat using a microtome blade. All samples were maintained in a PBS storage solution containing protease inhibitor at 4°C for up to 3 weeks before testing.

Testing was done in conjunction with Dr. Yongren Wu (Medical University of South Carolina) via Martin Groke. This testing was done on a DMA Q800 test frame (TA Instruments, New Castle, DE) equipped with a 5mm diameter confining chamber, 5 mm diameter impounder, and a porous bottom platen (**Figure 28D)**. Each FT-AFRP (n=6) was loaded into the confining chamber and loaded to an average preload of 0.064 N for height determination. A PBS solution was added to the chamber and samples were then subjected to a strain of 3% of total sample height. Samples equilibrated for 30 minutes at the 3% strain and final static force measured was used as the creep test pre-load force. Samples then underwent a 1-hour creep period in which a ramp force of 120% of the pre-load force was applied and held. Time and strain data was exported to Origin Pro software and fit to a biphasic model modified by Kuo et al. to determine dimensionless variables p and K (**Figure 28C**).[134] Aggregate modulus (H_A) and permeability (k) values were then calculated using the following equations: $p = \frac{P_0}{H_A}$ and $K = \frac{H_A k \pi^2}{h^2}$.

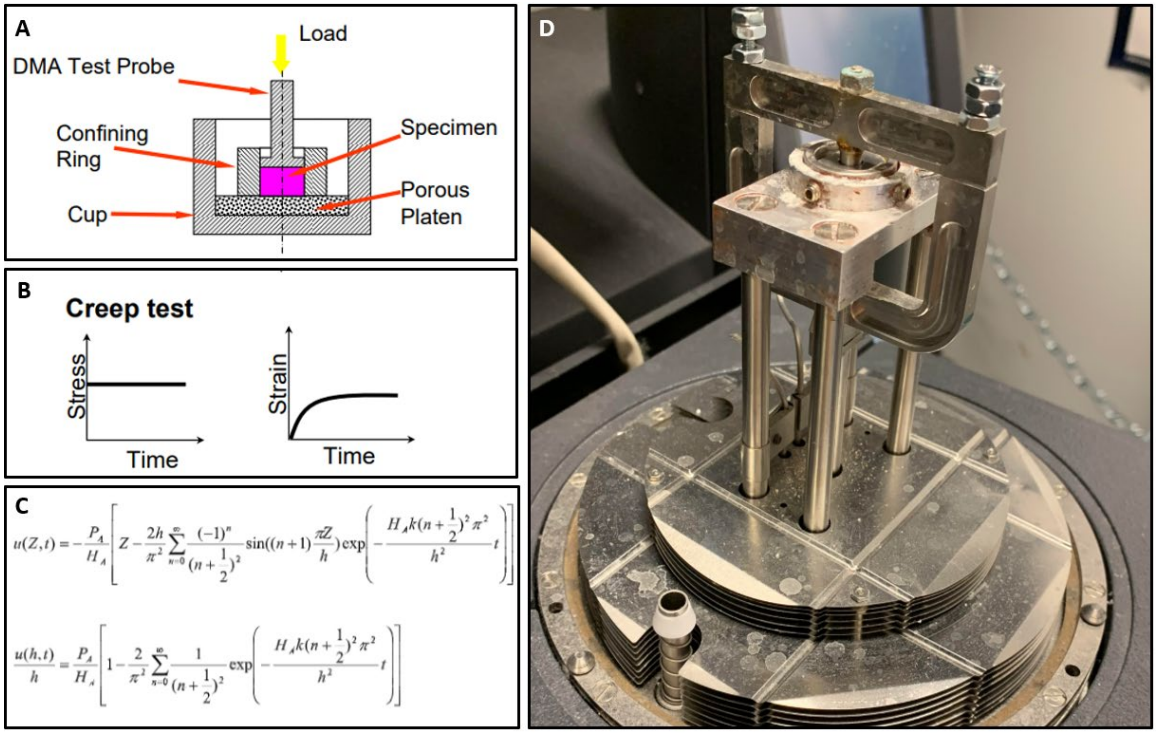

Figure 28: Study design for confined compression of FT-AFRP samples. Images depicting A) confining chamber setup, B) stress and strain representations of creep tests, C) biphasic model used to determine aggregate modulus and permeability values, D) DMA Q800 test frame setup. [134]

Statistical analysis was performed on permeability and aggregate modulus values of FT-AFRPs using Microsoft Excel software. Values were compared to human AF sample values using an unpaired two-tail t-test. Results are represented as mean ± standard error of the mean (SEM). Significance was defined as ($p \leq 0.05$).

3.2.2 Biomechanical Evaluation of IVD Repair Model Axial Kinematics

FT-AFRPs were fabricated using decellularized sheets of porcine pericardium. Pericardium was crosslinked as previously described. Plugs were fabricated through 24 individual layers of fiber aligned pericardium, a 6 mm biopsy punch, and a dip coating of alginate. 3-layer multi-laminate AFRPs were also fabricated from decellularized

pericardium. Compacted and crosslinked NP replacement material (ABNP) was fabricated using a previously developed method.[135] All samples were maintained in a PBS storage solution containing protease inhibitor at 4℃ for up to 2 week before testing.

Bovine caudal tails were obtained from a local grocer, Publix (Clemson, SC). Functional spinal units (FSUs: vertebrae-IVD-vertebrae) were harvested from the top caudal level (cc1-2) of each tail. Excess tissue and ligaments were removed from the vertebral bodies and IVDs via dissection. With posterior elements attached, the vertebral bodies of each FSU were cut to a flat and even edge using a band saw. The FSUs were potted using 3mm steel rods and urethane potting resin. The steel rods were intended to further prevent slippage of FSUs out of the potting material during testing. The IVDs of potted FSUs were wrapped with gauze saturated with PBS, stored in zip-lock bags, and frozen at -80℃. Prior to testing, FSUs were thawed in zip-lock storage bags by submerging in water at ambient temperature for four hours.

FSUs (n=6/group) underwent kinematic testing according to methods previously described by our group with slight modifications.[124] FSUs were tested in the following groups: uninjured, injured, repair using a native bovine AF plug, and repair using the FT-AFRP (**Figure 29A**). To produce an injury, a 6mm biopsy punch was used to remove AF tissue. NP material was then removed through the AF perforation with forceps and a scalpel. Repairs were done by physically compacting ABNP to remove excess fluid, implanting ABNP until the center region of the IVD was filled, implanting either the previously punched out native AF or FT-AFRP, and closure of the annular defect using an AFRP. Attachment of the AFRP consisted of suturing at all four corners and all four edges

of the square patch using 4-0 FiberWire suture. Before each group was tested, FSUs were allowed to equilibrate in PBS solution with protease inhibitor at 4°C for twelve hours. FSUs were repaired prior to swelling for the two repair groups. Testing order for the two different repairs was randomized for each FSU to avoid testing order bias. Wet and dry weights of all removed and implanted material were taken and compared. Dry weights were taken by freeze drying samples before massing.

Testing was done on a Bose ElectroForce model 3220 (TA Instruments) equipped with a 100-lb. load cell and test chamber filled with 1xPBS and protease inhibitor at ambient temperature. Samples were loaded to a mean amplitude level of -0.125 MPa before undergoing a 1-hour creep period at -0.50 MPA (**Figure 29C**). Samples were then returned to the -0.125 MPa amplitude level before undergoing 35 cycles of axial compression and tension at amplitude levels of -0.50 MPa and 0.25 MPa respectively at 0.1 Hz. Samples finally underwent a slow-rate compressive ramp at 1 N/s from the -0.125 mean amplitude level to -0.50 MPa (**Figure 29B**). Tensile and compressive stiffness was determined using a linear fit of the loading force-displacement curve from 60-100% of peak stress the 35^{th} cycle. Axial range of motion was determined from the total peak-to-peak displacement of the IVD in the 35^{th} cycle. The constant-rate slow-ramp compression stiffness was determined using a linear fit of the load displacement response. A custom MATLAB code was written to properly extract the 35^{th} cycle and determine all previously described parameters. The program was also used to graph the 35^{th} cycle and slow ramp curves with colors coordinating to the 60-100% loading regions (**Figure 29D**). A second MATLAB code was written to determine creep and step displacement values from creep data. The

step displacement was defined as the IVD displacement when loading from -0.125 MPa to -0.50 MPa. Creep displacement was defined as the displacement of the IVD during the 1-hour dwell at -0.50 MPa. A four parameter rheological equation: $\frac{d(t)}{L_o} = \frac{1}{\Psi_1}\left(1 - e^{\frac{-t\Psi_1}{\eta_1}}\right) + \frac{1}{\Psi_2}\left(1 - e^{\frac{-t\Psi_2}{\eta_2}}\right)$ was fit to creep data using GraphPad Prism 7 software. This fit determined elastic (Ψ) and viscous (η) damping coefficients for the short term (η_1 and Ψ_1) and long-term (η_2 and Ψ_2) response of the IVD.

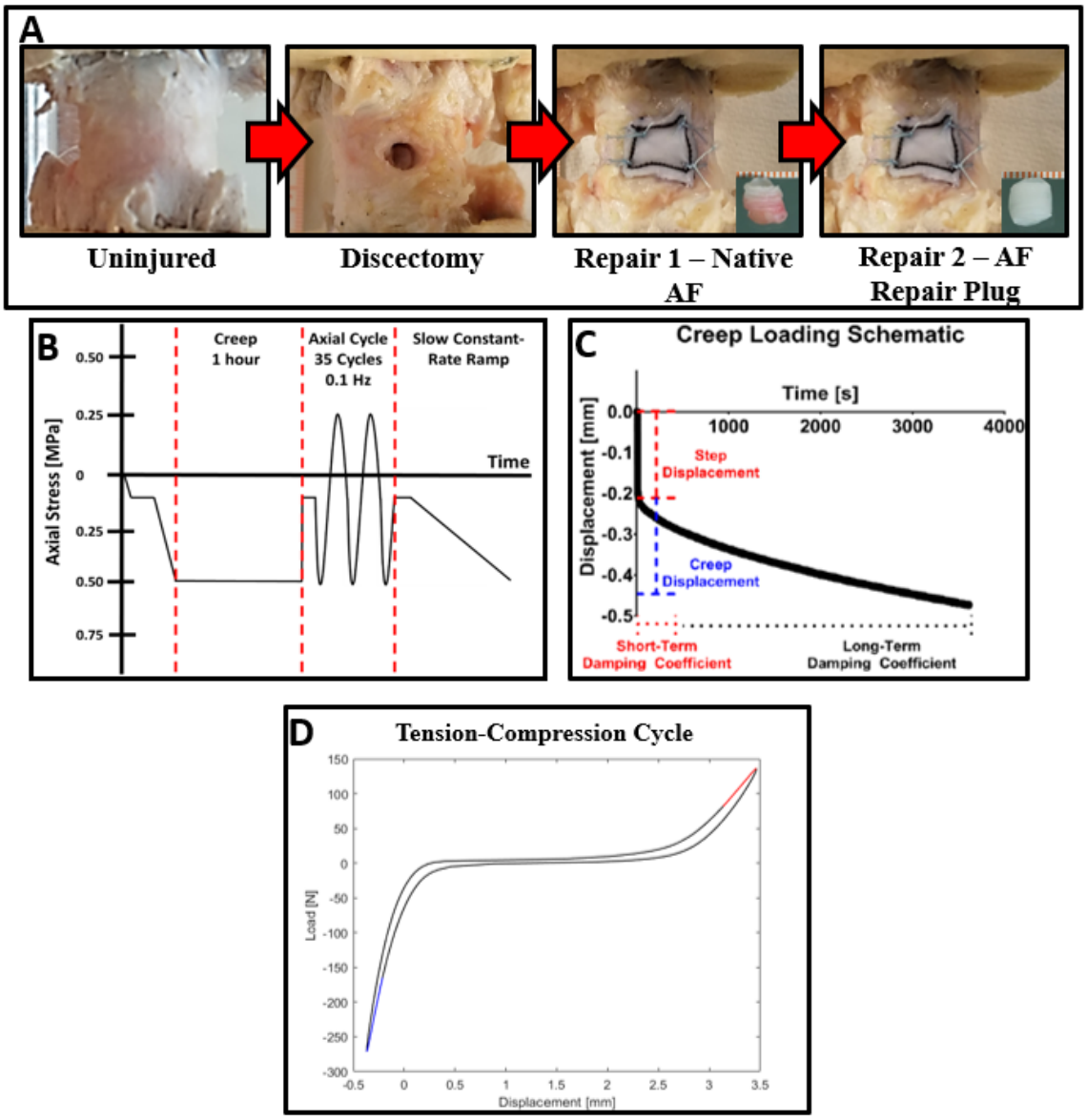

Figure 29: Study design for *in situ* kinematic testing of bovine IVD FSUs using annulus fibrosus repair plugs. A) Representative images of the testing progress of each FSU (the order of repair 1 and repair 2 was randomized). B) Loading scheme for FSU testing depicting creep loading, axial cyclic tension compression loading, and constant-rate slow ramp loading. C) Representative graph of creep loading and displacement parameters. D) Representative image of a 35th tension-compression cycle isolated using MATLAB code with red and blue lines depicting the region of 60-100% of peak amplitude.[68]

Statistical analysis was performed on raw data using GraphPad Prism 7 software. Results are represented as mean ± standard error of the mean (SEM). Significance was defined as ($p \leq 0.05$). Tissue weights were evaluated using a paired t-test. Kinematic data were evaluated using a one-way repeated measures ANOVA.

3.3 Results

3.3.1 Analysis of AF Repair Scaffold and Human AF in Confined Compression

FT-AFRP samples measured an average height of 2.10 ± 0.21 mm. Aggregate modulus and permeability values for FT-AFRP samples averaged 141.52 ± 17.59 kPa and 756.28 ± 219.51 $\times 10^{-16}$ m^4/N s, respectively. These values differed significantly from human AF samples as seen in **Figure 30**.

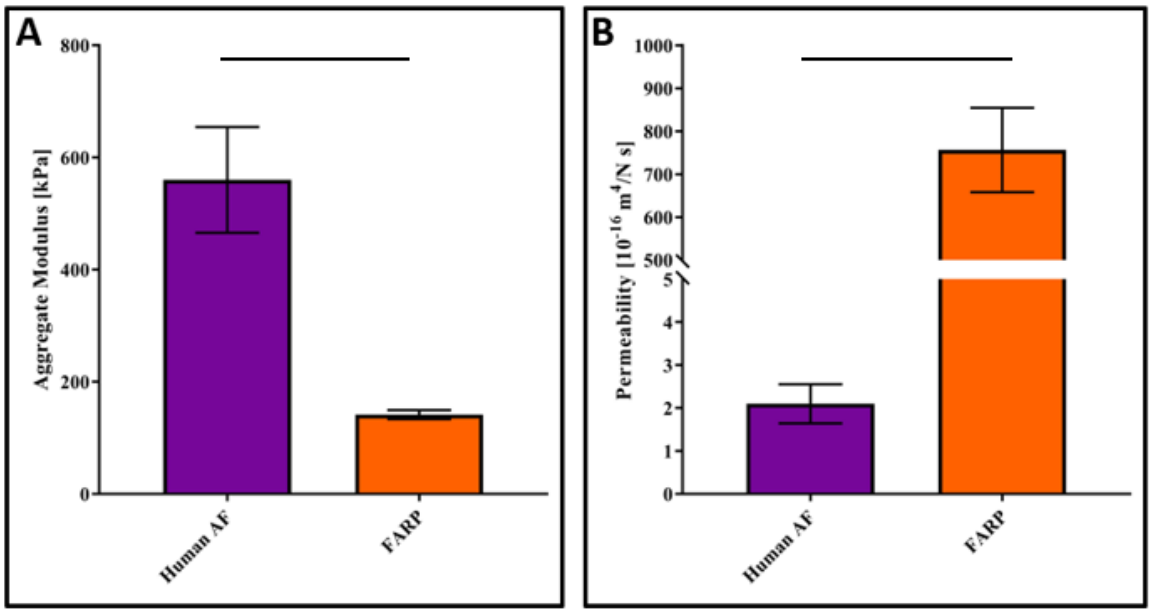

Figure 30: Results of FT-AFRP in confined compression and compared to human AF values for A) aggregate modulus and B) permeability. Solid lines connecting groups indicates significant different ($p<0.05$).

3.3.2 Biomechanical Evaluation of Functional Spinal Unit Axial Kinematics

An average of 109.67 ± 1.14 mg dry weight of tissue was removed from each IVD for the injury group. This included both NP and AF tissue. Average total material re-implanted for repair with native and repair with FT-AFRP were 85.10 ± 1.26 and 69.33 ± 0.62 mg dry weight respectively (**Figure 31**). While amount of material re-implanted was significantly lower than removed material for both repair groups, there was no significant difference between the two repair groups.

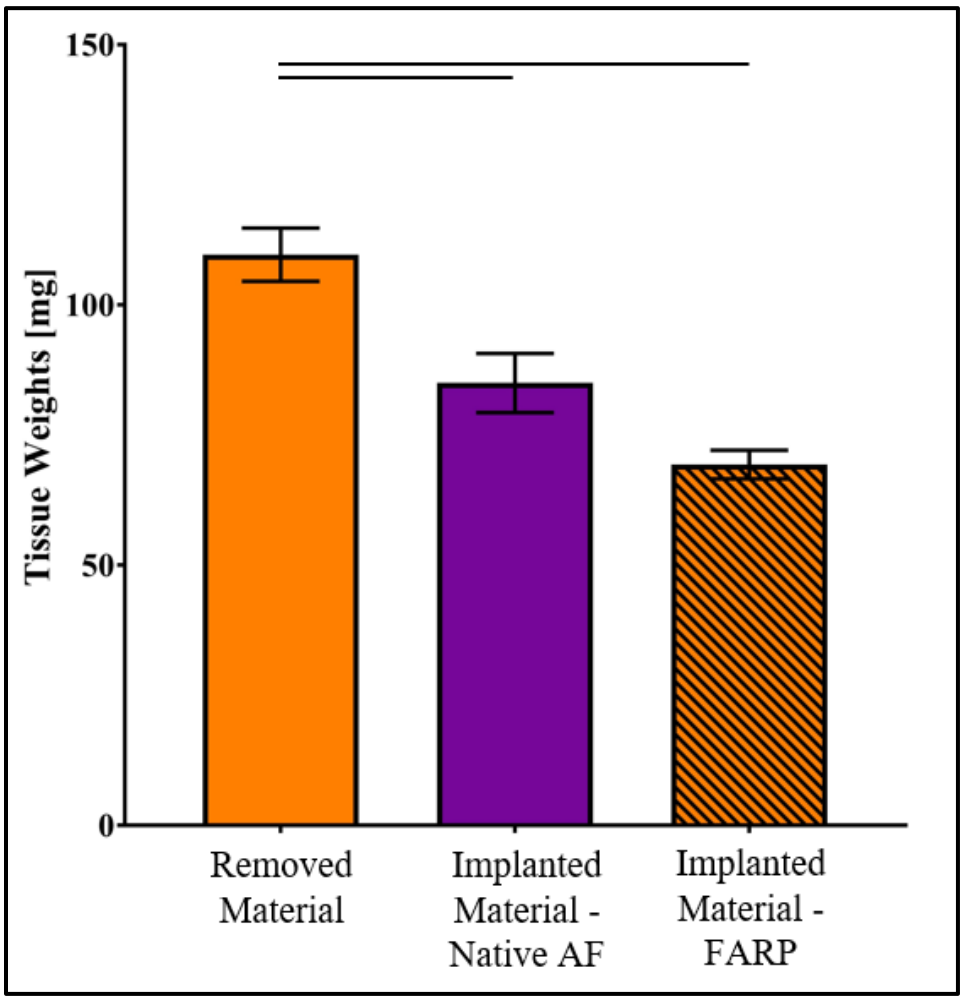

Figure 31: Average amounts of removed and re-implanted material. Solid lines connecting groups indicates significant different ($p<0.05$).

Axial cyclic kinematic testing of FSUs with a discectomy defect significantly altered compressive stiffness, slow-ramp compressive stiffness, tensile stiffness, and axial range of motion values compared to uninjured controls. Repair with either the native plug or AF repair plug further altered tensile stiffness (Native AF: 130.25 ± 3.80, Repair Plug: 131.84 ± 7.31 N/mm) and axial range of motion values (Native AF: 4.20 ± 0.24, Repair Plug: 4.22 ± 0.22 mm) compared to uninjured control and injury groups (**Figure 32C&D**). While still significantly altered, native AF and repair plug values began to return to control values for compressive stiffness (Native AF: 626.97 ± 34.75, Repair Plug: 609.16 ± 36.62 N/mm) and slow-ramp compressive stiffness (Native AF: 431.62 ± 17.14, Repair Plug: 419.40 ± 16.04 N/mm)(**Figure 32A&B**). There were no significant differences seen between repair with native AF and the repair plug.

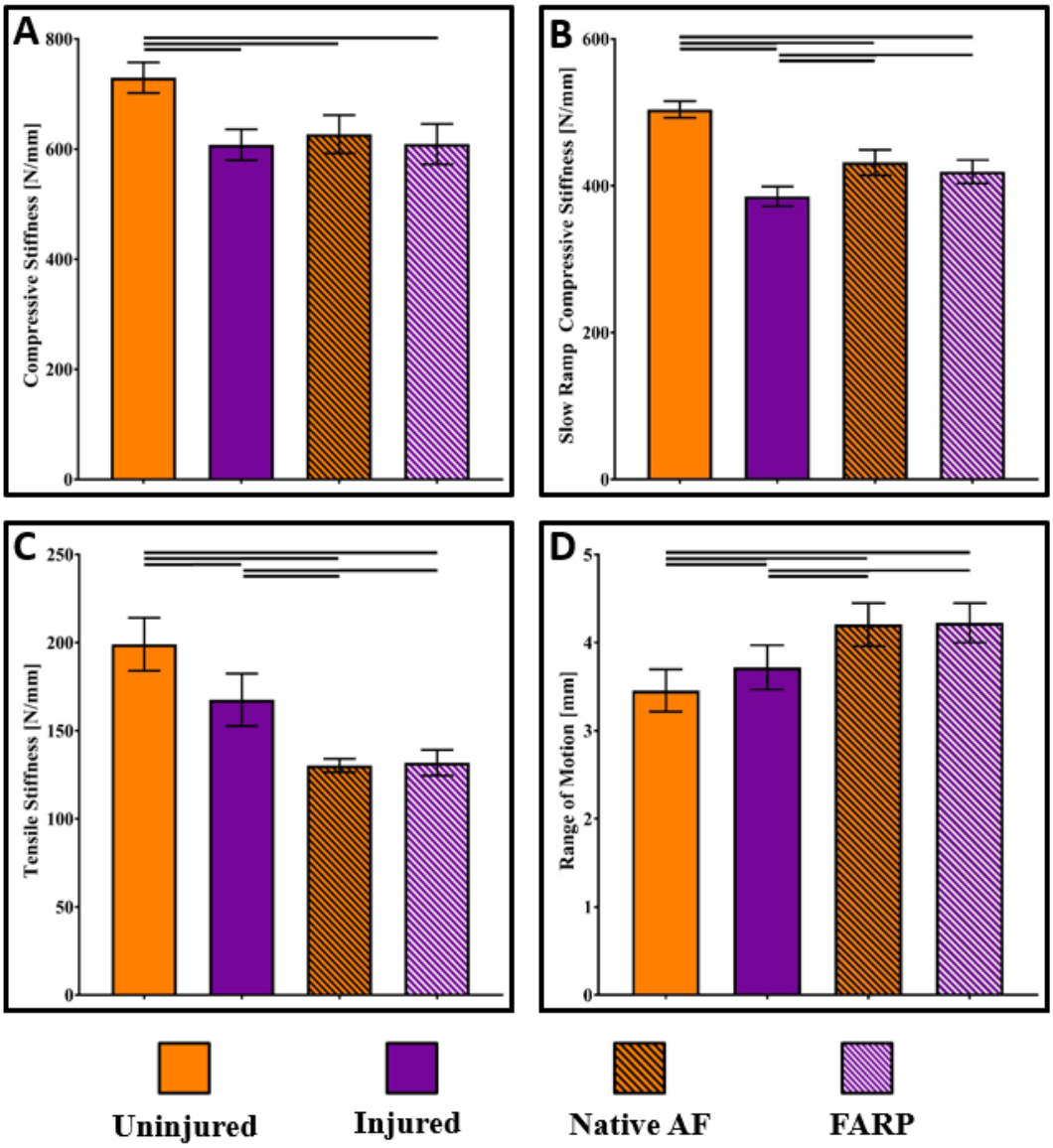

Figure 32: Axial cyclic tension compression kinematic testing results of bovine IVD FSUs. Graphs of A) compressive stiffness, B) slow-ramp compressive stiffness, C) tensile stiffness, D) axial range of motion. Solid lines connecting groups indicates significant different ($p<0.05$).

Creep loading of FSUs with a discectomy injury did not significantly alter step displacement or short-term viscous, long-term elastic, or long-term viscous damping coefficients compared to the uninjured control group (**Figure 33B&D-F**). Parameters were significantly altered through injury and remained altered after either repair group for creep

displacement and short-term elastic damping coefficient compared to the control group (**Figure 33A&C**). While not initially altered through injury, the short-term viscous damping coefficient for FT-AFRP repair was not significantly different from the control group while Native AF repair was significantly different (Native AF: 4170.50 ± 595.41N/mm, p=0.026, FT-AFRP: 5422.17 ± 835.32 N/mm, p=0.376) (**Figure 33D**). Although still significantly altered compared to uninjured controls, FT-AFRP repair was closer to maintaining or restoring parameters to control levels than native AF repair for step displacement (Native AF: 0.52 ± 0.03 mm, p=0.003, FT-AFRP: 0.46 ± 0.03 mm, p=0.047) and short-term elastic damping coefficient (Native AF: 308.41 ± 21.00 mm, p=0.003, FT-AFRP: 332.87 ± 18.88 N/mm, p=0.010) (**Figure 33B&C**).

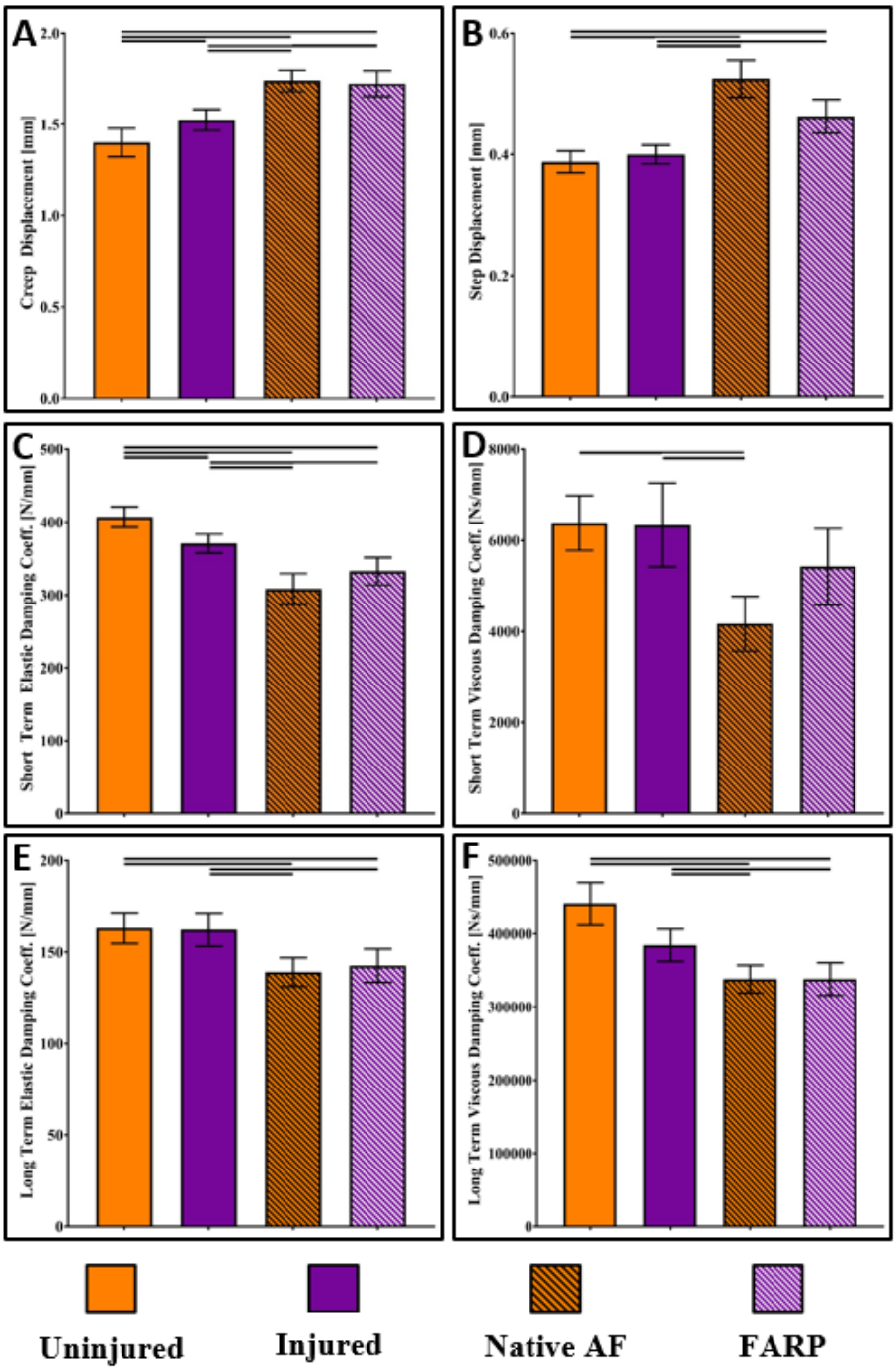

Figure 33: Creep kinematic testing results of bovine IVD FSUs. Graphs of A) creep displacement, B) step displacement, C) short-term elastic damaging coefficient, D) short-term viscous damaging coefficient, E) long-term elastic damaging coefficient, E) long-term viscous damaging coefficient. Solid lines connecting groups indicates significant different ($p<0.05$).

3.4 Discussion

3.4.1 Confined Compression

The annulus fibrosus is made up of 15-25 fiber-aligned concentric lamellae rich in collagen type I. These fibers play a crucial role in the strength of healthy AF tissue to support the hoop stresses brought on from NP force distribution. The FT-AFRP was constructed to mimic the ECM components and fiber orientation of native AF. Therefore, it is essential to understand the ability of the FT-AFRP to also mimic the mechanical properties of native AF tissue. The confined compression studies herein demonstrated that the FT-AFRP and native human AF tissue have significantly different but comparable aggregate moduli and a severely different permeability. While the fiber orientation of the AF may play an important role in tensile properties, the replication of the alignment with the FT-AFRP may not be enough to completely replicate compressive properties of native tissue. While the collagen content and fiber alignment are similar between pericardium and native AF lamellae, there are various components missing from the FT-AFRP that could also contribute to compressive properties. The lamellae in native AF are connected by collagen cross-fibers as well as a GAG- and elastin-rich gel. Thus, the inclusion of an adhering GAG gel between layers could further improve similarities. The GAG gel between layers may play an even more important role in correcting the permeability values of FT-AFRPs.

The permeability of the AF contributes to the ability of fluid to flow through the tissue, ultimately dictating its mechanical response. The mechanical behavior of the IVD is often described as a product of the biphasic properties of each of its tissue components;

that is, the elastic, permeability, and swelling properties of the AF and NP.[136] Measuring the associated biphasic parameters is an important benchmark in tissue engineering to better model the AFs mechanical behavior and fluid transport. The higher permeability value associated with the FT-AFRP compared to human AF may be advantageous for increased nutrient transport throughout the generally avascular tissue but could ultimately affect the mechanical response negatively. Lowering the permeability value further could be achieved and potentially fine-tuned by the previously mentioned GAG gel. Additionally, cell seeding and subsequent tissue remodeling could play a role in the mechanical properties of the FT-AFRP.

While the permeability and aggregate modulus values of the FT-AFRP failed to replicate that of native tissue in this study, other reported values in the literature have varied significantly as seen in **Table 2**. The FT-AFRPs aggregate modulus falls within the range of values reported in the literature, but its permeability value was not. Studies using confined compression and the biphasic model have widely been accepted as sufficient in modeling the AF, but procedural differences produce significantly different results.[136] Despite this, the results herein are compared to human AF tested under the same conditions as FT-AFRPs warranting future adjustment of modulus and permeability values.

Table 2: Reported biphasic parameters of native AF tissue from various groups as reported by Cortes et al.[136]

Parameter	Native AF Value
Aggregate Modulus (H_A) [kPa]	380
	116
	560
	29.9
	5000-7000
Permeability (k) [m^4/Ns]	2.4
	130
	19.2
	2.1

3.4.2 Kinematics

The main function of the IVD is to allow for adequate stability and flexibility in the spine. This is achieved through a dynamic interplay between healthy AF and NP tissue contributing to normal spinal kinematics. One key kinematic parameter used to define spinal motion is total range of motion of the spinal segment. Normal values for range of motion for healthy lumbar spine segments in flexion, extension, and lateral bending are 7.6º, 3.8º, and 6.6º respectively.[137] These values change under pathologic discogenic conditions like IVDD and IVDH.[138] An additional consideration for overall IVD function is the ability to bear load. Human Lumbar IVDs can experience axial compressive loads of up to 1200N during daily activity and up to 2350 N during overly strenuous activities.[139] Therefore, it is essential to understand the ability of the FT-AFRP to contribute to restoring normal spinal segment kinematics under similar conditions.

The FT-AFRP showed little success in restoring parameters such as tensile stiffness, compressive stiffness and range of motion in a bovine FSU repair model. Range of motion values continued to increase, even after implantation of repair materials, potentially pointing towards tissue fatigue after multiple sample runs. The same can potentially be said about tensile stiffness values which are unlikely to be restored without complete integration between implanted repair scaffolds and surrounding native tissue. A method to directly re-incorporate the FT-AFRP with native tissue may aid in reversing these altered parameters. Compressive stiffness values remained significantly altered after repair with both native AF and FT-AFRPs but began to rise back up to control values. Compressive forces imparted on the IVD are primarily borne by the NP and secondly supported by the AF. While the altered compressive stiffness parameters could be caused by an inadequate NP replacement material, an equally important aspect is the ability of the FT-AFRP to keep NP replacement in the center of the IVD. Removal of tissue after testing revealed that NP material still migrated into the AF region even with an AF replacement. This further points to the need for mechanical integration of the FT-AFRP with surrounding tissue to provide a more sufficient annular seal, and ultimately, further improved compressive, tensile, and range of motion properties. Furthermore, an average of approximately 70% of dry weight of material removed from injury groups was re-implanted in repair groups. While this number is higher than what has been previously seen by our group and could be caused by density differences, a more efficient packing method could result in more material contributing to IDP restoration and ultimately restored parameters.

Creep response of the IVD is generally associated with the NP in the short-term and with the AF in the long-term.[140] This was partially supported by the study herein. Both long- and short-term model parameters were altered through induced injury but a limited ability to restore these altered parameters was seen for either repair group. The short-term viscous damping coefficient was not altered through injury or FT-AFRP repair but did show significant differences with native AF repair. Additionally, the short-term elastic damping coefficient remained altered but was closer to uninjured control values with the FT-AFRP repair compared to native AF repair. This illustrates that the FT-AFRP is aiding in keeping NP material in the center of the disc better than the native AF plug replacement, allowing the NP to more properly dictate the short-term response. Despite this, significant changes in long-term coefficients remained following repair with either scaffold. The hoop stresses associated with the load bearing of healthy AF tissue may be the missing component in the void filling FT-AFRP. Even if proper retention of NP material to the center of the disc were achieved, long-term kinematic parameters would potentially remain altered unless the proper tension was restored throughout the AF through re-integration with adjacent tissue. Our group is currently working on a suture technique to secure AF repair tissue to adjacent native tissue.

Different patterns in parameter restoration were seen between this study and previous kinematic studies done by our group. These discrepancies may be due to the inclusion of a swelling period between each testing group. Allowing IVD tissue to re-swell could change the defect volume, shape, and subsequent repair. Additionally, studies herein were adapted from previous procedures from our group but optimized to be run entirely on

one test frame. This also could have contributed to differences between this and previous kinematic repair studies using bovine FSUs. Overall, with few significant differences between native AF plug and FT-AFRP repairs, it can be said that the FT-AFRP scaffold itself can mimic native AF tissue in a repair model, but that a space filling AF scaffold may not be sufficient in restoring IVD function without proper stabilization to adjacent tissue.

CHAPTER FOUR

AIM 3

4.1 Introduction and Purpose

The need for regenerative strategies has been identified for IVD, and more specifically, AF repair due to a low intrinsic healing capacity. Regenerative strategies aid in slowing the degenerative process of the IVD and are often achieved through cell and gene-based therapies. Cell based therapies have shown moderate clinical success but need a competent scaffold to support long term proliferation and promote proper differentiation in the case of stem cell implantation.[62] Additionally, it has been shown that implanted cells alone do not have the ability to produce adequate amounts of GAG and aggrecan needed to restore AF tissue.[106] These limitations warrant a scaffold that supports cell life and differentiation but also mimics native tissue for mechanical restoration and potential long-term integration with surrounding tissue. The need for a cell-based therapy and a competent scaffold warrants the investigation of how the two items interact.

Native cells of the outer AF are elongated and fibroblast-like. Inner AF regions transition to a mixed cell morphology with an increased amount of rounded, chondrocyte-like cells closest to the NP.[23] The elongated cells of the AF align their cell processes along the fibers of each lamellae, functioning to produce the highly organized collagenous matrix.[23] Considering this, a tissue engineered scaffold that mimics the angle-ply architecture of native AF must also provide the correct cues to produce similar cell alignment. Additionally, the scaffold must provide adequate support for cell life. To

achieve these goals, the FT-AFRP was engineered. The studies herein aim to determine the FT-AFRP's influence on cell alignment and viability.

Difficulties in obtaining healthy and autologous AF cells has shifted focus to the use of stem cells with hopes of differentiation into relevant cell types. In either case of AF cell or stem cell implantation, a fibroblast-like elongated cell type is desirable to mimic native AF cells. The studies herein use cells isolated from bovine AF tissue. While this cell type may not be viable in clinical applications due to immunogenic complications, it provides a meaningful representation of how autologous human AF cells or properly differentiated stem cells may act upon implantation into FT-AFRPs.

As described previously and shown in **Figure 17**, the fibrous pericardium used for FT-AFRP production is attached to a layer of parietal pericardium. Removing the parietal layer results in only fibrous tissue and acts as a means to expose the individual collagen fibers. In order to allow interaction between cells and fibers, cells were seeded on the fiber-exposed side of pericardium.

4.2 Materials and Methods

4.2.1 Bovine AF Primary Cell Isolation and Treatment

Primary bovine AF cells (bAFCs) between passage 4 and 6 (P4-P6) were used for all studies. Cells were previously isolated from fresh bovine caudal IVDs, passaged 2 times, and frozen in liquid nitrogen. Before each study, cells were thawed and expanded between P4 and P6. Cell culture media (CCM) was composed of 88% Dulbecco's Modified Eagles Medium (DMEM), 10% Fetal Bovine Serum (FBS), 1% antibiotic/antimycotic (ab/am) solution, and 1% 200mM L-glutamine.

4.2.2 Investigation of bAFC Cell Alignment on Decellularized Pericardium

Sheets of porcine pericardium were decellularized and crosslinked as previously described. Pericardium samples were cut to squares approximately 2 x 2 cm^2. To ensure cells were seeded on the fiber exposed side of pericardium, samples were analyzed using bright field microscopy and a polarizing light filter. Samples were subsequently marked with a tissue pen to indicating the fiber exposed side. All samples underwent a sterilization procedure including a 2-hour submersion in pH neutral 0.1% peracetic acid and three subsequent washed in sterile PBS. Sterile pericardium scaffolds were then neutralized overnight in a 50% DMEM and 50% FBS.

Samples (n=4/timepoint) were placed in an untreated 12-well plate. bAFCs were counted, suspended in CCM, and diluted to a concentration of 1,000,000 cells/mL. 200,000 cells were seeded dropwise onto each sample of pericardium. Seeded samples were placed in an incubator at 37°C and 5% CO_2 for two hours to allow cells to adhere to scaffolds. After 2 hours, 2 mL of CCM was added to each well and samples were placed back in the incubator.

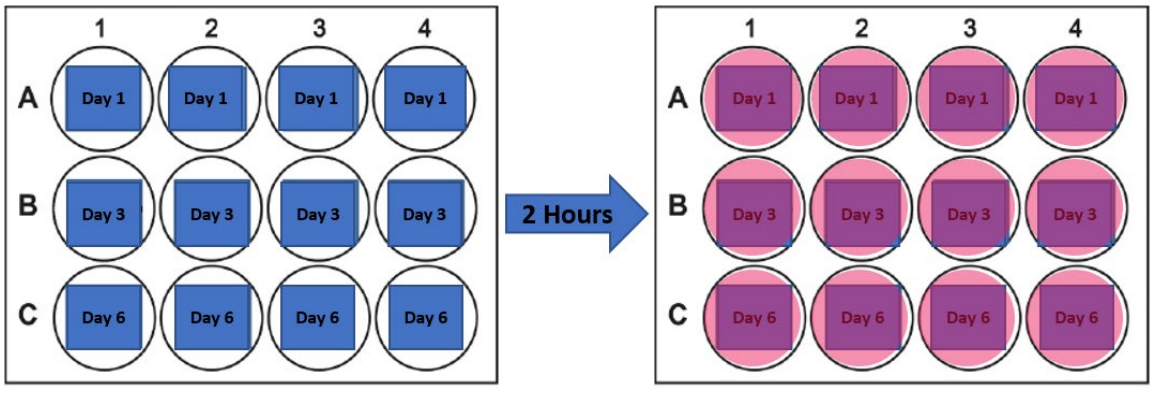

Figure 34: Overview of cell alignment study of bAFCs on decellularized pericardium. Figure depicting samples (n=4/timepoint) after initial cell seeding (left) and with CCM added after a 2-hour adherence period (right).

Samples were cultured to 1, 3, and 6 days. CCM was changed on days 1 and 3. At each timepoint, samples (n=4) were removed from CCM, rinsed twice by dipping in 1x PBS, placed in a new well plate, and stained with a solution of 10μM Calcein AM and 2μM Ethidium homdimer-III (EthD-III). Calcein AM permeates through intact cell membranes and stains the cytoplasm of viable cells. EthD-III cannot penetrate intact cell membranes and therefore stains cytoplasm of non-viable cells after the cell membrane is damaged. Samples were left in the staining solution for 30-45 minutes, shielded from light at room temperature. Axio Zeiss Vert. A1 camera microscopy with Axio Vision SE64 Rel 4.9.1 software was used for imaging all samples. First, live and dead cells were imaged using fluorescence microscopy. Live cells appeared green under blue fluorescent light. Dead cells appeared red under green fluorescent light. Without moving samples, the microscope was switched to brightfield microscopy and the polarizing filter was added to image the fiber orientation of samples.

Viability was assessed by manually counting the number of live and dead cells across various samples for each time point. Images taken at 200x total magnification were used for all viability counts. Viability was taken as $\%\, Viability = \frac{Live\ Cells}{Total\ Cells} \times 100$. Statistical analysis was performed to compare viability across various timepoint. Graphpad Prism 7 software was used to perform a one-way ANOVA with significance denoted as ($p<0.05$).

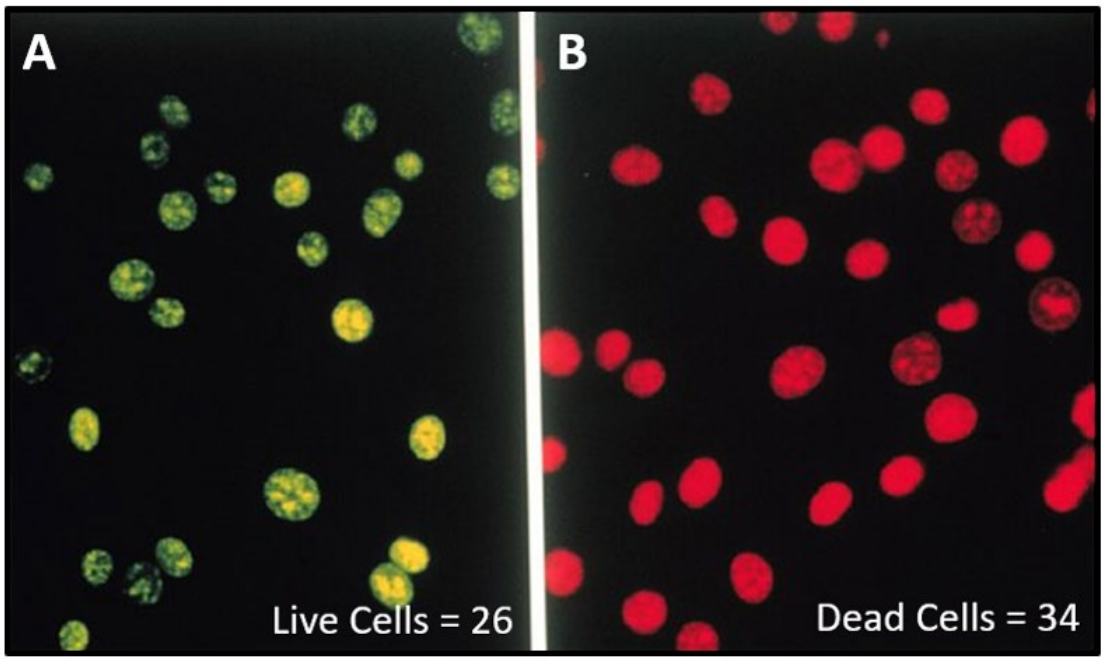

Figure 35: Example image of A) counted live cells stained with calcein AM, B) counted dead cells stained with EthD-III, C) calculation of percent viability.[141]

A follow-up study was conducted to investigate the ability of bAFCs to align on the non-fibrous side of decellularized pericardium. Pericardium samples (n=3) were marked on the non-fibrous side, seeded as previously described, and cultured for three days. Samples were imaged and viability counts were made as previously described.

4.2.3 Investigation of the FT-AFRPs ability to support bAFCs

Trial 1

Decellularized sheets of pericardium (approximately 4x4 cm^2) were sterilized as previously described. Nine sheets of pericardium were seeded with 800,000 cells at a concentration of 1,000,000 cells/mL. Seeded pericardium layers were placed in the

incubator for 2 hours to allow cells to adhere. Alginic acid sodium salt powder was sterilized using a 12-hour ethylene oxide treatment and subsequently used to create a sterile alginate solution. $CaCl_2$ crosslinker solution was sterile filtered prior to use. The 3-D printed fabrication base was autoclaved prior use.

15-layer sterile plugs (n=4/timepoint) were fabricated by stacking sterile pericardium layers onto the 3-D printed base. Three seeded layers were incorporated into each plug. The 1^{st}, 8^{th}, and 15^{th} layer of each plug was a seeded pericardium layer. Once staked, plugs were punched using a 6mm biopsy punch, dipped in sterile alginate, and dropped into sterile $CaCl_2$ crosslinker solution for 10 minutes. Plugs were then placed into separate wells of a 96 well plate and 250 μL of CCM was added on top of each plug. The plugs were placed in the well plate such that walls of the plug fit against the walls of the well. This was intended to simulate a reduced nutrient environment by only allowing CCM to diffuse through the plug to reach bottommost layers. Samples were placed in an incubator at 37℃ and 5% CO_2. Sample imaging timepoints were 1, 3, and 6 days. CCM was changed every 24 hours.

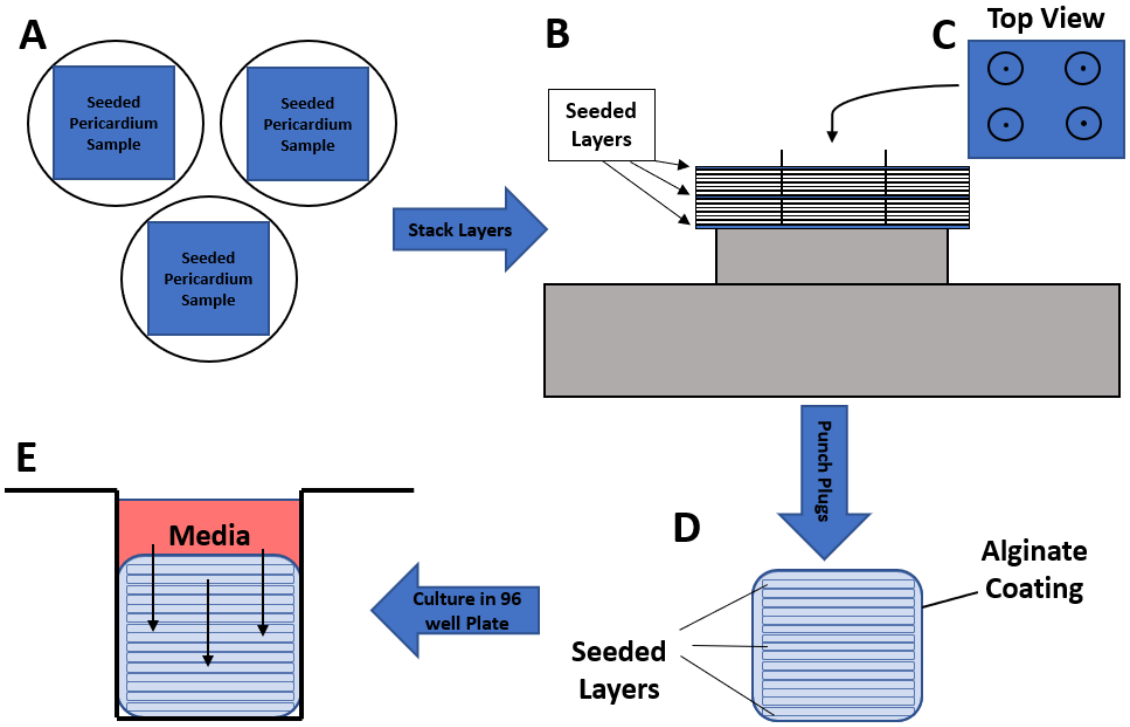

Figure 36: Fabrication of seeded FT-AFRPs for cell viability study. Figures representing A) pericardium layers in petri dishes seeded with bAFCs, B) 3 seeded and 12 unseeded layers of pericardium stacked onto the 3D printed fabrication base, C) a top down view of the stacked layers with circles and points representing biopsy punch locations and needle punctures respectively, D) a seeded FT-AFRP after being punched from stacked pericardium and dip coated in alginate, E) culture environment for FT-AFRPs in 96 well plate with arrows indicating direction of nutrient transport through pericardium layers.

At imaging timepoints, FT-AFRPs were removed from the 96 well plate and dipped into a sodium citrate chelator solution for 20 seconds. Layers were separated one at a time, rinsed twice by dipping in sterile PBS, and placed in separate wells of a 24 well plate. Live/dead staining was performed using a Calcein AM and EthD-III solution as described in section 4.2.2. Samples were immersed in staining solution for 30 minutes at room temperature shielded from light. Samples were then imaged using fluorescent light to view

live and dead cells. Viability was calculated by manually counting the number of live and dead cells across various sample images at 200x total magnification.

Trial 2

A similar procedure to trial 1 was used with slight modifications. 800,000 cells were seeded onto sheets of pericardium but at an increased suspended density of 1,250,00 cells/mL of CCM. Enough sheets were seeded to allow for three seeded layers in each FT-AFRP as well as a control sample for each time point. Once cells were seeded, scaffolds were placed in the incubator at 37°C for 2 hours to allow cell adherence to scaffolds. CCM was then added to each sheet of seeded pericardium and cells were cultured overnight to allow further interaction between cells and pericardium. After 24 hours of culture, 15-layer plugs were fabricated following the procedure from trial 1. Precaution was taken to prevent overhandling or shear stresses exerted on seeded layers. Stacked layers were punched with a 6mm biopsy punch, dipped in alginate, and dropped in $CaCl_2$ for 10 minutes.

Seeded FT-AFRPs (n=3/timepoint) were cultured for 1,3, and 6 days in a 12 well plate, submerged in CCM. CCM was changed on day 1 and 3. The control sample for each timepoint was cultured under the same conditions for 1, 3, and 6 days.

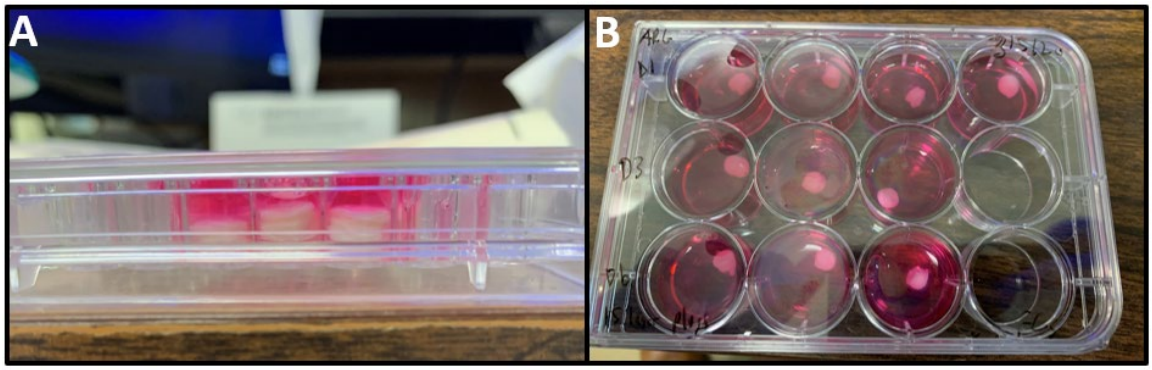

Figure 37: Culture condition comparison between A) trial 1 and B) trial 2 of cell viability study.

On day 1 and 3, plugs (n=3) were removed from CCM and rinsed twice by dipping in PBS. Whole FT-AFRPS, with alginate coating intact, were submerged in live/dead solution for 30 minutes shielded from light. Day 6 samples were stained using the procedure from trial 1. That is, FT-AFRP layers were split apart and rinsed in PBS before placing into live/dead stain for 30 minutes. The control sample for the corresponding timepoint was also rinsed and stained. FT-AFRPs were removed from staining solution and layers were split apart. All layers were imaged using florescence microscopy to visualize live and dead cells. Viability was calculated as previously described for FT-AFRPs at all time points as well as for control samples. Statistical analysis was performed to compare viability across various timepoint. Graphpad Prism 7 software was used to perform a one-way ANOVA with significance denoted as ($p<0.05$).

4.3 Results

4.3.1 Investigation of bAFC Cell Alignment on Decellularized Pericardium

BAFCs cultured on the fibrous side of decellularized pericardium began to show alignment as early as day 1. The AF cells possessed a primarily elongated cell shape with the processes of most cells pointing in the same direction. A lower occurrence of a more rounded cell type was evenly spread throughout samples. Regional differences in cell alignment, cell density, and cell shape were seen within each sample. Similar trends were seen for day 3 samples. Scaffolds seemed to be slightly more crowded and aligned, but still showed regions of a mixed cell type including rounded cells. Day 6 showed the most substantial alignment and scaffold crowding. A lower occurrence of rounded cells seemed to be present on day 6 compared to days 1 and 3.

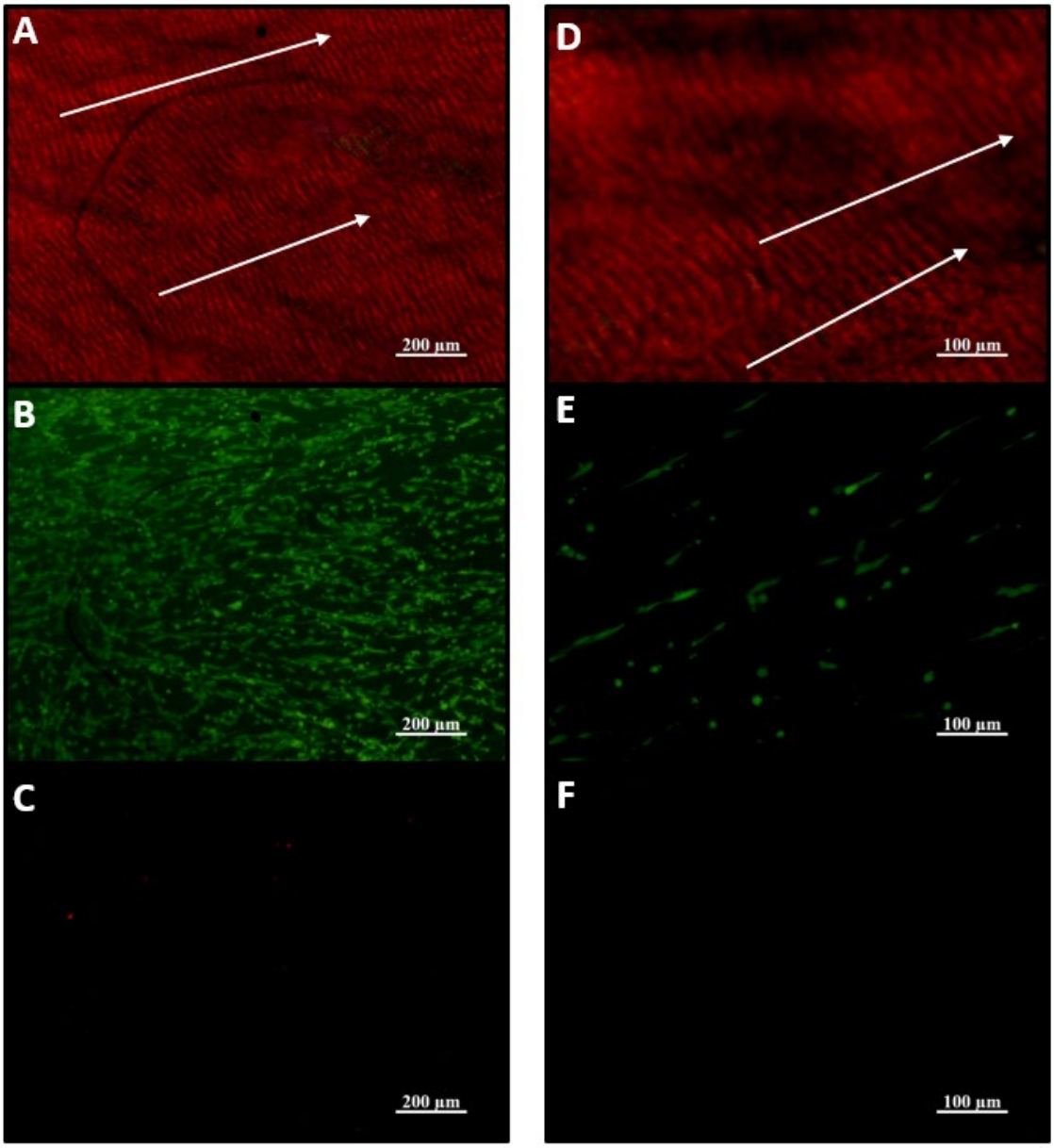

Figure 38: Day 1 samples of decellularized pericardium seeded with bAFCs. Representative images at 100x and 200x total magnification of A&C) fiber direction indicated by white arrows, B&D) live cells, and C&F) dead cells.

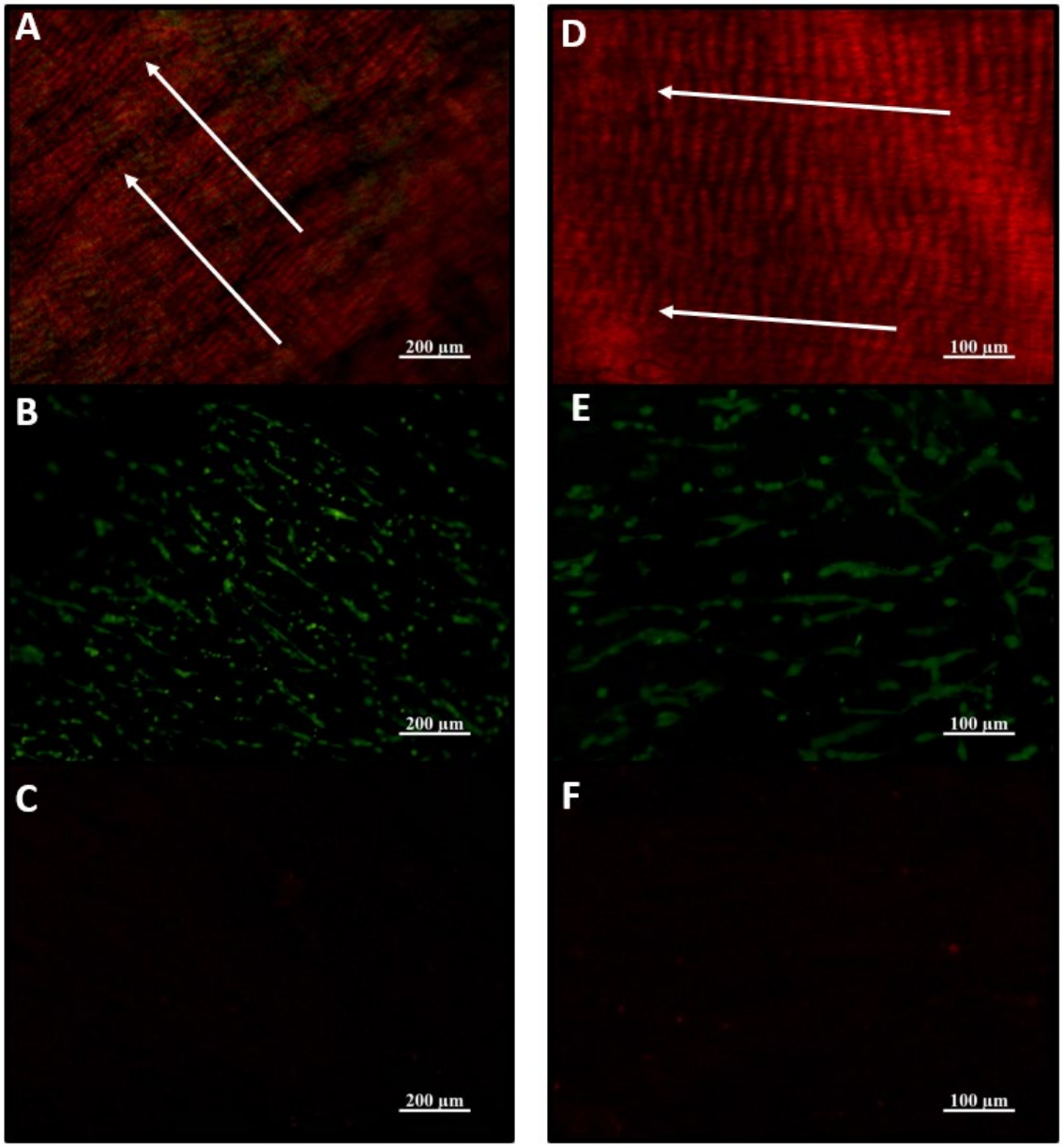

Figure 39: Day 3 samples of decellularized pericardium seeded with bAFCs. Representative images at 100x and 200x total magnification of A&C) fiber direction indicated by white arrows, B&D) live cells, and C&F) dead cells.

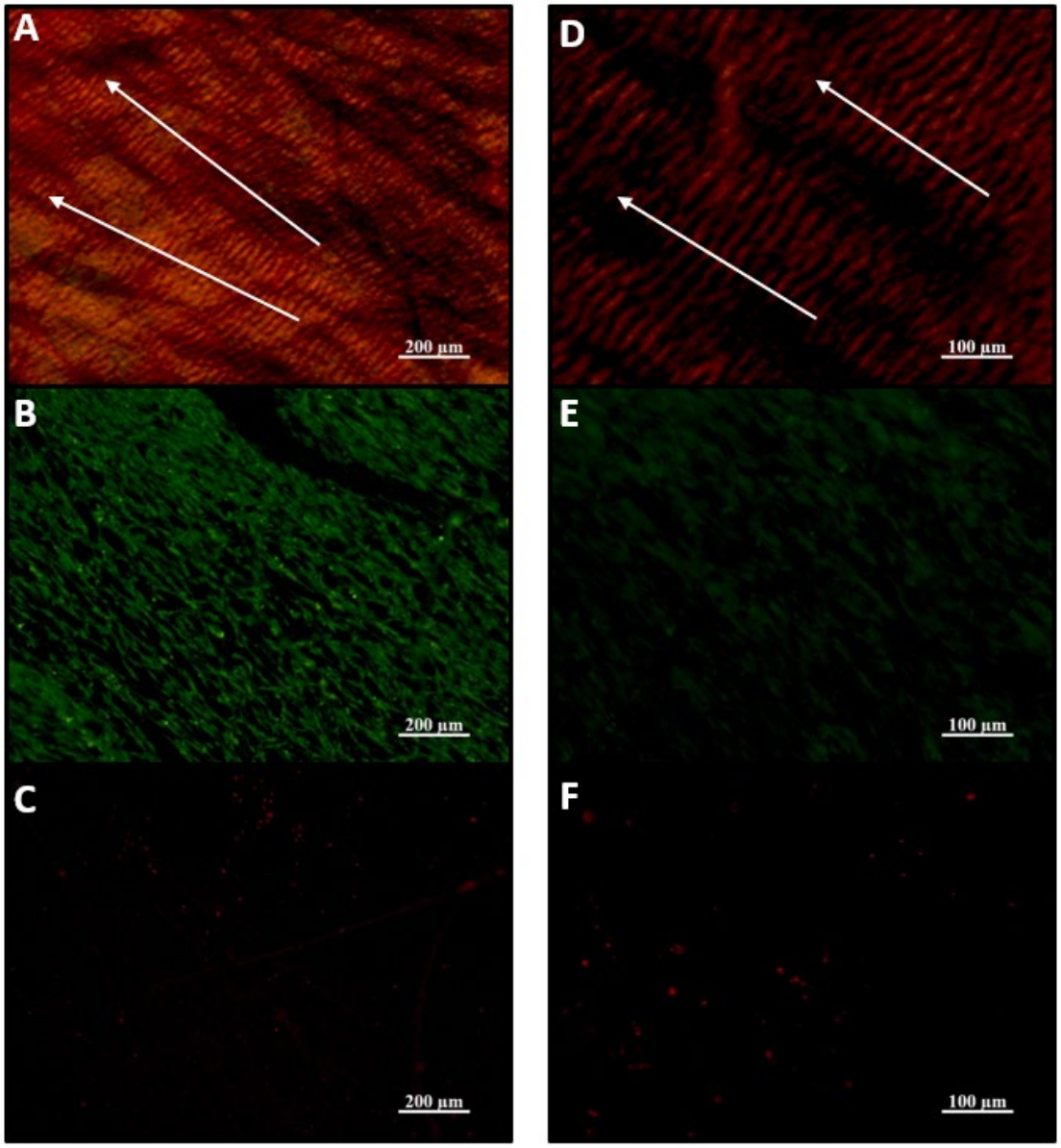

Figure 40: Day 6 samples of decellularized pericardium seeded with bAFCs. Representative images at 100x and 200x total magnification of A&C) fiber direction indicated by white arrows, B&D) live cells, and C&F) dead cells.

Percent viability for days 1, 3, and 6 were 98.65 ± 1.60%, 90.18 ± 6.26%, and 86.18 ± 7.25% respectively **(Figure 41)**. No significant differences were noted between groups for ($p<0.05$). The average across samples from all timepoints was 91.57 ± 7.72%.

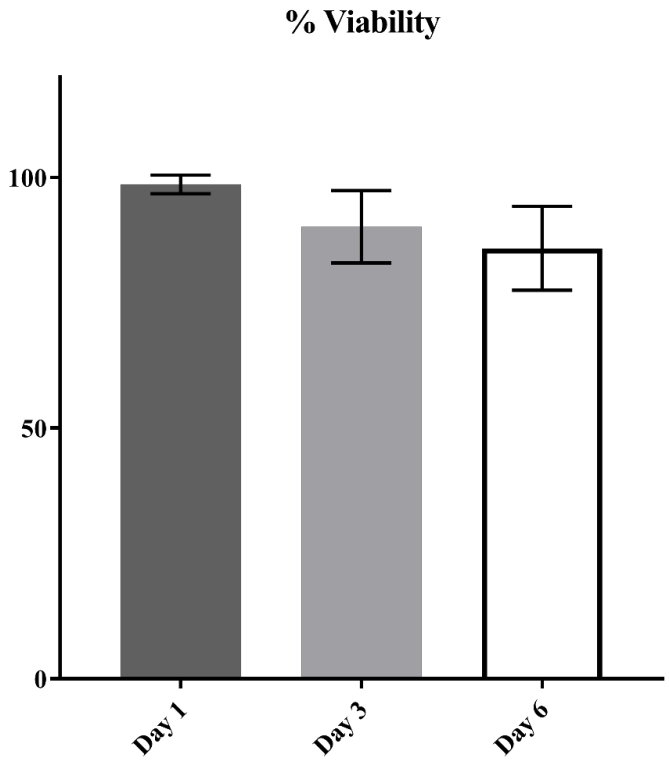

Figure 41: Average percent viability of bAFCs seeded on decellularized pericardium.

Cells seeded on the non-fibrous side of decellularized pericardium showed less alignment compared to day 3 samples with cells seeded on the fibrous side of pericardium. Additionally, the primary cell shape was rounded. Small regions of partially aligned elongated cells were seen throughout samples. Percent viability averaged 91.77 ± 2.76% which did not different significantly from day samples seeded with bAFCs on the fibrous side.

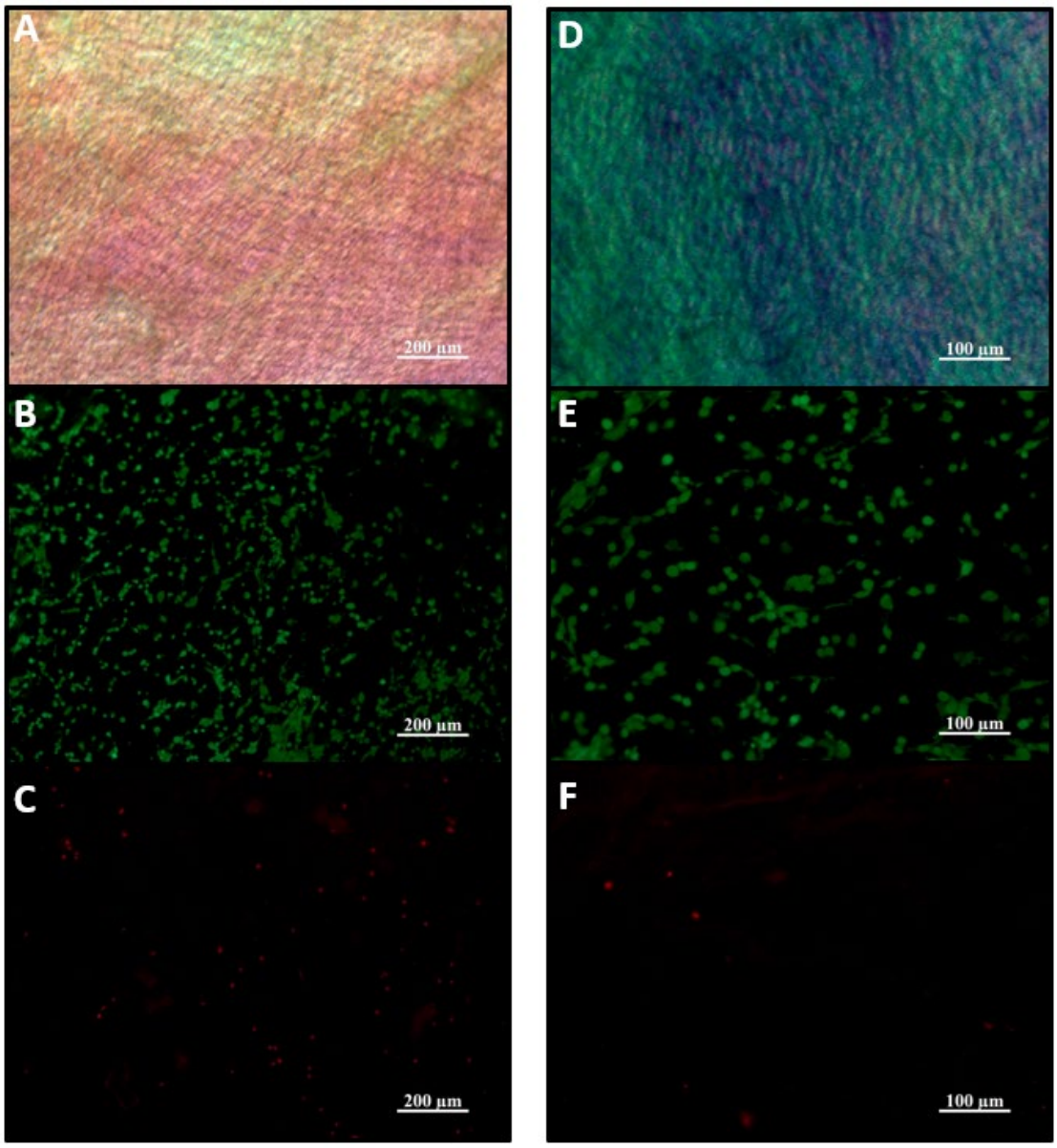

Figure 42: Day 3 samples of decellularized pericardium seeded with bAFCs on the non-fibrous side. Representative images at 100x and 200x total magnification of A&C) lack of fiber orientation, B&D) live cells, and C&F) dead cells.

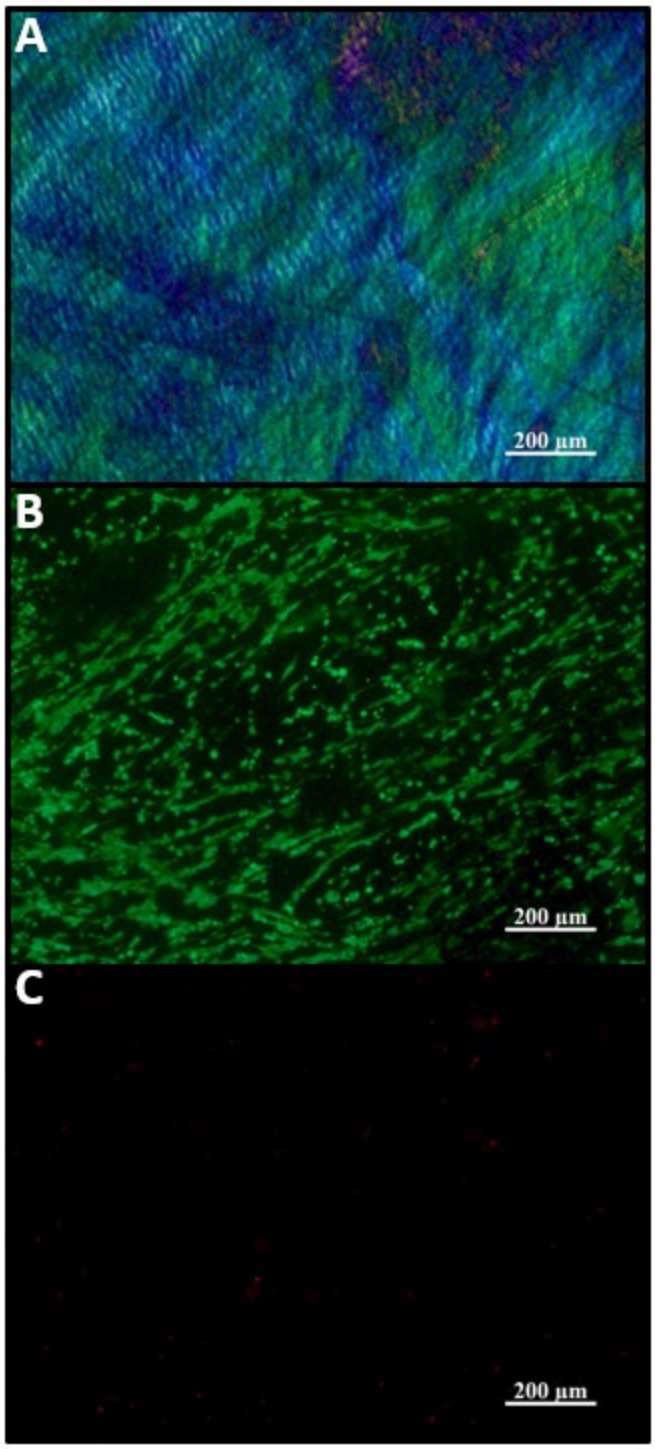

Figure 43: bAFCs seeded on the non-fibrous side of decellularized pericardium. A) Fiber orientation, B) live cells, and C) dead cells in a region showing moderate alignment and elongated cell shape.

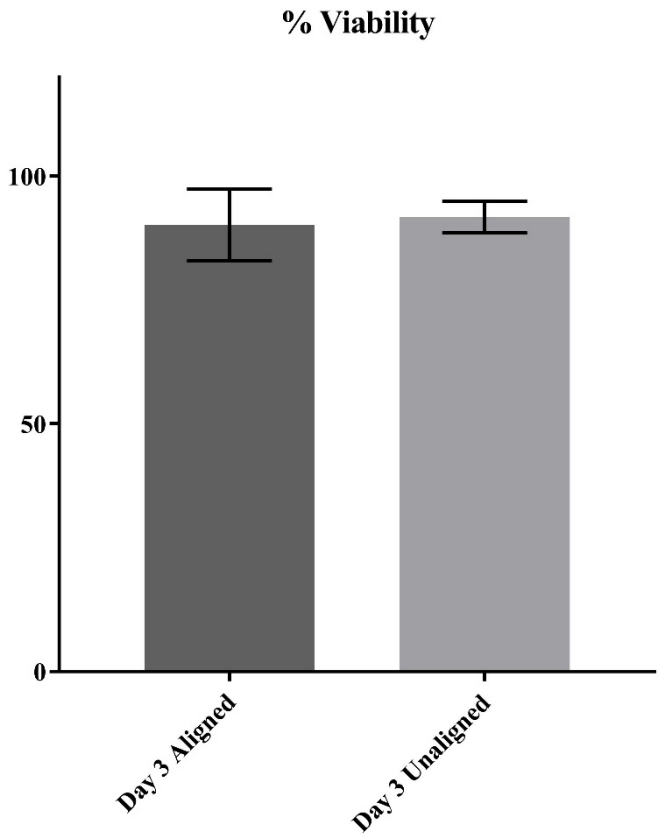

Figure 44: Average percent viability of day 3 samples seeded with bAFCs on the fibrous (aligned) and non-fibrous (unaligned) side.

4.3.2 Investigation of the FT-AFRPs ability to support bAFCs

Trial 1 resulted in little to no viable cells across all samples. On day 1, dead cells were found on all three seeded layers of various FT-AFRP samples. Viable cells that were found were in clusters of 2-10 cells and had a rounded shape. The majority of viable cells found were located on the top layers of the FT-AFRPS, closest to the CCM in the 96 well plate. While viable cells were seen, there were too few to obtain an accurate estimation of average percent viability. These results were confirmed in day 3 samples with even fewer

viable cells found. Due to the projected continued lack of viable cells, day 6 samples were not imaged.

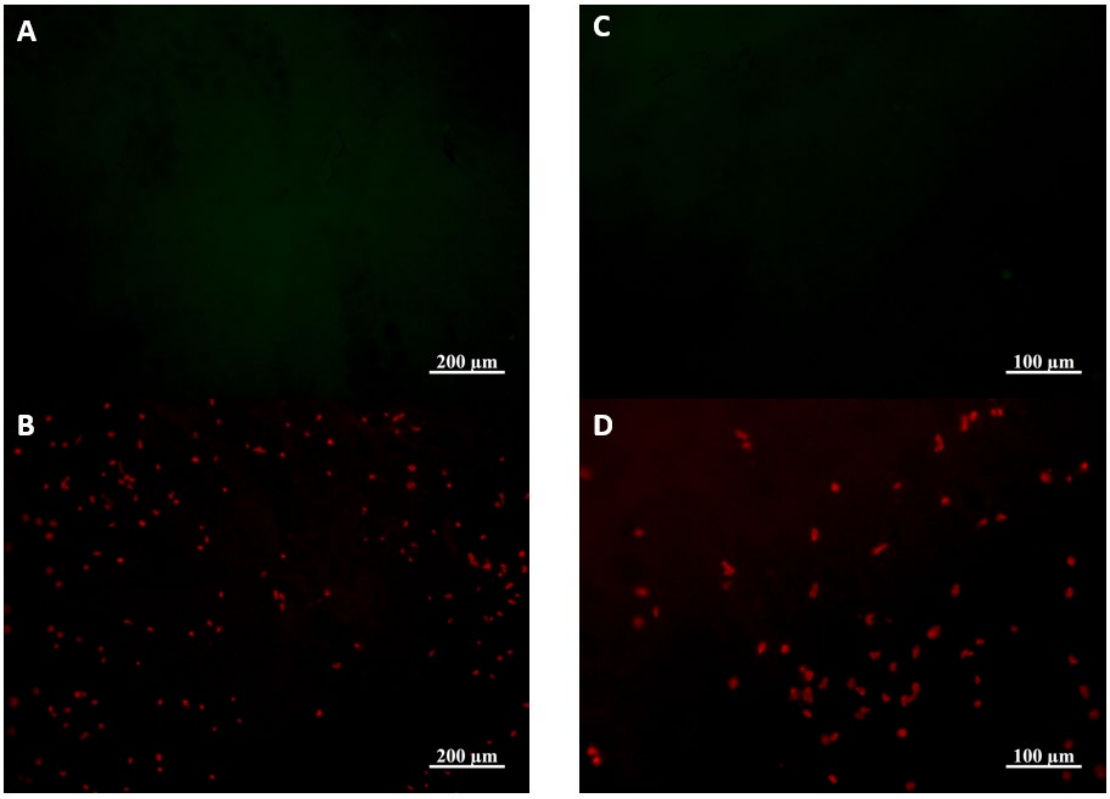

Figure 45: Trial 1 of FT-AFRPs seeded with bAFCs. Representative images at 100x and 200x total magnification of A&C) live cells and B&D) dead cells on single layers of pericardium from FT-AFRPs.

Regions found with live cells were inconsistent, normally showing a small cluster of 2-4 cells. One region of a top layer of seeded pericardium showed approximately 15 viable cells (**Figure 46)**. This region exhibited a much higher quantity of dead cells than live cells.

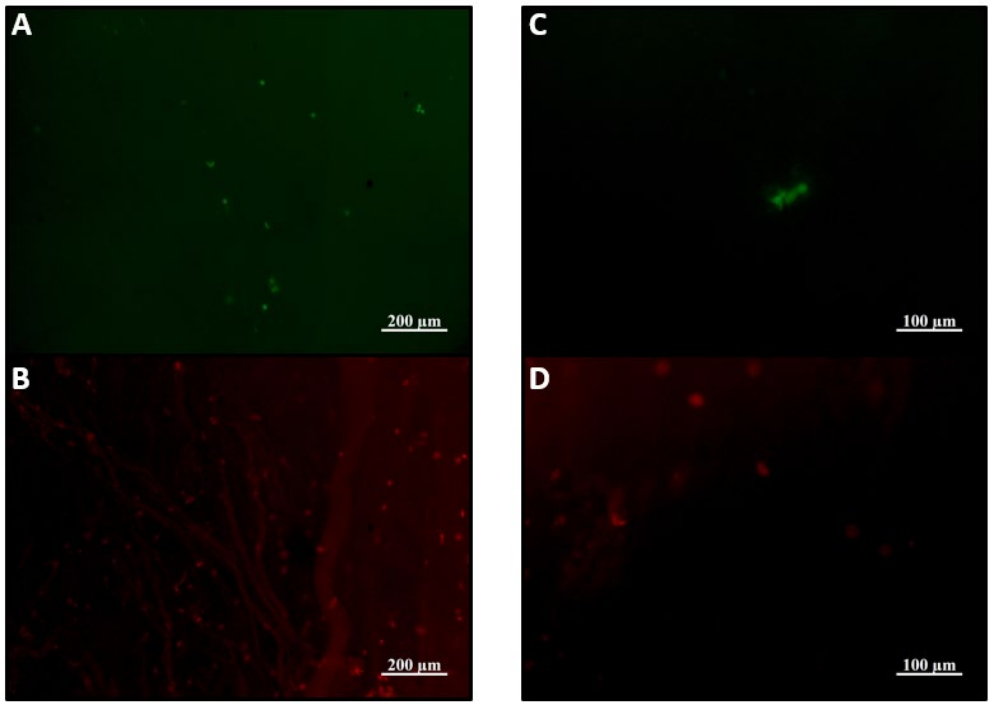

Figure 46: Small regions of viable cells found on the top layer of FT-AFRPs. Images showing A&C) live cells and B&D) dead cells.

Trial 2 samples imaged on day 1 showed no cells, live or dead. The day 1 control sample of seeded pericardium showed elongated and aligned cells with a viability of approximately 99%. Day 3 FT-AFRPs and the corresponding control sample showed similar results to Day 1, with a control viability of approximately 97%. No viability data was obtained from the day 1 or 3 FT-AFRPs due to the lack of stained cells. Day 6 samples, which reverted back to the staining method from trial 1, showed both live and dead cells across various layers of FT-AFRP samples. While the samples were not abundantly populated with cells compared to the controls, large clusters of both live and dead cells were found with primarily rounded cell type. Average viability for all layers of seeded pericardium from day 6 FT-AFRPs was 70.37 ± 14.37%. The control sample for day 6 had a viability of approximately 92%.

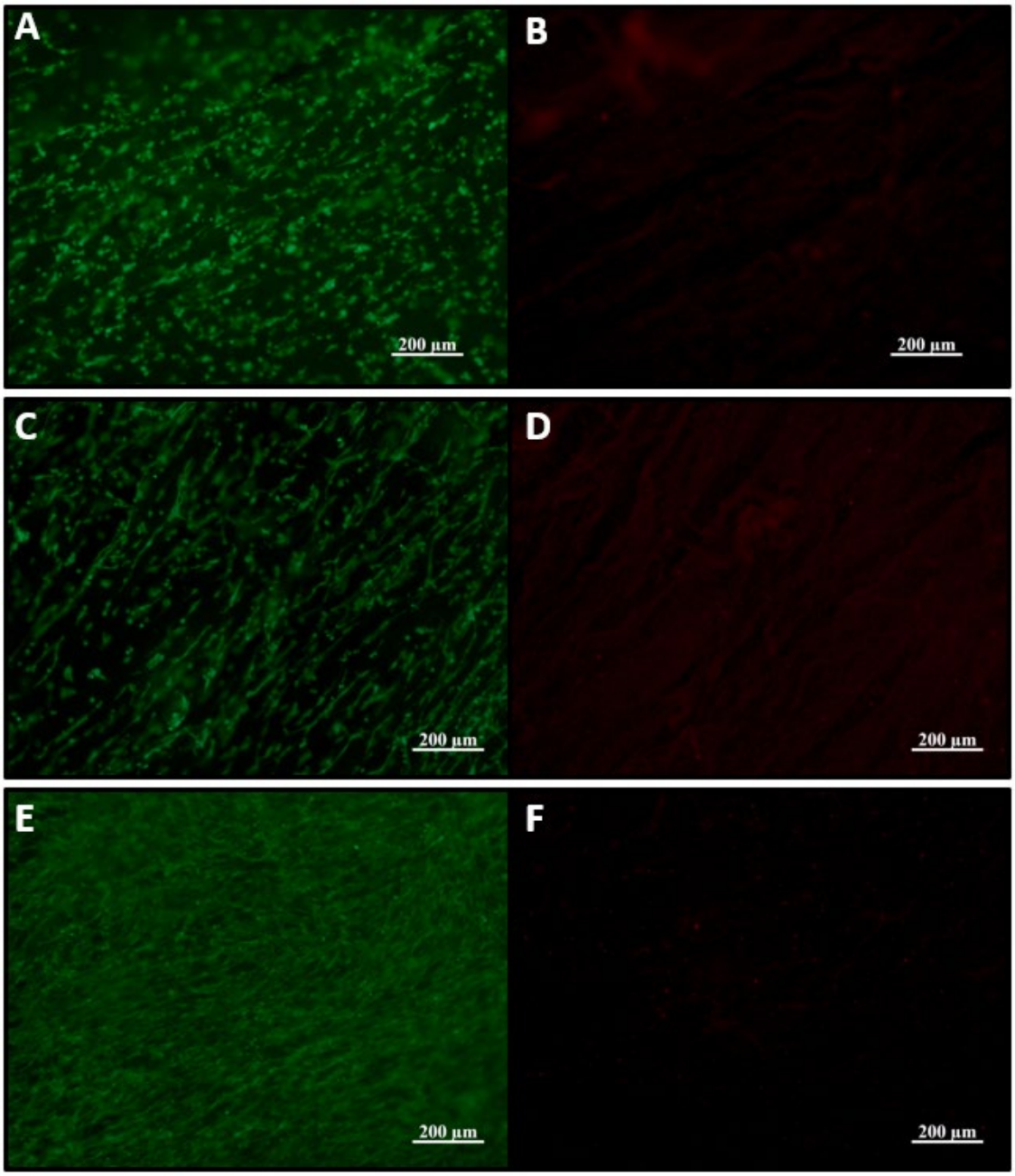

Figure 47: Live/Dead control images of bAFCs on sheets of pericardium for FT-AFRP cell viability study. Pairs representing A&B) day 1, B&C) day 2, and E&F) day 3. Image pairs show live cells (A,C and E) and dead cells (B, D, and F).

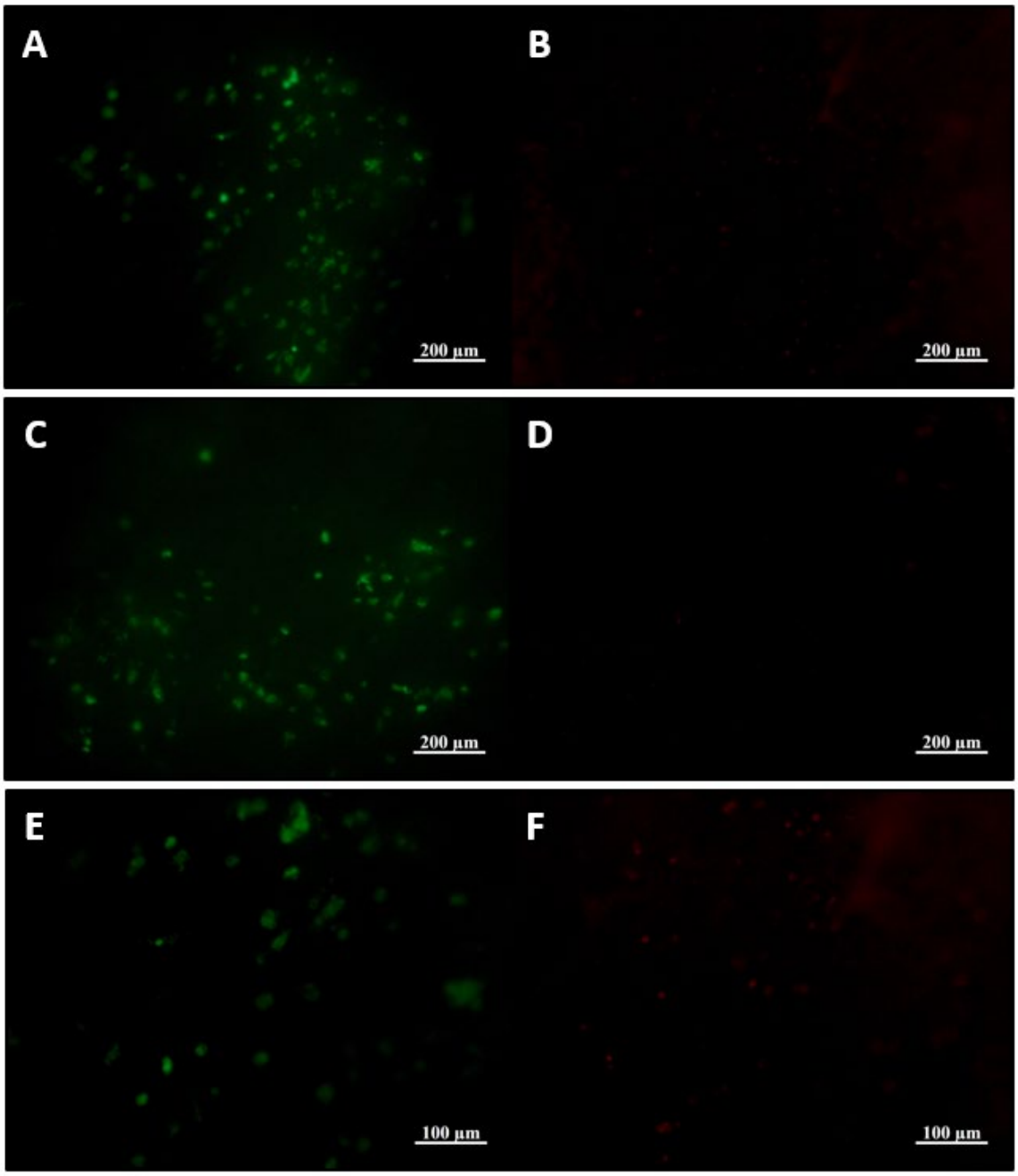

Figure 48: Day 6 FT-AFRP samples seeded with bAFCs. Representative image pairs of various layers of pericardium stained for live (A,C,E) and dead (B,D,F) cells.

4.4 Discussion

The use of cells along with mechanically competent scaffolds is an identified necessity for AF repair to help maintain ECM structure through maintaining the long-term homeostatic balance of matrix turnover in damaged IVDs. To achieve this, the FT-AFRP must be cytocompatible with relevant cell types. In addition, an important goal in tissue engineering the AF is to allow for potential integration between the repair scaffold and surrounding native tissue through infiltration of host cells. The implications of the FT-AFRP on these items was tested by incorporating bovine AF cells on singular sheets of pericardium as well as throughout FT-AFRPs. Human AF cells were not used due to a general difficulty in obtaining healthy samples of cells. Additionally, while stem cells may be more relevant for clinical use, the aim of this study was to investigate the general viability and alignment of a relevant end stage phenotype of native AF. This was achieved using readily available bAFCs. The studies herein proved that decellularized pericardium, as singular layers, can support bAFC proliferation and provide correct cues to maintain a properly elongated cell shape. Despite this, the incorporation of bAFCs into FT-AFRPs was only moderately successful as indicated by a lowered cell density compared to control samples as well as a round cell shape.

4.4.1 Investigation of bAFC Cell Alignment on Decellularized Pericardium

While previous studies by our group have identified the ability of decellularized pericardium to support cell life, no investigations have been done specifically targeted at identifying cell alignment and shape after seeding scaffolds. Bovine AF cells began to show alignment as early as one day after seeding indicated by staining viable cells with

calcein AM. Cells continued to proliferate and further align through 6 days of culture. The ability of these cells to remain elongated without incorporating tensile stresses is an important finding for future development. While bAFCs did not need tensile stimulus to align, it is possible that a tensile stimulus may still be required to achieve proper differentiation if stem cells were used. Tensile stimuli could also play a role in ECM production and biochemical output of cells. While most cells were elongated, viable rounded cells were also observed, especially in regions of lowered overall alignment. This points towards the inconsistencies in pericardium tissue but also further supports that the cells need cues from collagen fibers to properly align. These rounded cell types may also be useful in mimicking different regions of the AF as a higher proportion of rounded cells are seen in inner native AF tissue. Percent viability did lower the longer pericardium sheets were cultured, but values did not differ significantly. Cells seemed to become much denser by day 6. Therefore, the lowered viability at the end timepoint could be due to general overcrowding of the scaffolds.

The follow up study of seeding bAFCs on the non-fibrous side of pericardium also supported the need for collagen fibers to provide cellular cues for alignment and cell shape. Cells attached to and were supported by both sides of the pericardium as indicated by day 3 viability calculations but showed little alignment and a primarily rounded cell shape in this follow-up study. This study provided concrete support for always seeding pericardium layers on the fibrous side when fabricating FT-AFRPs an AFRPs when aiming for elongated and aligned cells. While mimicking the native AF cell population will primarily require elongated and aligned cells, layers of pericardium seeded with cells on the non-

fibrous side could be incorporated into the bottom-most layer of FT-AFRPs to mimic the mixed cell morphology seen in the inner AF.

4.4.2 Investigation of the FT-AFRPs ability to support bAFCs

While bAFCs seeded on singular sheets of pericardium showed positive outcomes towards using the material for AF repair, further investigation was needed to confirm cells could live in a multilayered construct sealed with an alginate gel such as the FT-AFRP. The initial trial of incorporating bAFCs onto FT-AFRPs was unsuccessful. A large amount of mechanical compression and shearing was imparted onto scaffolds through the fabrication process. Additionally, fabricated FT-AFRPs were placed into a highly nutrient reduced environment. The 96 well plate culture condition was a potentially aggressive model of the way nutrients would flow in the native AF. The combination of shear stresses and lack of nutrients were most likely the largest contributors to cell death.

In the second trial, data was not obtained for day 1 and 3 FT-AFRPs samples due to a flawed staining procedure. The staining solution may have inadequately penetrated through the alginate coating of the FT-AFRP when whole plugs were stained. Additionally, if the stain was able to penetrate the alginate, it may not have gotten to cell locations due to a seal between stacked pericardium layers. The issue arising from inadequate stain penetration was supported by readily visible and highly viable cells seen on control samples stained with the same solution. The revert in procedure back to separating pericardium layers before staining fixed the issue. Day 6 samples showed an average viability of 70.37 ± 14.37%. While viability levels were not as high as control values, further refinement of the fabrication process to reduce negative mechanical stimulus could provide further

improvement. Overall, the study showed that bAFCs are moderately supported by FT-AFRP scaffolds and that the alginate coating does not pose a significant barrier to nutrient diffusion for cellular support. While the viability values alone supported moderate success, overall cell density and shape give rise to further challenges of incorporating cells in FT-AFRPs. Cell shape in the FT-AFRP was rounded and total cell counts were much lower than control samples. The reduced cell proliferation compared to singular sheets of pericardium could be due to some reduced nutrient flow imposed by the alginate and adjacent pericardium layers. The layers adjacent to seeded layers may have also posed a physical barrier for cell migration. The rounded cell shape is another concern which must be induced by the physical environment of adjacent layers touching seeded layers. While cells were initially seeded on the fibrous side of the pericardium, they could have been receiving cues from the non-fibrous layer that was placed in contact with seeded layer. Additionally, cells could have attached to the adjacent layer of pericardium, influencing cell shape. The layers of pericardium were pulled apart from one another for staining and imaging. This could have also altered cell shape if cells had indeed attach to both the pericardium layer that the cells were seeded on as well as the second layer stacked on top of it. Further investigation is needed to understand the root cause of the rounded cell shape as well as ways to fine tune it. Additionally, a more consistent method of cell incorporation with FT-AFRPs is needed.

CHAPTER FIVE

CONCLUSIONS AND FUTURE RESEARCH DIRECTIONS

5.1 Conclusions

The FT-AFRP was developed following the identified need for a full thickness AF repair material following outer AF closure. Tissue engineering constructs have been widely developed in recent years but continually fall short in mimicking the angle-ply structure of native AF or in providing adequate mechanical restoration to the IVD. However, we have developed a method to repeatably fabricate a full thickness annular plug using sheets of decellularized pericardium which possess a highly structured matrix of aligned collagen fibers. The AF repair plug possesses compressive properties suitable for the conditions within a repaired IVD, especially when further supported by an outer annular closure device such as the AFRP. Additionally, it has been demonstrated that the pericardium used to fabricate the FT-AFRPs adequately supports AF cell viability and provides cues for cell alignment and an elongated cell shape. The FT-AFRP provides the last major piece of a repair system including an NP replacement as well as an outer AF closure patch. This repair system is intended to repair the IVD following IVDH. Additionally, the repair system could provide a much-needed early stage intervention for patients with signs of IVDD. The inclusion of the FT-AFRP in our in situ bovine repair model demonstrated partially restored spinal kinematic parameters and hinderance of re-herniations. Despite these successes, future research is needed for further refinement of the FT-AFRP.

5.2 Future Research directions

Future studies should first focus on refining the method to adhere pericardium layers together to provide a more robust scaffold for implantation. Additionally, a suturing technique needs to be developed to instantly establish a mechanically competent connection between the FT-AFRP and surrounding tissue. The focus of this development will need to re-establish tensile pre-strain in the AF. Also, further cell studies need to be done with MSCs to determine the FT-AFRPs influence on differentiation into relevant cell types. This also warrants an investigation of the induced long-term tissue remodeling and regeneration on mechanical properties of the scaffold. Lastly, a GAG gel needs to be incorporated between FT-AFRP layers to further mimic native AF biochemical content. The influence of this gel on cellular and mechanical characteristics of the FT-AFRP will subsequently need to be investigated.

APPENDIX

CUSTOM MATLAB CODES

Tension Compression Cycle Data Analysis

```
Read In Data and Clean Up Data
Cyclic Tension and Compression
Compression
Range of Motion
Slow Ramp
Output
%Alex Garon     Ortho-X     7/17/2018

%Bose Cyclic and Slow Ramp Analysis

clear
clc
close all
Read In Data and Clean Up Data

raw = load('bFSU-1-UTC.txt'); %read in file

c1 = 1;
while abs(raw(c1,3)-raw(c1+5,3))<=1 %find where first cycle starts
   c1=c1+1;
end
raw = raw(c1:end,:); %remove everything before the found point

loc = find(raw(:,3)>=mean(raw(length(raw)-100:length(raw),3))+1); %find where slow
ramp ends
raw = raw(1:loc(end)+10,:); %remove points after found location

raw(:,1:2) = raw(:,1:2)-raw(1,1:2); %Set zero values for time and discplacemnt
Cyclic Tension and Compression

loc2 = find(raw(:,3)<=mean(raw(length(raw)-100:length(raw),3))+1); % Find the bottom
of a cycle, lines 25-27 are accuracy adjustments
loc2 = loc2(1)+10;
loc2 = find(min(raw(loc2-10:loc2+10,3))==raw(:,3));
loc2 = loc2(1);

points = 10/raw(2,1); %Estimating total data points in single cycle assuming .1 Hz
```

```
loc35start = round(loc2+(35*points)-round(points));%finding the start of the 35th cycle
(Max Compression -> Tension -> Max Compression)
loc35end = round(loc2+(35*points));
sine(:,1) = raw(loc35start:loc35end,2);
sine(:,2) = raw(loc35start:loc35end,3);
Compression

sixtypC = .6*min(sine(:,2)); % 60% of max compression
locC = find(sine(:,2)>sixtypC);%find 60% value in unloading compression curve
locC = locC(end);
compression = sine(locC+1:end,:); %isolting max to 60% max compression
cC = polyfit(compression(:,1),compression(:,2),1);
CStiff = cC(1);

%Tension
sixtypT = .6*max(sine(:,2));
maxT = find(sine(:,2)==max(sine(:,2)),1);
locT = find(sine(1:maxT,2)<sixtypT);
locT = locT(end);
tension = sine(locT+1:maxT,:);
cT = polyfit(tension(:,1),tension(:,2),1);
TStiff = cT(1);
Range of Motion

RoM = abs(max(sine(:,1))-min(sine(:,1))); %Total Range of Motion
inflectT =find(sine(:,2)>0,1)-1; %Location where tensile loading starts
inflectC =find(sine(maxT:end,2)<0,1)+maxT-1; %Loacation where compressive loading
starts
RoMC = abs(sine(inflectC-1,1)-sine(end,1)); %Compressive RoM
RoMT = abs(sine(inflectT+1,1)-sine(maxT,1)); %Tensile RoM

% Cyclic Plot
figure('color','w')
plot(sine(1:250,1),sine(1:250,2),'k','linewidth',1)
hold on
plot(sine(250:501,1),sine(250:501,2),'k','linewidth',1)
plot(tension(:,1),tension(:,2),'r','linewidth',1)
plot(compression(:,1),compression(:,2),'b','linewidth',1)
%plot([sine(inflectT,1),sine(inflectT,1)],[-200,200],'k-')
%plot([sine(inflectC,1),sine(inflectC,1)],[-200,200],'g-')
xlabel('Displacement [mm]')
ylabel('Load [N]')
```

Slow Ramp

```
locSR = find(abs(raw(:,3)-raw(1,3))<.1); %finding location of slow ramp start
locSR = locSR(end);
locSR = find(max(raw(locSR-50:locSR,3))==raw(:,3));
LocSR = locSR(end);
SR = raw(LocSR:end,:); %Isolating SR data points
figure('color','w')
SRPF = polyfit(SR(:,2),SR(:,3),1); %fitting the data
SRSlope = SRPF(1); %Slope of SR
plot(SR(:,2),SR(:,3))
grid on
hold on
xth = SR(1,2):-.01:SR(end,2);
yth = SRSlope*xth+SRPF(2);
plot(xth,yth,'R--') %Trendline
title('Slow Ramp')
xlabel('Displacement [mm]')
ylabel('Load [N]')
eq = sprintf('y = %.2fx+%.2f',SRPF(1),SRPF(2));
text(xth(round(length(xth)/2-1))-mean(xth)/length(xth)^2,yth(round(length(yth)/2)),eq)
```

Output

```
fprintf('CS: %.4f\nTS: %.4f\nSlowRamp: %.4f\nRoM: %.4f\nCompressive RoM:
%.4f\nTensile RoM: %.4f\n\n',CStiff,TStiff,SRSlope,RoM,RoMC,RoMT)
CS: 700.8293
TS: 169.1297
SlowRamp: 480.8606
RoM: 3.8340
Compressive RoM: 1.8290
Tensile RoM: 3.1710
Published with MATLAB® R2019b
```

Creep Data Analysis

```
%Alex Garon     Ortho-X     7/17/2018

%Program for data analysis of .TXT file from bose creep output
%Open .TXT file and delete all text from the file then re-save
%Enter file name into load comman (line 12) and run

clear
clc
```

```
close all
%%Load In Data
A = load('bFSU-6-R2.txt');
Add Adjustment Values

A(:,4) = A(:,1); %Time
A(:,5) = A(:,2)-A(1,2); %Adjusted Displacment
[R, C] = size(A);
Displacements

mxdis = min(A(:,3)); %Max Force
av=mean(A(find(abs(mxdis-A(:,3))<1,1):end,3));
loc = A(find(abs(av-A(:,3))<1,1),1);
endloc = 3600+loc; %Find where where sample has been under load for 3600 s
Step = A(find(abs(av-A(:,3))<1,1),5); %Step Displacement
Total = A(find(A(:,1)>=endloc,1),5); %Total Discplaement
Creep = Total - Step; %Creep Displacement
fprintf('Step: %.3f\nTotal: %.3f\nCreep: %.3f\n',Step,Total,Creep)
Step: -0.619
Total: -2.433
Creep: -1.814
Plot
%figure('color','w')
%plot(A(:,4),A(:,5),'linewidth',2)
%grid on
%title('Bose Creep Test') %Plot Title
%xlabel('Time [s]') %x axis label
%ylabel('Displacement (mm)') %y axis label
%hold on
%plot(A(find(abs(mxdis-A(:,3))<1,1),4),Step,'ro','markerfacecolor','r') %Step
Displacement Point
%close all
s = 367.9;
n = 5088;
w = 154;
m = 345597;
x = A(:,4);
y = -271.43*((1/s)*(1-exp(-x*s/n))+(1/w)*(1-exp(-x*w/m)));
%hold on

%plot (x,y)
```

Published with MATLAB® R2019b

REFERENCES

1. Nedresky D, Singh G. Anatomy, back, nucleus pulposus. In: *StatPearls.* Treasure Island (FL): StatPearls Publishing; 2020. http://www.ncbi.nlm.nih.gov/books/NBK535373/. Accessed Jan 28, 2020.

2. Freburger JK, Holmes GM, Agans RP, et al. The rising prevalence of chronic low back pain. *Archives of Internal Medicine*. 2009;169(3):251-258. http://dx.doi.org/10.1001/archinternmed.2008.543. doi: 10.1001/archinternmed.2008.543.

3. Crow WT, Willis DR. Estimating cost of care for patients with acute low back pain: A retrospective review of patient records. *Journal of the American Osteopathic Association*. 2009;109(4):229. http://www.jaoa.org/cgi/content/abstract/109/4/229.

4. Charbonneau DH, Healy AM. Intervertebral disc disease. *Journal of Consumer Health On the Internet*. 2005;9(4):61-68. http://www.tandfonline.com/doi/abs/10.1300/J381v09n04_07. doi: 10.1300/J381v09n04_07.

5. Herper M. Making back surgery obsolete. 2010/06/11/back-surgery-medtronic-healthcare-business-j-and-j-spine. Updated 2010. Accessed January 27, 2020.

6. Sharifi S, Bulstra SK, Grijpma DW, Kuijer R. Treatment of the degenerated intervertebral disc; closure, repair and regeneration of the annulus fibrosus. *Journal of tissue engineering and regenerative medicine*. 2015;9(10):1120-1132.

https://www.narcis.nl/publication/RecordID/oai:ris.utwente.nl:publications%2F72d4e493-a8b0-496a-955f-715e0ec4a25e. doi: 10.1002/term.1866.

7. Hartvigsen J, Hancock MJ, Kongsted A, et al. What low back pain is and why we need to pay attention. *The Lancet*. 2018;391(10137):2356-2367. https://www.sciencedirect.com/science/article/pii/S014067361830480X. doi: 10.1016/S0140-6736(18)30480-X.

8. Taylor VM, Deyo RA, Cherkin DC, Kreuter W. Low back pain hospitalization. recent united states trends and regional variations. *Spine*. 1994;19(11):1207-1212; discussion 13. Accessed Jan 27, 2020. doi: 10.1097/00007632-199405310-00002.

9. Wipf JE, Deyo RA. Low back pain. *Med Clin North Am*. 1995;79(2):231-246. Accessed Jan 27, 2020. doi: 10.1016/s0025-7125(16)30065-7.

10. Low back pain fact sheet. https://www.ninds.nih.gov/Disorders/Patient-Caregiver-Education/Fact-Sheets/Low-Back-Pain-Fact-Sheet. Updated 2019. Accessed 1/27/, 2020.

11. Zheng C, Chen J. Disc degeneration implies low back pain. *Theoretical biology & medical modelling*. 2015;12(1):24. https://www.ncbi.nlm.nih.gov/pubmed/26552736. doi: 10.1186/s12976-015-0020-3.

12. Buser Z, Buser Z, Chung A, et al. The future of disc surgery and regeneration. *International Orthopaedics (SICOT)*. 2019;43(4):995-1002. https://www.ncbi.nlm.nih.gov/pubmed/30506089. doi: 10.1007/s00264-018-4254-7.

13. Understanding spinal anatomy: Intervertebral discs. . Updated 2016. Accessed Mar 6, 2020.

14. Lundon K, Bolton K. Structure and function of the lumbar intervertebral disk in health, aging, and pathologic conditions. *The Journal of orthopaedic and sports physical therapy*. 2001;31(6):291-306. https://www.ncbi.nlm.nih.gov/pubmed/11411624. doi: 10.2519/jospt.2001.31.6.291.

15. Antoniou J, Steffen T, Nelson F, et al. The human lumbar intervertebral disc: Evidence for changes in the biosynthesis and denaturation of the extracellular matrix with growth, maturation, ageing, and degeneration. *The Journal of clinical investigation*. 1996;98(4):996-1003. https://www.ncbi.nlm.nih.gov/pubmed/8770872.

16. Smith LJ, Nerurkar NL, Choi K, Harfe BD, Elliott DM. Degeneration and regeneration of the intervertebral disc: Lessons from development. *Disease models & mechanisms*. 2011;4(1):31-41. https://www.ncbi.nlm.nih.gov/pubmed/21123625. doi: 10.1242/dmm.006403.

17. Nosikova YS, Santerre JP, Grynpas M, Gibson G, Kandel RA. Characterization of the annulus fibrosus–vertebral body interface: Identification of new structural features.

Journal of Anatomy. 2012;221(6):577-589. https://onlinelibrary.wiley.com/doi/abs/10.1111/j.1469-7580.2012.01537.x. doi: 10.1111/j.1469-7580.2012.01537.x.

18. Iatridis JC, MacLean JJ, O'Brien M, Stokes IAF. Measurements of proteoglycan and water content distribution in human lumbar intervertebral discs. *Spine*. 2007;32(14):1493-1497. https://www.ncbi.nlm.nih.gov/pubmed/17572617. doi: 10.1097/BRS.0b013e318067dd3f.

19. Chen S, Fu P, Wu H, Pei M. Meniscus, articular cartilage and nucleus pulposus: A comparative review of cartilage-like tissues in anatomy, development and function. *Cell Tissue Res*. 2017;370(1):53-70. https://www.ncbi.nlm.nih.gov/pubmed/28413859. doi: 10.1007/s00441-017-2613-0.

20. Varki A, Cummings R, Esko J, Freeze H, Hart G, Marth J. *Proteoglycans and glycosaminoglycans.* Cold Spring Harbor Laboratory Press; 1999. https://www.ncbi.nlm.nih.gov/books/NBK20693/. Accessed Jan 29, 2020.

21. Cassidy JJ, Hiltner A, Baer E. Hierarchical structure of the intervertebral disc. *Connect Tissue Res*. 1989;23(1):75-88. Accessed Feb 11, 2020. doi: 10.3109/03008208909103905.

22. Langlais T, Desprairies P, Pietton R, et al. Microstructural characterization of annulus fibrosus by ultrasonography: A feasibility study with an in vivo and in vitro approach. *Biomech Model Mechanobiol*. 2019;18(6):1979-1986.

https://www.ncbi.nlm.nih.gov/pubmed/31222527. doi: 10.1007/s10237-019-01189-3.

23. Turner KG, MASc, Ahmed N, PhD, Santerre JP, PhD, Kandel RA, MD. Modulation of annulus fibrosus cell alignment and function on oriented nanofibrous polyurethane scaffolds under tension. *Spine Journal, The*. 2014;14(3):424-434. https://www.clinicalkey.es/playcontent/1-s2.0-S1529943013014952. doi: 10.1016/j.spinee.2013.08.047.

24. Moon S, Yoder J, Wright A, Smith L, Vresilovic E, Elliott D. Evaluation of intervertebral disc cartilaginous endplate structure using magnetic resonance imaging. *Eur Spine J*. 2013;22(8):1820-1828. https://www.ncbi.nlm.nih.gov/pubmed/23674162. doi: 10.1007/s00586-013-2798-1.

25. Jensen GM. Biomechanics of the lumbar intervertebral disk: A review. *Phys Ther*. 1980;60(6):765-773. https://academic.oup.com/ptj/article/60/6/765/2727048. Accessed Jan 30, 2020. doi: 10.1093/ptj/60.6.765.

26. Urban JPG, Roberts S. Degeneration of the intervertebral disc. *Arthritis research & therapy*. 2003;5(3):120-130. https://www.ncbi.nlm.nih.gov/pubmed/12723977. doi: 10.1186/ar629.

27. Boos N, Weissbach S, Rohrbach H, Weiler C, Spratt KF, Nerlich AG. Classification of age-related changes in lumbar intervertebral discs: 2002 volvo award in basic

science. *Spine*. 2002;27(23):2631-2644. Accessed Jan 31, 2020. doi: 10.1097/00007632-200212010-00002.

28. Miller JA, Schmatz C, Schultz AB. Lumbar disc degeneration: Correlation with age, sex, and spine level in 600 autopsy specimens. *Spine*. 1988;13(2):173-178. Accessed Jan 31, 2020.

29. Adams MA. *The biomechanics of back pain.* 2nd ed. ed. Edinburgh: Churchill Livingstone Elsevier; 2006.

30. Fujii K, Yamazaki M, Kang JD, et al. Discogenic back pain: Literature review of definition, diagnosis, and treatment. *JBMR Plus*. 2019;3(5):e10180-n/a. https://onlinelibrary.wiley.com/doi/abs/10.1002/jbm4.10180. doi: 10.1002/jbm4.10180.

31. Ito K, Creemers L. Mechanisms of intervertebral disk degeneration/injury and pain : A review. *Global Spine Journal*. 2013;3(3):145-152. https://www.narcis.nl/publication/RecordID/oai:pure.tue.nl:publications%2F38645c5e-ffaa-4707-a337-79f26956e13b. doi: 10.1055/s-0033-1347300.

32. Roberts S, Eisenstein SM, Menage J, Evans EH, Ashton IK. Mechanoreceptors in intervertebral discs. morphology, distribution, and neuropeptides. *Spine*. 1995;20(24):2645-2651. Accessed Jan 31, 2020. doi: 10.1097/00007632-199512150-00005.

33. Vo NV, Hartman RA, Patil PR, et al. Molecular mechanisms of biological aging in intervertebral discs. *Journal of Orthopaedic Research*. 2016;34(8):1289-1306. https://onlinelibrary.wiley.com/doi/abs/10.1002/jor.23195. doi: 10.1002/jor.23195.

34. Frobin w, Brinckmann P, Kramer M, Hartwig E. Height of lumbar discs measured from radiographs compared with degeneration and height classified from MR images . *Europe Radiology*. 2001;11.

35. Brinjikji W, Luetmer PH, Comstock B, et al. Systematic literature review of imaging features of spinal degeneration in asymptomatic populations. *AJNR. American journal of neuroradiology*. 2015;36(4):811-816. https://www.ncbi.nlm.nih.gov/pubmed/25430861. doi: 10.3174/ajnr.A4173.

36. Deyo RA, Mirza SK. Herniated lumbar intervertebral disk. *The New England Journal of Medicine*. 2016;374(18):1763-1772. http://dx.doi.org/10.1056/NEJMcp1512658. doi: 10.1056/NEJMcp1512658.

37. Dulebohn SC, Ngnitewe Massa R, Mesfin FB. Disc herniation. In: *StatPearls.* Treasure Island (FL): StatPearls Publishing; 2020. http://www.ncbi.nlm.nih.gov/books/NBK441822/. Accessed Jan 31, 2020.

38. Amin R, Andrade N, Neuman B. Lumbar disc herniation. *Curr Rev Musculoskelet Med*. 2017;10(4):507-516. https://www.ncbi.nlm.nih.gov/pubmed/28980275. doi: 10.1007/s12178-017-9441-4.

39. Wong JJ, Côté P, Sutton DA, et al. Clinical practice guidelines for the noninvasive management of low back pain: A systematic review by the ontario protocol for traffic injury management (OPTIMa) collaboration. *European Journal of Pain*. 2017;21(2):201-216. https://onlinelibrary.wiley.com/doi/abs/10.1002/ejp.931. doi: 10.1002/ejp.931.

40. Van Tulder M, Becker A, Bekkering T, et al. European guidelines for the management of acute nonspecific low back pain in primary care. *Eur Spine J*. 2006;15(S2):s169-s191. https://www.ncbi.nlm.nih.gov/pubmed/16550447. doi: 10.1007/s00586-006-1071-2.

41. Roger Chou, Amir Qaseem, Vincenza Snow, et al. Diagnosis and treatment of low back pain: A joint clinical practice guideline from the american college of physicians and the american pain society. *Annals of Internal Medicine*. 2007;147(7):478. http://www.annals.org/content/147/7/478.abstract. doi: 10.7326/0003-4819-147-7-200710020-00006.

42. Saal JA, Saal JS. Intradiscal electrothermal treatment for chronic discogenic low back pain: Prospective outcome study with a minimum 2-year follow-up. *Spine*. 2002;27(9):966-973. https://www.ncbi.nlm.nih.gov/pubmed/11979172. doi: 10.1097/00007632-200205010-00017.

43. Daffner SD, MD, Hymanson HJ, BS, Wang JC, MD. Cost and use of conservative management of lumbar disc herniation before surgical discectomy. *Spine Journal,*

The. 2010;10(6):463-468. https://www.clinicalkey.es/playcontent/1-s2.0-S152994301000104X. doi: 10.1016/j.spinee.2010.02.005.

44. Peul WC, van Houwelingen HC, van den Hout, Wilbert B., et al. Surgery versus prolonged conservative treatment for sciatica. *N Engl J Med*. 2007;356(22):2245-2256. Accessed Feb 4, 2020. doi: 10.1056/NEJMoa064039.

45. Weinstein JN, Lurie JD, Tosteson TD, et al. Surgical vs nonoperative treatment for lumbar disk herniation: The spine patient outcomes research trial (SPORT) observational cohort. *JAMA*. 2006;296(20):2451-2459. http://dx.doi.org/10.1001/jama.296.20.2451. doi: 10.1001/jama.296.20.2451.

46. Bai D, Liang L, Zhang B, et al. Total disc replacement versus fusion for lumbar degenerative diseases - a meta-analysis of randomized controlled trials. *Medicine (Baltimore)*. 2019;98(29):e16460. Accessed Feb 9, 2020. doi: 10.1097/MD.0000000000016460.

47. Zhang Y, Shan J, Liu X, Li F, Guan K, Sun T. Comparison of the dynesys dynamic stabilization system and posterior lumbar interbody fusion for lumbar degenerative disease. *PloS one*. 2016;11(1):e0148071. https://www.ncbi.nlm.nih.gov/pubmed/26824851. doi: 10.1371/journal.pone.0148071.

48. Rajaee SS, Bae HW, Kanim LEA, Delamarter RB. Spinal fusion in the united states: Analysis of trends from 1998 to 2008. *Spine*. 2012;37(1):67-76.

https://www.ncbi.nlm.nih.gov/pubmed/21311399. doi: 10.1097/BRS.0b013e31820cccfb.

49. Martin B, Mirza S, Spina N, Spiker W, Lawrence B, Brodke D. Trends in lumbar fusion procedure rates and associated hospital costs for degenerative spinal diseases in the united states, 2004 to 2015. *SPINE*. 2019;44(5):369-376. https://www.ncbi.nlm.nih.gov/pubmed/30074971. doi: 10.1097/BRS.0000000000002822.

50. Chou W, Hsu C, Chang W, Wong C. Adjacent segment degeneration after lumbar spinal posterolateral fusion with instrumentation in elderly patients. *Arch Orthop Trauma Surg*. 2002;122(1):39-43. https://www.ncbi.nlm.nih.gov/pubmed/11995879. doi: 10.1007/s004020100314.

51. Andersson G, Watkins-Castillo S. Spinal fusion. https://www.boneandjointburden.org/2014-report/iie1/spinal-fusion. Updated 2014. Accessed Feb 9, 2020.

52. Fritzell P, Hägg O, Wessberg P, Nordwall A. Chronic low back pain and fusion: A comparison of three surgical techniques: A prospective multicenter randomized study from the swedish lumbar spine study group. *Spine*. 2002;27(11):1131-1141. Accessed Feb 9, 2020. doi: 10.1097/00007632-200206010-00002.

53. Golden N. 2019 position statement from the international society for the advancement of spine surgery on cervical and lumbar disc replacements – ISASS – the

international society for the advancement of spine surgery. . . https://www.isass.org/public-policy/policy-statements/2019-position-statement-from-the-international-society-for-the-advancement-of-spine-surgery-on-cervical-and-lumbar-disc-replacements/. Accessed February 9, 2020.

54. Zigler J, Delamarter R, Spivak JM, et al. Results of the prospective, randomized, multicenter food and drug administration investigational device exemption study of the ProDisc-L total disc replacement versus circumferential fusion for the treatment of 1-level degenerative disc disease. *Spine*. 2007;32(11):1155-1162; discussion 1163. Accessed Feb 9, 2020. doi: 10.1097/BRS.0b013e318054e377.

55. Zigler JE, Delamarter RB. Five-year results of the prospective, randomized, multicenter, food and drug administration investigational device exemption study of the ProDisc-L total disc replacement versus circumferential arthrodesis for the treatment of single-level degenerative disc disease. *J Neurosurg Spine*. 2012;17(6):493-501. Accessed Feb 9, 2020. doi: 10.3171/2012.9.SPINE11498.

56. Harrop JS, Youssef JA, Maltenfort M, et al. Lumbar adjacent segment degeneration and disease after arthrodesis and total disc arthroplasty. *Spine*. 2008;33(15):1701-1707. Accessed Feb 9, 2020. doi: 10.1097/BRS.0b013e31817bb956.

57. Garcia RJ, Yue JJ, Blumenthal S, et al. Lumbar total disc replacement for discogenic low back pain: Two-year outcomes of the activL multicenter randomized controlled IDE clinical trial. *Spine*. 2015;40(24):1873–1881.

https://journals.lww.com/spinejournal/fulltext/2015/12150/lumbar_total_disc_replacement_for_discogenic_low.1.aspx. Accessed Feb 9, 2020. doi: 10.1097/BRS.0000000000001245.

58. Veruva SY, Steinbeck MJ, Toth J, Alexander DD, Kurtz SM. Which design and biomaterial factors affect clinical wear performance of total disc replacements? A systematic review. *Clin Orthop Relat Res*. 2014;472(12):3759-3769. Accessed Feb 9, 2020. doi: 10.1007/s11999-014-3751-2.

59. Othman YA, Verma R, Qureshi SA. Artificial disc replacement in spine surgery. *Annals of Translational Medicine*. 2019;7(S5):S170. https://search.proquest.com/docview/2307155253. doi: 10.21037/atm.2019.08.26.

60. Kitzen J, Schotanus M, Kujik S, et al. Long-term clinical results following charite III lumbar total disc replacement. *The Spine Journal*. 2019;18(6):917-925. http://dx.doi.org/10.1016/j.spinee.2017.08.252. doi: 10.1016/j.spinee.2017.08.252.

61. Lumbar artificial disc replacement. . . https://midwestbonejoint.com/lower-back/lumbar-artificial-disc-replacement/. Accessed Feb 10, 2020.

62. Guterl CC, See EY, Blanquer SBG, et al. Challenges and strategies in the repair of ruptured annulus fibrosus. *European cells & materials*. 2013;25:1-21. https://www.narcis.nl/publication/RecordID/oai:pure.rug.nl:publications%2F2482c523-9a3a-4201-9a95-6e392351908e.

63. Martin BI, Mirza SK, Flum DR, et al. Repeat surgery following lumbar decompression for herniated disc: The quality implications of hospital and surgeon variation. *The Spine Journal*. 2011;12(2):89-97. https://www.openaire.eu/search/publication?articleId=od_____267::c53a5117e086c1b7bcb34693d77e223c. doi: 10.1016/j.spinee.2011.11.010.

64. Barth M, Diepers M, Weiss C, Thomé C. Two-year outcome after lumbar microdiscectomy versus microscopic sequestrectomy: Part 2: Radiographic evaluation and correlation with clinical outcome. *Spine*. 2008;33(3):273-279. Accessed Feb 7, 2020. doi: 10.1097/BRS.0b013e31816201a6.

65. Yorimitsu E, Chiba K, Toyama Y, Hirabayashi K. Long-term outcomes of standard discectomy for lumbar disc herniation: A follow-up study of more than 10 years. *Spine*. 2001;26(6):652-657. Accessed Feb 7, 2020. doi: 10.1097/00007632-200103150-00019.

66. Cherkin DC, Deyo RA, Loeser JD, Bush T, Waddell G. An international comparison of back surgery rates. *Spine*. 1994;19(11):1201-1206. Accessed Feb 10, 2020. doi: 10.1097/00007632-199405310-00001.

67. Thomé C, Barth M, Scharf J, Schmiedek P. Outcome after lumbar sequestrectomy compared with microdiscectomy: A prospective randomized study. *J Neurosurg Spine*. 2005;2(3):271-278. Accessed Feb 10, 2020. doi: 10.3171/spi.2005.2.3.0271.

68. Borem R. *Development of a biomimetic, collagen-based scaffold for the repair and regeneration of the annulus fibrosus.* Clemson University; 2018.

69. Bron JL, Helder MN, Meisel HJ, van Royen BJ, Smit TH. Repair, regenerative and supportive therapies of the annulus fibrosus: Achievements and challenges. *Eur Spine J*. 2009;18(3):301-313. https://www.narcis.nl/publication/RecordID/oai:pure.atira.dk:publications%2F12e7ce9a-346e-429d-8464-744a349a9d07. doi: 10.1007/s00586-008-0856-x.

70. Chiang C, Cheng C, Sun J, Liao C, Wang Y, Tsuang Y. The effect of a new anular repair after discectomy in intervertebral disc degeneration: An experimental study using a porcine spine model. *Spine*. 2011;36(10):761-769. Accessed Feb 11, 2020. doi: 10.1097/BRS.0b013e3181e08f01.

71. Heuer F, Ulrich S, Wilke H. Biomechanical evaluation of conventional anulus fibrosus closure methods requrie nucleus replacement. *Journal of Neurosurgery*. 2008;9(3):307-313. https://thejns.org/spine/view/journals/j-neurosurg-spine/9/3/article-p307.xml.

72. Bailey A, Araghi A, Blumenthal S, Huffmon G. Prospective, multicenter, randomized, controlled study of anular repair in lumbar discectomy: Two-year follow-up. *Spine*. 2013;38(14):1161-1169. https://www.ncbi.nlm.nih.gov/pubmed/23392414. doi: 10.1097/BRS.0b013e31828b2e2f.

73. Montanaro L, Arciola CR, Cenni E, et al. Cytotoxicity, blood compatibility and antimicrobial activity of two cyanoacrylate glues for surgical use. *Biomaterials*. 2000;22(1):59-66. http://dx.doi.org/10.1016/S0142-9612(00)00163-0. doi: 10.1016/S0142-9612(00)00163-0.

74. Thumwanit V, Kedjarune U. Cytotoxicity of polymerized commercial cyanoacrylate adhesive on cultured human oral fibroblasts. *Aust Dent J*. 1999;44(4):248-252. Accessed Feb 12, 2020. doi: 10.1111/j.1834-7819.1999.tb00228.x.

75. Intrinsic Therapeutics, inventor; Intrinsic Therapeutics, assignee. Barricaid® Anular Closure Device (ACD). patent P160050. Fri, 12/20/ - 20:25, 2019.

76. Choy WJ, Phan K, Diwan AD, Ong CS, Mobbs RJ. Annular closure device for disc herniation: Meta-analysis of clinical outcome and complications. *BMC musculoskeletal disorders*. 2018;19(1):290. https://www.ncbi.nlm.nih.gov/pubmed/30115053. doi: 10.1186/s12891-018-2213-5.

77. Klassen PD, Bernstein DT, Köhler H, et al. Bone-anchored annular closure following lumbar discectomy reduces risk of complications and reoperations within 90 days of discharge. *Journal of pain research*. 2017;10:2047-2055. https://www.ncbi.nlm.nih.gov/pubmed/28894388. doi: 10.2147/JPR.S144500.

78. Meisel H, Ganey T, Hutton W, Libera J, Minkus Y, Alasevic O. Clinical experience in cell-based therapeutics: Intervention and outcome. *Eur Spine J*. 2006;15(S3):397-

405. https://www.ncbi.nlm.nih.gov/pubmed/16850291. doi: 10.1007/s00586-006-0169-x.

79. Larson JW, Levicoff EA, Gilbertson LG, Kang JD. Biologic modification of animal models of intervertebral disc degeneration. *J Bone Joint Surg Am*. 2006;88 Suppl 2:83-87. Accessed Feb 12, 2020. doi: 10.2106/JBJS.F.00043.

80. Sobajima S, Kim JS, Gilbertson LG, Kang JD. Gene therapy for degenerative disc disease. *Gene Ther*. 2004;11(4):390-401. Accessed Feb 12, 2020. doi: 10.1038/sj.gt.3302200.

81. Melrose J, Smith S, Little C, Moore R, Vernon-Roberts B, Fraser R. Recent advances in annular pathobiology provide insights into rim-lesion mediated intervertebral disc degeneration and potential new approaches to annular repair strategies. *Eur Spine J*. 2008;17(9):1131-1148. https://www.ncbi.nlm.nih.gov/pubmed/18584218. doi: 10.1007/s00586-008-0712-z.

82. Hegewald AA, Neumann K, Kalwitz G, et al. The chemokines CXCL10 and XCL1 recruit human annulus fibrosus cells. *Spine*. 2012;37(2):101-107. Accessed Feb 19, 2020. doi: 10.1097/BRS.0b013e318210ed55.

83. Henriksson H, Thornemo M, Karlsson C, et al. Identification of cell proliferation zones, progenitor cells and a potential stem cell niche in the intervertebral disc region: A study in four species. *Spine*. 2009;34(21):2278-2287. Accessed Feb 19, 2020. doi: 10.1097/BRS.0b013e3181a95ad2.

84. Blanco JF, Graciani IF, Sanchez-Guijo FM, et al. Isolation and characterization of mesenchymal stromal cells from human degenerated nucleus pulposus: Comparison with bone marrow mesenchymal stromal cells from the same subjects. *Spine*. 2010;35(26):2259-2265. Accessed Feb 19, 2020. doi: 10.1097/BRS.0b013e3181cb8828.

85. Feng G, Yang X, Shang H, et al. Multipotential differentiation of human anulus fibrosus cells: An in vitro study. *J Bone Joint Surg Am*. 2010;92(3):675-685. Accessed Feb 19, 2020. doi: 10.2106/JBJS.H.01672.

86. Liu L, Huang B, Li C, Zhuang Y, Wang J, Zhou Y. Characteristics of stem cells derived from the degenerated human intervertebral disc cartilage endplate. *PLoS ONE*. 2011;6(10):e26285. Accessed Feb 19, 2020. doi: 10.1371/journal.pone.0026285.

87. Wuertz K, Vo N, Kletsas D, Boos N. Inflammatory and catabolic signalling in intervertebral discs: The roles of NF-κB and MAP kinases. *Eur Cell Mater*. 2012;23:103-120. Accessed Feb 19, 2020. doi: 10.22203/ecm.v023a08.

88. Smith JW, Walmsley R. Experimental incision of the intervertebral disc. *J Bone Joint Surg Br*. 1951;33-B(4):612-625. Accessed Feb 20, 2020.

89. Key JA, Ford LT. Experimental intervertebral-disc lesions. *J Bone Joint Surg Am*. 1948;30A(3):621-630. Accessed Feb 20, 2020.

90. Moore RJ, Osti OL, Vemon-Roberts B, Fraser RD. Changes in endplate vascularity after an outer anulus tear in the sheep. *Spine*. 1992;17(8):874–878. https://journals.lww.com/spinejournal/Abstract/1992/08000/Changes_in_Endplate_Vascularity_After_an_Outer.3.aspx. Accessed Feb 20, 2020.

91. Melrose J, Ghosh P, Taylor T, Vernon-Roberts B, Latham J, Moore R. Elevated synthesis of biglycan and decorin in an ovine annular lesion model of experimental disc degeneration. *Eur Spine J*. 1997;6(6):376-384. https://www.ncbi.nlm.nih.gov/pubmed/9455664. doi: 10.1007/BF01834063.

92. Hampton D, Laros G, McCARRON R, Franks D. Healing potential of the anulus fibrosus. *Spine*. 1989;14(4):398–401. https://journals.lww.com/spinejournal/Abstract/1989/04000/Healing_Potential_of_the_Anulus_Fibrosus.9.aspx. Accessed Feb 20, 2020.

93. Ganey T, Libera J, Moos V, et al. Disc chondrocyte transplantation in a canine model: A treatment for degenerated or damaged intervertebral disc. *Spine*. 2003;28(23):2609–2620. https://journals.lww.com/spinejournal/Fulltext/2003/12010/Disc_Chondrocyte_Transplantation_in_a_Canine.9.aspx. Accessed Feb 20, 2020. doi: 10.1097/01.BRS.0000097891.63063.78.

94. Ethier DB, Cain JE, Yaszemski MJ, et al. The influence of anulotomy selection on disc competence: A radiographic, biomechanical, and histologic analysis. *Spine*.

1994;19(18):2071–2076. https://journals.lww.com/spinejournal/Abstract/1994/09150/The_Influence_of_Anulotomy_Selection_on_Disc.12.aspx. Accessed Feb 20, 2020.

95. Ahlgren BD, Lui W, Herkowitz HN, Panjabi MM, Guiboux J. Effect of anular repair on the healing strength of the intervertebral disc: A sheep model. *Spine*. 2000;25(17):2165–2170. https://journals.lww.com/spinejournal/Fulltext/2000/09010/Effect_of_Anular_Repair_on_the_Healing_Strength_of.4.aspx. Accessed Feb 20, 2020.

96. Korecki CL, MacLean JJ, Iatridis JC. Dynamic compression effects on intervertebral disc mechanics and biology. *Spine*. 2008;33(13):1403–1409. https://journals.lww.com/spinejournal/Fulltext/2008/06010/Dynamic_Compression_Effects_on_Intervertebral_Disc.3.aspx. Accessed Feb 20, 2020. doi: 10.1097/BRS.0b013e318175cae7.

97. Thompson JP, Oegema TR, Bradford DS. Stimulation of mature canine intervertebral disc by growth factors. *Spine*. 1991;16(3):253-260. Accessed Feb 20, 2020. doi: 10.1097/00007632-199103000-00001.

98. Takegami K, Thonar, Eugene J. M. A., An HS, Kamada H, Masuda K. Osteogenic protein-1 enhances matrix replenishment by intervertebral disc cells previously exposed to interleukin-1. *Spine*. 2002;27(12):1318-1325. Accessed Feb 20, 2020. doi: 10.1097/00007632-200206150-00014.

99. Li YY, Diao HJ, Chik TK, et al. Delivering mesenchymal stem cells in collagen microsphere carriers to rabbit degenerative disc: Reduced risk of osteophyte formation. *Tissue Eng Part A*. 2014;20(9-10):1379-1391. https://www.ncbi.nlm.nih.gov/pmc/articles/PMC4011461/. Accessed Feb 20, 2020. doi: 10.1089/ten.tea.2013.0498.

100. Vadalà G, Sowa G, Hubert M, Gilbertson LG, Denaro V, Kang JD. Mesenchymal stem cells injection in degenerated intervertebral disc: Cell leakage may induce osteophyte formation. *J Tissue Eng Regen Med*. 2012;6(5):348-355. Accessed Feb 20, 2020. doi: 10.1002/term.433.

101. Cruz MA, Hom WW, DiStefano TJ, et al. Cell-seeded adhesive biomaterial for repair of annulus fibrosus defects in intervertebral discs. *Tissue Engineering Part A*. 2018;24(3-4):187-198. https://www.liebertpub.com/doi/abs/10.1089/ten.tea.2017.0334. doi: 10.1089/ten.tea.2017.0334.

102. Kandel R, Roberts S, Urban J. Tissue engineering and the intervertebral disc: The challenges. *Eur Spine J*. 2008;17(S4):480-491. https://www.ncbi.nlm.nih.gov/pubmed/19005701. doi: 10.1007/s00586-008-0746-2.

103. Gruber HE, Ingram JA, Davis DE, Hanley EN. Increased cell senescence is associated with decreased cell proliferation in vivo in the degenerating human

annulus. *Spine J*. 2009;9(3):210-215. Accessed Feb 21, 2020. doi: 10.1016/j.spinee.2008.01.012.

104. Stergar J, Gradisnik L, Velnar T, Maver U. Intervertebral disc tissue engineering: A brief review. *Bosnian journal of basic medical sciences*. 2019;19(2):130-137. https://www.ncbi.nlm.nih.gov/pubmed/30726701. doi: 10.17305/bjbms.2019.3778.

105. Richardson SM, Walker RV, Parker S, et al. Intervertebral disc cell-mediated mesenchymal stem cell differentiation. *Stem Cells*. 2006;24(3):707-716. Accessed Feb 21, 2020. doi: 10.1634/stemcells.2005-0205.

106. Loibl M, Wuertz-Kozak K, Vadala G, Lang S, Fairbank J, Urban JP. Controversies in regenerative medicine: Should intervertebral disc degeneration be treated with mesenchymal stem cells? *JOR Spine*. 2019. http://hdl.handle.net/20.500.11850/395120. doi: 10.3929/ethz-b-000395120.

107. Pettine KA, Murphy MB, Suzuki RK, Sand TT. Percutaneous injection of autologous bone marrow concentrate cells significantly reduces lumbar discogenic pain through 12 months. *STEM CELLS*. 2015;33(1):146-156. https://stemcellsjournals.onlinelibrary.wiley.com/doi/abs/10.1002/stem.1845. Accessed Feb 24, 2020. doi: 10.1002/stem.1845.

108. Smith LJ, Silverman L, Sakai D, et al. Advancing cell therapies for intervertebral disc regeneration from the lab to the clinic: Recommendations of the ORS spine

section. *JOR Spine*. 2018;1(4):e1036-n/a. https://onlinelibrary.wiley.com/doi/abs/10.1002/jsp2.1036. doi: 10.1002/jsp2.1036.

109. Bowles RD, Ph.D, Setton LA, Ph.D. Biomaterials for intervertebral disc regeneration and repair. *Biomaterials*. 2017;129:54-67. https://www.clinicalkey.es/playcontent/1-s2.0-S0142961217301564. doi: 10.1016/j.biomaterials.2017.03.013.

110. Borde B, Grunert P, Härtl R, Bonassar LJ. Injectable, high-density collagen gels for annulus fibrosus repair: An in vitro rat tail model. *Journal of Biomedical Materials Research Part A*. 2015;103(8):2571-2581. https://onlinelibrary.wiley.com/doi/abs/10.1002/jbm.a.35388. doi: 10.1002/jbm.a.35388.

111. Moriguchi Y, Borde B, Berlin C, et al. In vivo annular repair using high-density collagen gel seeded with annulus fibrosus cells. *Acta Biomaterialia*. 2018;79:230-238. http://dx.doi.org/10.1016/j.actbio.2018.07.008. doi: 10.1016/j.actbio.2018.07.008.

112. Long RG, Bürki A, Zysset P, et al. Mechanical restoration and failure analyses of a hydrogel and scaffold composite strategy for annulus fibrosus repair. *Acta Biomaterialia*. 2016;30:116-125. http://dx.doi.org/10.1016/j.actbio.2015.11.015. doi: 10.1016/j.actbio.2015.11.015.

113. Guterl CC, Torre OM, Purmessur D, et al. Characterization of mechanics and cytocompatibility of fibrin-genipin annulus fibrosus sealant with the addition of cell adhesion molecules. *Tissue Engineering Part A*. 2014;20(17-18):2536-2545. https://www.liebertpub.com/doi/abs/10.1089/ten.tea.2012.0714. doi: 10.1089/ten.tea.2012.0714.

114. Bron JL, Vonk LA, Smit TH, Koenderink GH. Engineering alginate for intervertebral disc repair. *J Mech Behav Biomed Mater*. 2011;4(7):1196-1205. Accessed Feb 25, 2020. doi: 10.1016/j.jmbbm.2011.04.002.

115. Gruber HE, Leslie K, Ingram J, Norton HJ, Hanley EN. Cell-based tissue engineering for the intervertebral disc: In vitro studies of human disc cell gene expression and matrix production within selected cell carriers. *Spine J*. 2004;4(1):44-55. Accessed Feb 25, 2020. doi: 10.1016/s1529-9430(03)00425-x.

116. Chang G, Kim H-, Kaplan D, Vunjak-Novakovic G, Kandel R. Porous silk scaffolds can be used for tissue engineering annulus fibrosus. *Eur Spine J*. 2007;16(11):1848-1857. https://www.ncbi.nlm.nih.gov/pubmed/17447088. doi: 10.1007/s00586-007-0364-4.

117. Bhunia BK, Kaplan DL, Mandal BB. Silk-based multilayered angle-ply annulus fibrosus construct to recapitulate form and function of the intervertebral disc. *Proceedings of the National Academy of Sciences of the United States of America*.

2018;115(3):477-482. https://www.ncbi.nlm.nih.gov/pubmed/29282316. doi: 10.1073/pnas.1715912115.

118. Nerurkar NL, Elliott DM, Mauck RL. Mechanics of oriented electrospun nanofibrous scaffolds for annulus fibrosus tissue engineering. *Journal of Orthopaedic Research*. 2007;25(8):1018-1028. https://onlinelibrary.wiley.com/doi/abs/10.1002/jor.20384. doi: 10.1002/jor.20384.

119. Nerurkar NL, Sen S, Huang AH, Elliott DM, Mauck RL. Engineered disc-like angle-ply structures for intervertebral disc replacement. *Spine*. 2010;35(8):867-873. https://www.ncbi.nlm.nih.gov/pubmed/20354467. doi: 10.1097/BRS.0b013e3181d74414.

120. Shamsah AH, Cartmell SH, Richardson SM, Bosworth LA. Tissue engineering the annulus fibrosus using 3D rings of electrospun PCL:PLLA angle-ply nanofiber sheets. *Frontiers in bioengineering and biotechnology*. 2019;7:437. https://www.ncbi.nlm.nih.gov/pubmed/31993415.

121. Kang R, Li H, Xi Z, et al. Surgical repair of annulus defect with biomimetic multilamellar nano/microfibrous scaffold in a porcine model. *Journal of Tissue Engineering and Regenerative Medicine*. 2018;12(1):164-174. https://onlinelibrary.wiley.com/doi/abs/10.1002/term.2384. doi: 10.1002/term.2384.

122. Blanquer SBG, Sharifi S, Grijpma DW. Development of poly(trimethylene carbonate) network implants for annulus fibrosus tissue engineering. *Journal of*

applied biomaterials & functional materials. 2012;10(3):177-184. https://www.narcis.nl/publication/RecordID/oai:pure.rug.nl:publications%2F28c58e47-9aed-427b-8419-909faca8985d. doi: 10.5301/JABFM.2012.10354.

123. McGuire R, Borem R, Mercuri J. The fabrication and characterization of a multi-laminate, angle-ply collagen patch for annulus fibrosus repair. *Journal of Tissue Engineering and Regenerative Medicine*. 2017;11(12):3488-3493. https://onlinelibrary.wiley.com/doi/abs/10.1002/term.2250. doi: 10.1002/term.2250.

124. Borem R, Madeline A, Walters J, Mayo H, Gill S, Mercuri J. Angle-ply biomaterial scaffold for annulus fibrosus repair replicates native tissue mechanical properties, restores spinal kinematics, and supports cell viability. *Acta Biomaterialia*. 2017;58:254-268. http://dx.doi.org/10.1016/j.actbio.2017.06.006. doi: 10.1016/j.actbio.2017.06.006.

125. Borem R, Madeline A, Vela J, Ricardo, Gill S, Mercuri J. Multi-laminate annulus fibrosus repair scaffold with an interlamellar matrix enhances impact resistance, prevents herniation and assists in restoring spinal kinematics. *Journal of the mechanical behavior of biomedical materials*. 2019;95:41-52. https://www.ncbi.nlm.nih.gov/pubmed/30953808. doi: 10.1016/j.jmbbm.2019.03.030.

126. Tedder ME, Liao J, Weed B, et al. Stabilized collagen scaffolds for heart valve tissue engineering. *Tissue Eng Part A*. 2009;15(6):1257-1268. Accessed Mar 2, 2020. doi: 10.1089/ten.tea.2008.0263.

127. Barnes R. Layers of the heart, pericarditis, and endocarditis. . 2017. https://heartstrongnurse.com/2017/06/20/layers-of-the-heart/. Accessed Mar 2, 2020.

128. Miller L, McGirt M, Garfin S, Bono C. Association of annular defect width after lumbar discectomy with risk of symptom recurrence and reoperation. *Spine*. 2018;43:E308-E315. https://www.ncbi.nlm.nih.gov/pmc/articles/PMC5815639/. Accessed Mar 2, 2020. doi: 10.1097/BRS.0000000000002501.

129. Janmey PA, Winer JP, Murray ME, Wen Q. The hard life of soft cells. *Cell Motil Cytoskeleton*. 2009;66(8):597-605. Accessed Mar 6, 2020. doi: 10.1002/cm.20382.

130. Kaklamani G, Cheneler D, Grover LM, Adams MJ, Bowen J. Mechanical properties of alginate hydrogels manufactured using external gelation. *Journal of the Mechanical Behavior of Biomedical Materials*. 2014;36:135-142. http://dx.doi.org/10.1016/j.jmbbm.2014.04.013. doi: 10.1016/j.jmbbm.2014.04.013.

131. Wang JY, Baer AE, Kraus VB, Setton LA. Intervertebral disc cells exhibit differences in gene expression in alginate and monolayer culture. *Spine*. 2001;26(16):1747-1751; discussion 1752. Accessed Mar 6, 2020. doi: 10.1097/00007632-200108150-00003.

132. Reitmaier S, Schmidt H, Ihler R, et al. Preliminary investigations on intradiscal pressures during daily activities: An in vivo study using the merino sheep. *PloS one*. 2013;8(7):e69610. https://www.ncbi.nlm.nih.gov/pubmed/23894509. doi: 10.1371/journal.pone.0069610.

133. Long R, Torre O, Hom W, Assael D, Iatridis J. Design requirements for annulus fibrosus repair: Review of forces, displacements, and material properties of the intervertebral disk and a summary of candidate hydrogels for repair. *Journal of Biomechanical Engineering*. 2016;138.

134. Kuo J, Zhang L, Bacro T, Yao H. The region-dependent biphasic viscoelastic properties of human temporomandibular joint discs under confined compression. *J Biomech*. 2010;43(7):1316-1321. https://www.ncbi.nlm.nih.gov/pmc/articles/PMC2857513/. Accessed Mar 9, 2020. doi: 10.1016/j.jbiomech.2010.01.020.

135. Walters JD, Gill SS, Mercuri JJ. Ethanol-mediated compaction and cross-linking enhance mechanical properties and degradation resistance while maintaining cytocompatibility of a nucleus pulposus scaffold. *Journal of Biomedical Materials Research Part B: Applied Biomaterials*. 2019;107(8):2488-2499. https://onlinelibrary.wiley.com/doi/abs/10.1002/jbm.b.34339. doi: 10.1002/jbm.b.34339.

136. Cortes DH, Jacobs NT, DeLucca JF, Elliott DM. Elastic, permeability and swelling properties of human intervertebral disc tissues: A benchmark for tissue engineering. *J Biomech*. 2014;47(9):2088-2094. https://www.ncbi.nlm.nih.gov/pmc/articles/PMC4047194/. Accessed Mar 9, 2020. doi: 10.1016/j.jbiomech.2013.12.021.

137. Panjabi MM. The stabilizing system of the spine. part II. neutral zone and instability hypothesis. *J Spinal Disord*. 1992;5(4):390-396; discussion 397. Accessed Mar 8, 2020. doi: 10.1097/00002517-199212000-00002.

138. McGregor AH, Cattermole HR, Hughes SP. Spinal motion in lumbar degenerative disc disease. *The Journal of bone and joint surgery. British volume*. 1998;80(6):1009-1013. https://www.ncbi.nlm.nih.gov/pubmed/9853494. doi: 10.1302/0301-620X.80B6.0801009.

139. Schultz A, Andersson G, Ortengren R, Haderspeck K, Nachemson A. Loads on the lumbar spine. validation of a biomechanical analysis by measurements of intradiscal pressures and myoelectric signals. *J Bone Joint Surg Am*. 1982;64(5):713-720. Accessed Mar 8, 2020.

140. Johannessen W, Cloyd JM, O'Connell GD, Vresilovic EJ, Elliott DM. Trans-endplate nucleotomy increases deformation and creep response in axial loading. *Ann Biomed Eng*. 2006;34(4):687-696. Accessed Mar 8, 2020. doi: 10.1007/s10439-005-9070-8.

141. ThermoFisher Scientific. Ethidium homodimer-2 (EthD-2) - 1 mM solution in DMSO. http://www.thermofisher.com/order/catalog/product/E3599. Accessed Mar 12, 2020.